UNIVERSITY OF CALIFORNIA
RIVERSIDE

Bridging the Gap Between Emission Simulators and Near-Road $PM_{2.5}$ Measurements

A Dissertation submitted in partial satisfaction
of the requirements for the degree of

Doctor of Philosophy

in

Chemical and Environmental Engineering

by

Ayla Marie Moretti

September 2021

Dissertation Committee:
Dr. David R. Cocker III, Co-Chairperson
Dr. Matthew J. Barth, Co-Chairperson
Dr. Kelley C. Barsanti

The Dissertation of Ayla Marie Moretti is approved:

Committee Co-Chairperson

Committee Co-Chairperson

University of California, Riverside

Acknowledgements

I would like to thank my advisors, Dr. David Coker and Dr. Matthew Barth for their support and expert guidance throughout my Ph.D. program. Thank you for always being available to help with revisions for writing and presentations, as well as helping me understand my data. Thank you for also teaching me so much about the field of atmospheric chemistry and vehicle emissions.

Additionally, I would like to thank my final committee member Dr. Kelley Barsanti for always being willing to answer any questions I had. I would also like to thank Dr. Ji Luo, Dr. Kanok Boriboonsomsin and Dr. Guoyuan Wu for all their support and guidance. Without their help and expertise none of this would have been possible.

Special thanks to Priyanka Sing for her endless support, Ryan Drover & Tom Eckel for their assistance during experiments and for being comic relief, and Dr. Patrick Roth for his assistance on training me on using the instruments in the APL and running chamber experiments. I appreciate the support and encouragement of Ben Bodenmiller as well as my family and friends, without you I would not have made it this far.

I would like to recognize the funding sources through the various projects. My personal funding though grant from the National Center for Sustainable Transportation (NCST), supported by the U.S. Department of Transportation (USDOT) through the graduate fellowship and the NCST dissertation award, and the Esther F. Hays Graduate Fellowship (Chapters 3 and 4). Next, I would like to acknowledge the Center for Advancing Research in Transportation Emissions, Energy, and Health (Chapter 2) and the CA Strategic Growth Council (Chapter 5).

Chapter 5, part or in full, is a reprint of the material as it appears in Transportation Research Record: Journal of the Transportation Research Board, Ayla Moretti, Ji Luo, Kanok Boriboonsomsin, Matthew Barth. “Reducing Community Exposure to Freight-related Air Pollution through Exposure-Based Truck Routing”. Transportation Research Record: Journal of the Transportation Research Board (under review).

Chapter 3 and 4 will be part or in full, submitted into academic journals upon completion.

Dedication

My Husband, Cats, Parents and Siblings

ABSTRACT OF THE DISSERTATION

Bridging the Gap Between Emission Simulators and Near-Road $PM_{2.5}$ Measurements

by

Ayla Marie Moretti

Doctor of Philosophy, Graduate Program in Chemical and Environmental Engineering
University of California, Riverside, September 2021
Dr. David R. Cocker III, Co-Chairperson
Dr. Matthew J. Barth, Co-Chairperson

Vehicle emissions are a major source of particulate matter ($PM_{2.5}$) in urban areas with emissions from on-road vehicles significantly impacting human health and the environment. Emission simulators and near-road ambient studies are used to estimate $PM_{2.5}$ exposure; however, studies are emerging that emission simulators underestimate the vehicle emitted $PM_{2.5}$ observed near-road. First, a statistical model examination of the relationship between weather parameters, traffic data, and the near-roadway $PM_{2.5}$ yielded $R^2 \leq 0.24$ indicating that something other than traffic and weather data was needed to better predict near-road $PM_{2.5.;}$ such as the gas-particle (G/P) partitioning of the organic $PM_{2.5}$. The underestimation is due to emission simulators treating all $PM_{2.5}$ as non-volatile and not accounting for the G/P partitioning of organics. Next, this dissertation describes a $PM_{2.5}$ correction factor (CF) to account for G/P partitioning of organics emitted from on-road gasoline and diesel vehicles. The CF accounts for sampling dilution and temperature, ambient temperature, background $PM_{2.5}$, distance from the vehicle, and the vehicle's initial reactive organic gas (ROG_i) concentration and elemental carbon to organic carbon (EC:OC). Using the CF, a look-up table and four Random Forest (RF) models were created.

In building the RF it was found that generally the ambient temperature, vehicle's EC:OC and ROG_i concentration were the most important variables in predicting the CF. Implementing the CF with emission simulators and/or dispersion models would allow for a more realistic $PM_{2.5}$ concentration thereby improving our understanding of how vehicle emissions affect human health, air quality, and the environment. Additionally, a case study is included within that evaluates the impacts of exposure-based routing in a Southern California disadvantaged community and demonstrates how the CF can be applied. Results indicated that re-routing heavy-duty diesel trucks along "low exposure routes" (LER) could reduce inhaled $PM_{2.5}$ by 14+% depending on meteorological and traffic conditions. The reduction in $PM_{2.5}$ inhalation could increase by an additional 50+% by selecting LER that are over 10m from the sensitive populations, and when accounting the CF.

Table of Contents

List of Figures

List of Tables

Chapter 1. Introduction

1.1 Introduction & Motivation

The World Health Organization (WHO) estimates that ambient air pollution accounts for about 4.2 million deaths per year with around 91% of the world's population living in places where the air quality levels exceed WHO limits [1]. One major outdoor pollution source is vehicles emissions. The major pollutants emitted from vehicles include particulate matter (PM), carbon monoxide (CO), carbon dioxide (CO_2), volatile organic compounds (VOCs), hydrocarbons (HCs), nitrogen oxides (NO_x), and polycyclic aromatic hydrocarbons (PAHs) [2,3]. Many epidemiological studies have shown risk of illness and mortality for drivers, and individuals living near roadways due to these emissions [3,4]. The main cause of this mortality is due to fine particulate matter ($PM_{2.5}$), particulate matter with an aerodynamic diameter less than 2.5 micrometers. In the United States, the Environmental Protection Agency (EPA) has established National Ambient Air Quality Standards (NAAQS) for $PM_{2.5}$ to help provide public health protection, especially for "sensitive" populations such as children and the elderly, as well as protect the environment. $PM_{2.5}$ poses a large health risk because it can penetrate deep into the lungs, leading to heart and lung diseases, and may even enter the bloodstream [5]. $PM_{2.5}$ is also the main cause of reduced visibility around the world and depending on chemical composition can lead to environmental damage such as: water acidification, damaging crops and soil, and contributing to acid rain [5].

In California, light duty vehicles account for 70% of the transportation emissions with the pollutants from transportation, especially $PM_{2.5}$, being a significant contributor to adverse health effects [6]. Researchers estimate, based on total population exposed to on-road transportation $PM_{2.5,}$ there are approximately 3,100 premature deaths in California per year due to cardiovascular diseases and other illnesses due to $PM_{2.5}$ exposure [7]. Emission simulators, such as the United States Environmental Protection Agency's (US EPA) MOtor Vehicle Emission Simulator (MOVES), can be used to estimate exposure to on-road gasoline and diesel vehicles. The emission factors from emission simulators can then be used to estimate annual exposure and health impacts of $PM_{2.5}$. Near-road ambient studies can be used to predict near-road air quality and validate emission simulators predictions. However, studies are finding that emission simulators substantially underestimate vehicle $PM_{2.5}$ emissions when comparing laboratory, on-board, tunnel, and near-road ambient studies to modelled data [8]. The difference between emission simulators and near-road ambient studies could be due to the gas-particle partitioning of the organic $PM_{2.5}$ and organic gases not currently accounted for by the emission simulators used for near roadway models.

This dissertation aims to bridge the gap between measured near-road ambient $PM_{2.5}$ concentration and emission simulator predicted near-road $PM_{2.5}$. First, an investigation is reported into the near-road correlation between $PM_{2.5}$ and NO_x concentrations, traffic and ambient parameters. An $PM_{2.5}$ correction factor was then developed to bridge the gap between the near-road ambient $PM_{2.5}$ measurements and emission simulators by introducing thermodynamics into emission simulators through a model accounting for gas-

particle partitioning. The correction factor is then applied to a case study of the contribution of heavy-duty diesel vehicle emissions to inhaled $PM_{2.5}$ in a near-by population. This dissertation specifically breaks down as follows:

Chapter 2 examines the relationship between air quality, traffic and weather parameters to gain a better understanding of the near-freeway air quality. $PM_{2.5}$ and nitrogen dioxide (NO_2) measurement data and weather data were obtained from two near-road air monitoring stations (AMS), managed by South Coast Air Quality Management District, along two different freeways in Southern California. The air pollutant concentrations were than statistically analyzed versus Caltrans Performance Measurement System (PeMS) traffic data and the AMS weather data.

Chapter 3 develops a novel $PM_{2.5}$ correction factor to bridge the gap between emission simulator predicted near-road $PM_{2.5}$ and the near-road ambient $PM_{2.5}$ measurements. The correction factor was created by using the volatility basis set to account for variability in gas-particle partitioning as a function of different emission measurement strategies. This correction factor adds thermodynamics into emission simulator estimates of ambient $PM_{2.5}$ by accounting for the gas-particle partitioning of the organics emitted from on-road gasoline and diesel vehicles that can then be applied to emission simulator outputs to better predict near-road $PM_{2.5}$.

Chapter 4 derives a look-up table and random forest model based on the correction factor introduced in Chapter 3. The look-up table uses MySQL; the random forest was created using the look-up table and Python version 3.9 and the package scikit-learn version

0.24. These novel tools allow the correction factor to be easily coupled with emission simulators or dispersion models to better predict the near-road $PM_{2.5}$ concentrations.

Chapter 5 evaluated the exposure-based routing in the San Bernardino Airport area, a largely disadvantaged community and demonstrates how the correction factor (derived in Chapters 3 and 4) can be applied. Exposure-based routing can navigate a heavy-duty-diesel-truck through a disadvantaged community in a way that lowers the total exposure of community members to the pollutant emissions ($PM_{2.5}$, NO_x, and CO_2) from the truck without significantly increasing travel time.

Chapter 6 summarizes the chapters and the broader impact of this dissertation and proposes future work.

Appendix A introduces a new instrument, an oxidation flow reactor (OFR), built and initially characterized in the University of California, Riverside Center for Environmental Research and Technology's Atmospheric Processes Laboratory.

1.2 References

1. World Health Organization. Air Pollution. https://www.who.int/health-topics/air-pollution#tab=tab_2
2. Wu, G., Pham, L., Hao, P., Jung, H., & Boriboonsomsin, K. (2017). Prediction of real-time particulate matter concentrations on highways using traffic information and emission model. *Transportation Research Board, 96th Annual Meeting*.
3. Zhang, K., & Batterman, S. (2013). Air pollution and health risks due to vehicle traffic. *Science of the Total Environment*, *450–451*, 307–316, http://doi.org/10.1016/j.scitotenv. 2013.01.074.

4. Wang, X., Ho, K. F., Chow, J. C., Kohl, S. D., Chan, C. S., Cui, L., … Watson, J. G. (2018). Hong Kong vehicle emission changes from 2003 to 2015 in the Shing Mun Tunnel. Aerosol Science and Technology, 6826, 1–14. https://doi.org/10.1080/02786826.2018.1456650.
5. United States Environmental Protection Agency. Particulate Matter (PM) Pollution [online]. Available: https://www.epa.gov/pm-pollution
6. Brown, A. L., Sperling, D., Austin, B., DeShazo, J., Fulton, L., Lipman, T., Murphy, C., Saaphores, J. D., Tal, G., Abrams, C., Chakraborty, D., Coffee, D., Babag, S., Davis, A., Delucchi, M. A., Fleming, K. L., Forest, K., Garcia, J., Hyland, M., … Yang, A. (2021). Driving California' s Transportation Emissions to Zero. https://doi.org/10.7922/G2MC8X9X
7. Union of Concerned Scientists. (2019). Inequitable Exposure to Air Pollution from Vehicles in California. January, 4. https://www.ucsusa.org/sites/default/files/attach/2019/02/cv-air-pollution-CA-web.pdf
8. Smit, R., Ntziachristos, L., & Boulter, P. (2010). Validation of road vehicle and traffic emission models - A review and meta-analysis. Atmospheric Environment, 44(25), 2943–2953. https://doi.org/10.1016/j.atmosenv.2010.05.022

Chapter 2. Understanding Air Quality Data, Traffic, and Weather Parameters Collected from Near-Road Stations

Ayla Moretti[1,2], Ji Luo[1], Guoyuan Wu[1], Brandon Feenstra[1,2], Kanok Boriboonsomsin[1], Matthew Barth[1,3]

1. Bourns College of Engineering, Center for Environmental Research and Technology (CE-CERT), University of California, 1084 Columbia Avenue, Riverside, California 92507, United States
2. Department of Chemical and Environmental Engineering, Bourns College of Engineering, University of California, Riverside, California 92521, United States
3. Department of Electrical and Computer Engineering, Bourns College of Engineering, University of California, Riverside, California 92521, United States

2.1 Abstract

Near-road air quality measurement serves as a fundamental method to understand the impact of transportation emissions on ambient air quality and public health. In this study, 5-minute average fine particulate matter ($PM_{2.5}$) and nitrogen dioxide (NO_2) measurement data were obtained from two near-freeway air monitoring stations (AMS) in Southern California. In addition, 13 variables and more than 26,000 rows of data, including weather parameters, traffic speed, and traffic volume near the AMS were obtained. The Multiple Linear Regression (MLR) and Multivariate Adaptive Regression Splines (MARS) models were used to examine the relationship among the weather parameters, traffic data, and near-freeway air pollutant concentration. Both MLR and MARS showed that all weather parameters (e.g., relative humidity, pressure, temperature, wind) were significant variables. MLR coefficients indicated that the traffic speed on the direction closest to the AMS had up to 13 times larger impact than the speed on the opposite direction. For State Route 60 AMS, MLR gave the adjusted R^2 as 0.18 and 0.27 for $PM_{2.5}$ and NO_2, respectively, and MARS gave the R^2 as 0.30 and 0.46, respectively. For Interstate-710 AMS, MLR gave the adjusted R^2 as 0.14 and 0.36 for $PM_{2.5}$ and NO_2, respectively, and MARS gave the R^2 as 0.21 and 0.57. Generally, NO_2 concentration can be better explained by the selected variables than $PM_{2.5}$. The test of traffic speed segmentation further indicates that the traffic speed has a considerable influence on near-road pollutant concentrations.

2.2 Introduction

Vehicle emissions are major contributors of urban air pollution. Due to the continued growth of vehicle use and greater occurrence of traffic congestion, vehicle emissions are predicted to grow in the coming years [1,2]. Among many strategies of emission estimation and subsequent mitigation, near-road air quality measurements serve as a fundamental method to understand the impact of the traffic emissions on ambient air quality and public health. Extensive near-road measurement studies were performed to assess a variety of research purposes, including examining the relationship among near-road air pollutants, exposure, and health effects [3,4,5,6], as well as evaluating the effects of traffic calming strategies [7,8,9]. For this study, a literature review was done focusing on studies which utilized near-road measurement data to analyze the impact of traffic, weather, and spatial parameters on the air quality in the road-side or other microenvironments [10,11,12,13]. For example, Zhang et al. (2011) found that hard vehicle acceleration can lead to an increase of hydrocarbon (HC) and carbon monoxide (CO) emissions due to the fuel rich mode, while deceleration can increase particulate matter (PM) and HC emissions due to unburned fuel. Based on a year-long road-side measurement campaign, Kimbrough et al. (2013) revealed that while the average wind speed appeared to be an important explanatory factor, the monthly average traffic volume and frequency of downwind conditions were not enough to explain the monthly average excess in monthly carbon monoxide concentrations. Bigazzi et al. (2012) combined 20-second interval freeway traffic data and in-vehicle ultrafine particulate (UFP) concentration data and found

that traffic states had a small but significant impact on in-vehicle UFP, and that vehicle ventilation was the dominant influence on in-vehicle UFP concentration.

In addition, near-road measurements have be applied to predict the near-road air quality or aggregated traffic emission factors based on models [14,15,16]. For instance, Venkatram et al. (2007) investigated near-road micrometeorology parameters and air quality measurements, with their dispersion model showing that the measured micrometeorology and air quality data agreed well with the predicted values. Choudhary et al. (2016) found that, during peak hour, emission factors of CO and HC were about 4-7 times higher than during off-peak hours, and that emission factor of nitrogen oxides (NO_x) was about 2 times higher than that of off-peak hour. Wu et al. (2017) applied a Multivariate Adaptive Regression Splines model to mobile air quality measurements and traffic data - and identified eleven traffic-related variables that had the most impacts on in-source PM concentration prediction.

In this study, fine PM ($PM_{2.5}$) and nitrogen dioxide (NO_2) measurement data (5-minute average) were obtained from two near-road air monitoring stations (AMS) which are managed by South Coast Air Quality Management District. The objective of this study was to examine the relationship between air quality, and traffic and weather parameters. Utilizing air quality measurement spanning over four months, a better understanding of the near-freeway concentration, traffic speed, traffic flow, and weather parameters was obtained.

2.3 Data Collection and Processing

2.3.1 Data Collection

2.3.1.1 Air Monitoring Stations

1-minute average concentration of $PM_{2.5}$ and NO_2 were obtained from two near-roadway air monitoring stations (AMS) managed by the South Coast Air Quality Management District (SCAQMD) [17]. The locations of the two stations are marked in Figure 2.1a with street view images in Figure 2.1b and Figure 2.1c. Figure 2.2 presents a more detailed image of each of the AMS in relationship to the traffic count data collected.

1. *Ontario SR-60 Near Road (60NR) AMS:* located at 2330 S Castle Harbour Pl, Ontario, CA 91761. 60NR is approximately 10 meters north to California State Route 60 (SR-60) between the Grove Ave and Vineyard Ave exits (figure 2a). The monitoring station is equipped with a Horiba APNA 370 NO_x instrument for NO_2 measurements and a Thermo-Scientific 5014i for continuous $PM_{2.5}$ measurements [18]. This site was selected by SCAQMD because this location is known for high traffic congestion during weekdays. The typical traffic mix is dominated by light duty vehicles.
2. *Long Beach I-710 Near Road (710NR) AMS:* located at 5895 Long Beach Blvd. Long Beach, CA 90805. 710NR is located 20 meters east to Interstate 710 (I-710) between the exits for W. Del Amo Boulevard and Long Beach Boulevard (figure 2b). The monitoring station is equipped with a Thermo-Scientific 42i NO_x instrument for NO_2 measurements and a Thermo-Scientific 5014i for continuous $PM_{2.5}$ measurements [19]. This site was selected by SCAQMD because this location

is known for having a significant amount of heavy-duty trucks accounting for the majority of freeway traffic.

The air quality data from the two AMS was collected from January 2018 through April 2018. The 1-minute concentration values were then averaged to 5-minute values to match the time resolution of the traffic count data.

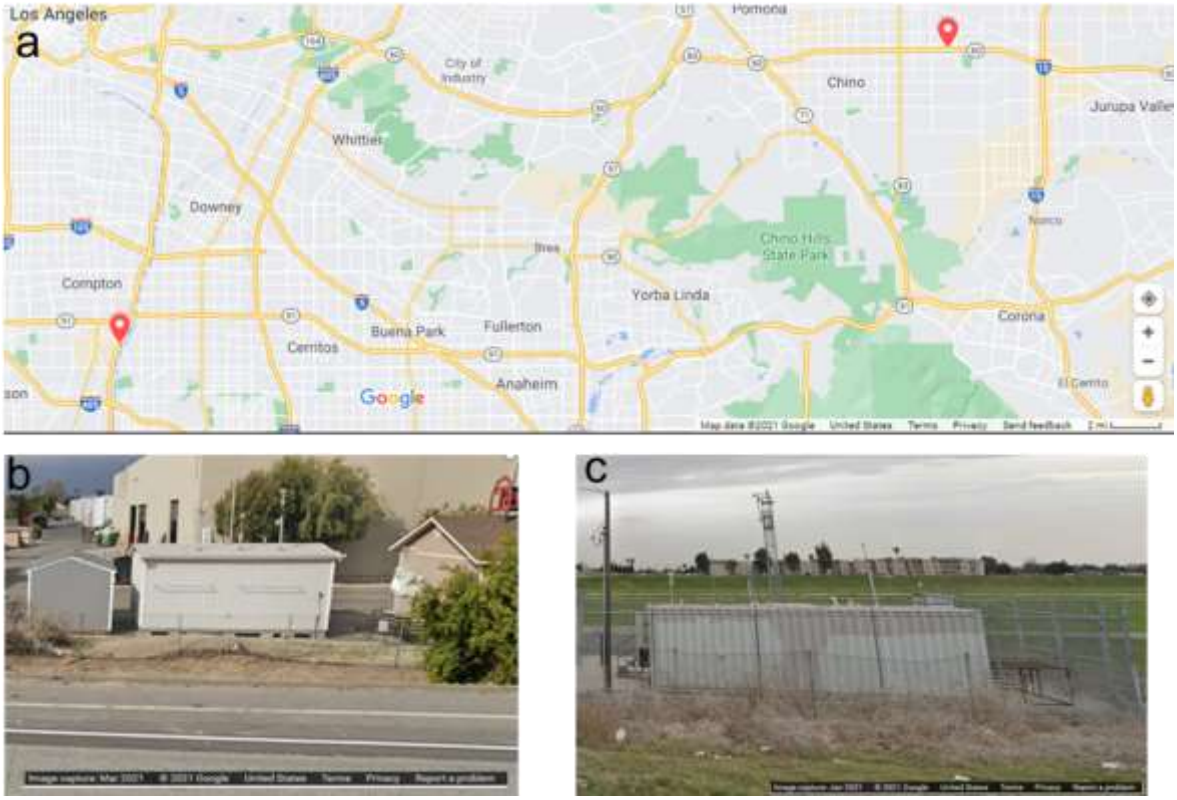

Figure 2.1: (a) Illustration of the SCAQMD near-roadway AMS sites selected for this study in Google Maps. (b) Street view of 60NR AMS and (c) street view of 710NR AMS.

2.3.1.2 Meteorological Data

Meteorological conditions are critical factors for near-road $PM_{2.5}$ and NO_2 concentration. The SCAQMD near-roadway AMS network also collects the following meteorological parameters: pressure, temperature, relative humidity (RH), wind direction

and wind speed. The 1-minute meteorological data was collected from January 2018 through April 2018 and processed into 5-minute averaged data to match the time resolution of the traffic count data. An arithmetic mean was applied to concentration, humidity, temperature, atmospheric pressure. For wind speed and wind direction, vector average method was used [20].

2.3.1.3 Traffic Parameters

The traffic metrics used in this study was obtained from the Caltrans Performance Measurement System (PeMS) [21]. PeMS receives real-time 30 second raw measurements on traffic count and lane occupancy from each inductive loop detector (ILD) throughout the California freeway system. The system detects missing and invalid data and would correct the wrong values or fill in the missing data [22]. Based on the traffic count and lane occupancy data for each lane, PeMS estimates an aggregated traffic speed at each inductive loop detector using the G-factor algorithm [23]. Raw data are aggregated at different temporal levels (e.g., per 5 minute, hourly, daily) in PeMS for different purpose. This study extracted the station-level 5-minute aggregated data. PeMS also records the latitude and longitude of each vehicle detection station (VDS) and the corresponding postmile. Using the PeMS "Station Metadata" and the nearest postmiles (Figure 2.2), the nearest upstream and downstream VDS along both directions for both the near-roadway AMS was identified. Data processing will be introduced in the next section.

Figure 2.2: Satellite images of the SCAQMD near-roadway AMS selected for this study (source: Google Maps and PeMS).

Note: Figure (a) Shows the SCAQMD site (red marker) adjacent to SR-60 and the corresponding postmiles (blue markers). Postmile A corresponds to PeMS abs postmile 36.32 for SR-60 Eastbound and PeMS abs postmile 36.31 for SR-60 Westbound. Postmile B corresponds to PeMS abs postmile 37.65 for SR-60 Eastbound and PeMS abs postmile 37.64 for SR-60 Westbound. (b) Shows the SCAQMD site (red marker) adjacent to I-710 and the corresponding postmiles (blue markers). Postmile A corresponds to PeMS abs postmile 6.04 for I-710 Northbound and PeMS abs postmile 5.99 for I-710 Southbound. Postmile B corresponds to PeMS abs postmile 7.17 for I-710 Northbound and PeMS abs postmile 6.93 for I-710 Southbound.

2.3.2 Data Preparation

2.3.2.1 Data Cleaning

The raw database obtained from near-road AMS and PeMS required further data processing, including examining outliers, averaging values, and removing missing values. All the data were within the reasonable range and there were no detectable outliers. For 5-minute average values, the entry would be labeled as null if there were more than 3 data points missing within the five minutes.

After synchronizing 5-minute data for concentration, traffic, and weather parameters, listwise deletion was applied to handle missing information, i.e., the row of

data would be removed if there were any null values (e.g. concentration, traffic, or weather parameters) in the row. There was one exception: all the atmospheric pressure data for 710NR AMS was missing, therefore the analysis of 710NR AMS excluded pressure values.

2.3.2.2 Variable Transformation

Box-cox transformation was performed to transform non-normal concentration values to a normal-distribution shape. Lambda of 0.5 was applied for $PM_{2.5}$ concentration ($\mu g/m^3$), and the comparison of before and after transformation is presented in Figure 2.3. Before the transformation, the $PM_{2.5}$ concentration distribution had a skewness of 1.501 (Figure 2.3a), and after the transformation it conformed much better to a normal distribution with a skewness of 0.235 (Figure 2.3b). The Box-cox transformation did not improve NO_2 distribution and therefore was not applied to NO_2 concentration values.

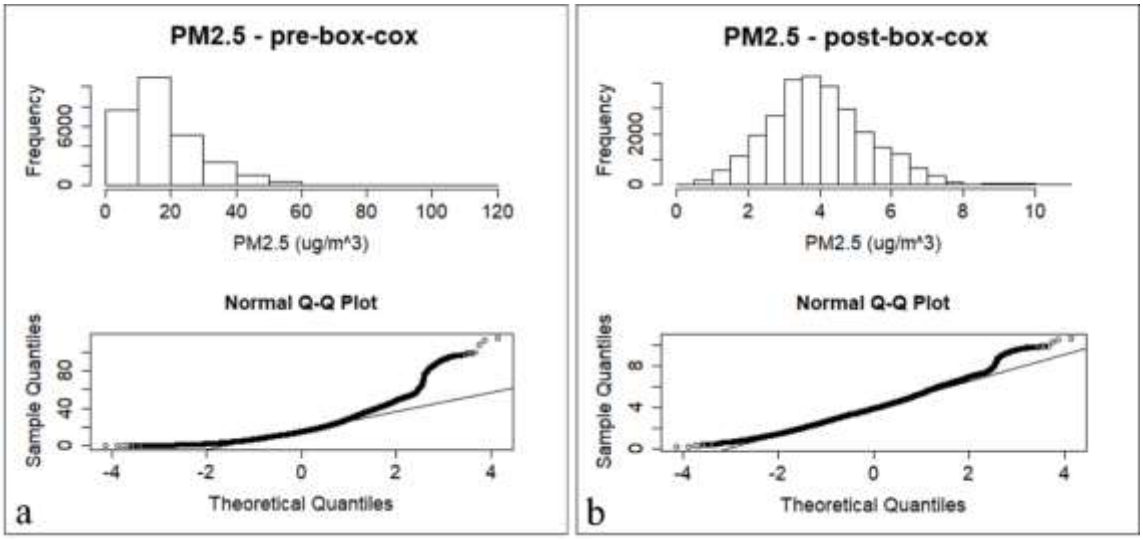

Figure 2.3: Histogram and Q-Q plot of $PM_{2.5}$ before and after box-cox transformation with $\lambda = 0.5$.

The Pearson correlation coefficients was calculated to examine the linear relationship between any two numerical variables [24]. This was done to identify potential

multicollinearity issues among the variables. The results indicated that the explanatory variables were not linearly related with each other.

2.4 Models and Results

Two different regression models were applied to the database: 1) multiple linear regression (MLR); and 2) multivariate adaptive regression splines (MARS). All the regression models were executed using R version 3.5.1 [25].

2.4.1 Multiple Linear Regression (MLR)

The Multiple Linear Regression (MLR) model is the simplest multivariate regression method that models the linear relationship between the explanatory variables on the observed traffic, and meteorological parameters on $PM_{2.5,}$ NO_2 concentration. The general equation for the MLR model can be written as

$$y = \beta_0 + \sum_i \beta_i * x_i + \varepsilon_i \quad (2.1)$$

where y represents the estimated model output; β_0 is the intercept; β_i is the regression coefficient associated with the i-th variable, x_i is the value of the i-th variable (Table 2.1); and ε_i is an independent, normally distributed, random error with zero mean and constant variance [26].

Table 2.1: Description of the explanatory variables for 60NR and 710NR

	60NR	**710NR**	
i	x_i	x_i	**unit**
0	Intercept		-
1	Relative Humidity		%
2	Temperature		Fahrenheit
3	Pressure	-	Hg bar
4	Wind Speed		MPH
5	Wind Direction		Degree
6	Speed West – Postmile A	Speed North – Postmile A	MPH
7	Speed West – Postmile B	Speed North – Postmile B	MPH
8	Speed East – Postmile A	Speed South – Postmile A	MPH
9	Speed East – Postmile B	Speed South – Postmile B	MPH
10	Flow West – Postmile A	Flow North – Postmile A	Vehicle/5 minutes
11	Flow West – Postmile B	Flow North – Postmile B	Vehicle/5 minutes
12	Flow East – Postmile A	Flow South – Postmile A	Vehicle/5 minutes
13	Flow East – Postmile B	Flow South – Postmile B	Vehicle/5 minutes

2.4.1.1 MLR Results at 60NR AMS

The results of MLR analysis for NO_2 and $PM_{2.5}$ measured from the two near-roadway AMS are shown in Table 2.2. At 60NR AMS, results indicated that for both $PM_{2.5}$ and NO_2, all the weather parameters are significant with at 5% α-level. Relative humidity and temperature are positively related with $PM_{2.5}$ concentration, however, the two factors are negatively related with NO_2 concentration. Atmospheric pressure is positively related with both pollutant concentrations. Wind speed is always negatively related with both pollutant concentrations, indicating that higher wind speeds, and unstable atmospheric conditions, will lead to lower near-road air pollution concentrations.

Table 2.2: List of regression coefficients for 60NR and 710NR MLR analysis of $PM_{2.5}$ and NO_2

		MLR							
		60NR				710NR			
		$PM_{2.5}$		NO_2		$PM_{2.5}$		NO_2	
i*		β_i	p-value	β_i	p-value	β_i	p-value	β_i	p-value
0	Intercept	**-6.46E+01**	< 2e-16	-4.65E+01	9.22E-02	**3.93E+00**	< 2e-16	**7.84E+01**	< 2e-16
1	Relative Humidity	**1.49E-02**	< 2e-16	**-1.80E-01**	< 2e-16	**7.56E-03**	< 2e-16	**-2.61E-01**	< 2e-16
2	Temperature	**4.56E-02**	< 2e-16	**-1.83E-01**	< 2e-16	**1.57E-02**	< 2e-16	**-5.29E-02**	2.58E-04
3	Pressure	**2.27E+00**	< 2e-16	**4.72E+00**	4.33E-07	-	-	-	-
4	Wind Speed	**-1.90E-01**	< 2e-16	**-2.99E+00**	< 2e-16	**-1.87E-01**	< 2e-16	**-3.16E+00**	< 2e-16
5	Wind Direction	**3.39E-04**	5.56E-06	**-3.00E-02**	< 2e-16	**1.55E-04**	1.97E-02	**3.52E-03**	1.32E-07
6	Speed West/North A	**5.59E-03**	1.87E-02	1.69E-02	4.61E-01	**-1.95E-02**	< 2e-16	**-1.90E-01**	< 2e-16
7	Speed West/North B	**-1.28E-02**	5.86E-09	**-1.42E-01**	1.84E-11	-3.25E-06	9.98E-01	**-1.12E-01**	3.25E-15
8	Speed East/South A	-6.45E-05	8.39E-01	**-8.22E-03**	7.28E-03	**3.53E-04**	3.47E-06	**2.24E-03**	3.31E-03
9	Speed East/South B	4.29E-04	2.30E-01	9.46E-04	7.84E-01	**1.14E-03**	2.11E-08	**-8.41E-03**	3.51E-05
10	Flow West/North A	**-6.35E-03**	4.25E-04	-2.04E-02	2.40E-01	**-3.63E-03**	6.65E-04	**-1.17E-01**	< 2e-16
11	Flow West/North B	**4.88E-03**	8.67E-03	**-3.16E-01**	< 2e-16	**4.19E-03**	1.91E-02	**4.18E-02**	1.98E-02
12	Flow East/South A	**6.69E-03**	< 2e-16	**8.55E-02**	< 2e-16	**4.08E-04**	7.85E-03	**2.55E-02**	< 2e-16
13	Flow East/South B	**-7.34E-03**	< 2e-16	**-8.10E-02**	< 2e-16	**-1.16E-03**	4.49E-08	**-1.75E-02**	< 2e-16
Degree of Freedom		27600		27600		26327		26327	
Residual Standard Error		1.263		12.18		1.316		13.21	
Multiple R-Squared		0.1763		0.273		0.1409		0.3575	
Ajusted R-Squared		0.1759		0.2726		0.1405		0.3572	
F-Statistic P-Value		< 2.2e-16		< 2.2e-16		< 2.2e-16		< 2.2e-16	

Variables in boldface are statistically significant at 5% α-level

* Refer to Table 1 for the description of each index i

For $PM_{2.5}$, traffic speed on west bound at both postmiles is significant, and traffic flow on both directions is significant, with p-values less than 5%. As shown in Figure 2.1 and Figure 2.2, the west bound of SR-60 is directly facing the AMS, therefore it could be expected that the traffic speed on west bound had a more significant impact than that of east bound. However, because similar traffic volume could reflect different traffic speed/congestion levels, flow's influence on the pollutant concentration is not consistent and cannot be well explained. However, because similar traffic volume could reflect different traffic speed/congestion levels, flow's influence on the pollutant concentration is not consistent and cannot be well explained. To further consider the impact of traffic speed, a segmented regression and MARS will be applied in the following sections.

At 60NR AMS, the adjusted R^2 values are 0.27 and 0.18 for the NO_2 and $PM_{2.5}$, respectively, implying that NO_2 could be better explained by the explanatory variables than $PM_{2.5}$.

2.4.1.2 MLR Results at 710NR AMS

At 710NR AMS, similar as that of 60NR AMS, all meteorological parameters are statistically significant. The similar effects of relative humidity, temperature, and wind speed are observed for both air pollutants at the 710NR AMS as that of 60NR site. Table 2.2 also showed that for $PM_{2.5}$, all variables are statistically significant except for the traffic speed at north bound postmile B (downstream to AMS). For NO_2, all the explanatory variables become statistically significant at 5% α-level. The magnitude of the coefficient of the north bound traffic speed (e.g. -1.12E-1 at postmile A) is 13 times larger than that of the south bound (e.g. -8.41E-3 at postmile A) traffic speed, which is reasonable as the 710NR AMS is directly adjacent to the north bound lanes (Figure 2.2). Similarly, the results of total flow could not be well explained by the relative locations and hypothesis. Future improvements, truck flow and near-road carbon dioxide measurement could help explain the concentration variations.

The adjusted R^2 values are 0.36 and 0.14 for NO_2 and $PM_{2.5}$, respectively, which also implies that NO_2, for both 710NR and 60NR, could be better explained by the selected variables than $PM_{2.5}$. The hypothesis for this observation was that on-road traffic contributes a large portion to the ambient primary NO_2. On the other hand, a large percentage of $PM_{2.5}$ comes from secondary formation, therefore $PM_{2.5}$ cannot be well explained by simultaneous traffic and weather factors. Figure 2.4 illustrates the comparison between observed and MLR-modelled NO_2 and $PM_{2.5}$ concentrations for both 60NR and 710NR. For $PM_{2.5}$, there is a small number of points which stand outside of the point cloud.

For NO_2, the cluster is tighter with less scattered points. Generally, MLR tends to underestimate the averaged near-road concentrations.

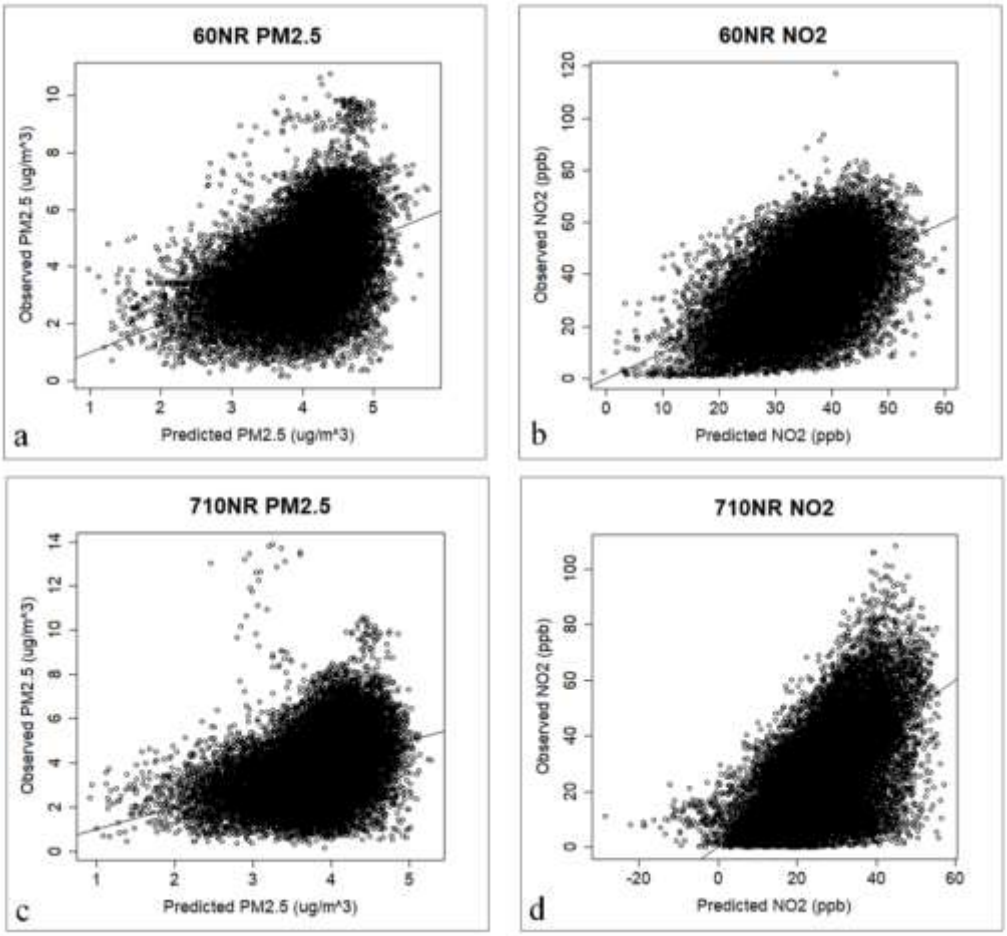

Figure 2.4: Predicted vs. observed graphs using the MLR model (a) 60NR $PM_{2.5}$ (b) 60NR NO_2 (c) 710NR $PM_{2.5}$ (d) 710NR NO_2. The axes for the $PM_{2.5}$ figures (a and c) are raised to the 0.5 due to the Box-cox transformation.

2.4.1.3 Traffic Speed Segmentation

Due to the non-linearity between traffic speed and volume, segmenting the traffic speed could help to better understand the impact of traffic speed and volume. Four different congestion speeds as well as a transition period are tested using the MLR model. As listed in the first two rows in Table 2.3, for example, considering SR-60 West, it was assumed that congestion would occur when all speeds become less than 30 mph at both postmiles,

and free-flow status would return when all speeds were greater than or equal to 30 mph in the West direction, with no speed constraints for the east direction. One transition period between 30 to 45 mph is considered as shown in the second to the last row in Table 2.3.

The segmenting speed improved nearly all adjusted R^2 values when compared with Table 2.2, except for a few cases. In the congestion section, nearly all the adjusted R^2 values improved significantly, especially for the SR-60 West and I-710 North, which are directly adjacent to the AMS.

Table 2.3: MLR adjusted R^2 values for 60NR and 710NR speed segment results.

MLR model		**60NR**					**710NR**			
adjusted R^2 values (Number of data points)		**SR-60 West**		**SR-60 East**			**I-710 North**		**I-710 South**	
		$PM_{2.5}$	**NO_2**	**$PM_{2.5}$**	**NO_2**		**$PM_{2.5}$**	**NO_2**	**$PM_{2.5}$**	**NO_2**
≥ 30 MPH	**Free-Flow**	0.175 (27,294)	0.274 (27,294)	0.175 (27,200)	0.274 (27,200)		0.143 (25,760)	0.358 (25,760)	0.14 (24,719)	0.35 (24,719)
< 30 MPH	**Congestion**	0.582 (114)	0.61 (114)	0.226 (111)	0.468 (111)		0.762 (18)	- (18)	0.679 (58)	0.209 (58)
≥ 35 MPH	**Free-Flow**	0.173 (26,906)	0.27 (26,906)	0.176 (26,337)	0.274 (26,337)		0.143 (22,513)	0.357 (22,513)	0.138 (24,006)	0.346 (24,006)
< 35 MPH	**Congestion**	0.44 (232)	0.49 (232)	0.102 (406)	0.534 (406)		0.386 (75)	0.541 (75)	0.394 (153)	0.414 (153)
≥ 40 MPH	**Free-Flow**	0.171 (26,175)	0.266 (26,175)	0.178 (25,409)	0.272 (25,409)		0.135 (24,441)	0.359 (24,441)	0.137 (23,427)	0.346 (23,427)
< 40 MPH	**Congestion**	0.394 (564)	0.507 (564)	0.105 (1,116)	0.51 (1,116)		0.262 (197)	0.533 (197)	0.301 (283)	0.447 (283)
≥45 MPH	**Free-Flow**	0.17 (25,343)	0.265 (25,343)	0.177 (24,723)	0.273 (24,723)		0.133 (21,899)	0.358 (21,899)	0.139 (22,799)	0.347 (22,799)
< 45 MPH	**Congestion**	0.298 (1,131)	0.469 (1,131)	0.133 (1,880)	0.482 (1,880)		0.167 (308)	0.531 (308)	0.264 (436)	0.389 (436)
≥ 45 MPH	**Free-Flow**	0.17 (25,343)	0.265 (25,343)	0.177 (24,723)	0.273 (24,723)		0.133 (21,899)	0.358 (21,899)	0.139 (22,799)	0.347 (22,799)
30 - 45	**Transition**	0.219 (842)	0.493 (842)	0.158 (1,515)	0.475 (1,515)		- (14)	- (14)	0.3 (268)	0.413 (268)
< 30 MPH	**Congestion**	0.582 (114)	0.61 (114)	0.226 (111)	0.468 (111)		0.762 (18)	- (18)	0.679 (58)	0.209 (58)

2.4.2 Multivariate Adaptive Regression Splines (MARS)

To further explore the impacts of selected variables, a nonparametric regression technique, Multivariate Adaptive Regression Splines (MARS) model [27], is also applied to the dataset used in this study. Even though the statistical properties of the resulting estimators are more difficult to determine, compared to the MLR model, the non-parametric regression techniques require fewer assumptions and can provide a better fit than the parametric techniques. The following description of MARS referenced Wu *et al*., 2017 [15]. The MARS model can also be regarded as an extension of the linear models that automatically captures nonlinearities and interactions using the equation:

$$f(x) = \sum_i c_i * B_i(x) \tag{2.2}$$

where f(x) is the estimated model output; $B_i(x)$ is the *i-th* basis function which can be a constant 1, a hinge function, or a product of two or more hinge functions. With the hinge function can take the form:

$$\max(0, x - const.) \tag{2.3}$$

or,

$$\max(0, const. - x) \tag{2.4}$$

and automatically partition the input data so that the effects of any outliers can be attenuated. The MARS model tends to have a good bias-variance tradeoff due to the flexible but sufficiently constrained form of the basis functions to model nonlinearity with relatively low bias and variance.

2.4.2.1 MARS Results at 60NR AMS

In Table 2.4, results for $PM_{2.5}$ indicates that the explanatory variables of importance include all meteorological parameters, traffic speed on west bound postmile A (downstream to AMS), traffic speed on east bound for both postmiles, and traffic volume on east bound for both postmiles. For NO_2, the important variables also include all the meteorological parameters, traffic speed on west bound postmile A (downstream to AMS) and east bound postmile B (downstream to AMS), and all the traffic flow factors on both freeway directions for both postmiles.

The variable of importance as well as the values in the corresponding basis functions represents the associated values that are critical to the partitioning for that set of explanatory variables. For example, looking at x_4 (wind speed) for $PM_{2.5}$ in Table 2.4, 5.06 mph is a critical partitioning point for the wind speed values. The R^2 values are 0.298 for $PM_{2.5}$ and 0.456 for NO_2, which are improvements compared to that of the MLR model.

Table 2.4: List of basis functions and the associated coefficients for MARS analysis at 60NR AMS

MARS				
	60NR			
	$PM_{2.5}$		NO_2	
i	c_i	$B_i(\cdot)$	c_i	$B_i(\cdot)$
1	9.0921522	Intercept	24.1888258	Intercept
2	-0.1039223	$\max(0,x_1-23.4757)$	-1.22574	$\max(0,24.6593-x_1)$
3	-0.1289832	$\max(0,56.1789-x_1)$	-0.2701166	$\max(0,x_1-24.6593)$
4	0.1083492	$\max(0,x_1-56.1789)$	0.042974	$\max(0,69.0225-x_2)$
5	-0.1710971	$\max(0,x_1-92.0911)$	0.5483144	$\max(0,x_2-69.0225)$
6	-0.0217847	$\max(0,50.0921-x_2)$	-17.8840408	$\max(0,29.1997-x_3)$
7	0.0538777	$\max(0,x_2-50.0921)$	-25.2079524	$\max(0,x_3-29.1997)$
8	0.0362095	$\max(0,x_2-62.7371)$	2.5181552	$\max(0,10.1248-x_4)$
9	-7.3152284	$\max(0,29.02-x_3)$	-0.0598559	$\max(0,-29.9224-x_5)$
10	1.5009418	$\max(0,x_3-29.02)$	-0.0814862	$\max(0,x_5- -29.9224)$
11	0.2132374	$\max(0,5.05813-x_4)$	-1.1133425	$\max(0,x_6-59.2)$
12	-0.0460445	$\max(0,x_4-5.05813)$	7.5724357	$\max(0,x_6-66.4)$
13	-0.0051891	$\max(0,-13.4998-x_5)$	-5.9893867	$\max(0,x_6-67.1)$
14	-0.0028538	$\max(0,x_5- -13.4998)$	0.3087225	$\max(0,66.6-x_9)$
15	0.0089976	$\max(0,66.8-x_6)$	-0.112624	$\max(0,x_9-66.6)$
16	0.0437147	$\max(0,x_6-66.8)$	0.0414866	$\max(0,431-x_{10})$
17	0.0086899	$\max(0,56.9-x_8)$	0.0124535	$\max(0,x_{10}-431)$
18	-0.0232322	$\max(0,x_8-56.9)$	-0.0537269	$\max(0,278-x_{11})$
19	-0.0200148	$\max(0,59.7-x_9)$	0.0109178	$\max(0,x_{11}-278)$
20	-0.0273413	$\max(0,x_9-59.7)$	-0.1143703	$\max(0,364-x_{12})$
21	-0.0045964	$\max(0,492-x_{12})$	0.0965363	$\max(0,x_{12}-364)$
22	0.01029	$\max(0,x_{12}-492)$	0.1150449	$\max(0,392-x_{13})$
23	-0.0054454	$\max(0,x_{13}-77)$	-0.0476433	$\max(0,x_{13}-392)$
R^2	0.2983778		0.4555687	

Refer to Table 1 for the description of each index x_i

2.4.2.2 MARS Results at 710NR AMS

Similar to the MARS results at 60NR AMS and previous MLR results, all the meteorological parameters are important variables for near-road concentration (note that pressure data were missing for 710NR). For traffic parameters, Table 2.5 shows that the variables of importance are traffic speed on north bound for both postmiles and south bound at postmile B (upstream to AMS) for $PM_{2.5}$. For NO_2, except for traffic speed and volume on south bound at postmile B (upstream to AMS), all other variables are significant. Therefore, it can be seen that the traffic conditions on north bound, where the AMS is directly next to, always play an important role on the near-road pollutant

concentration. The R^2 values are 0.208 and for $PM_{2.5}$ and 0.568 for NO_2. When comparing the MARS results for NO_2, (Table 2.4 & Table 2.5) 710NR has a higher R^2 value than that of 60NR. When comparing the MARS results for $PM_{2.5}$ (Table 2.4 & Table 2.5), the R^2 value for the 60NR is higher than that of 710NR. The comparisons are consistent with what are observed based on the MLR results.

Table 2.5: List of basis functions and the associated coefficients for MARS analysis of $PM_{2.5}$ and NO_2 at 710NR AMS

MARS				
	710NR			
	$PM_{2.5}$		NO_2	
i	c_i	$B_i(\cdot)$	c_i	$B_i(\cdot)$
1	3.5339768	Intercept	39.920506	Intercept
2	-0.1717258	max(0,x_1-15.88)	-1.030523	max(0,24.8391-x_1)
3	-0.2256506	max(0,25.3236-x_1)	-0.240284	max(0,x_1-24.8391)
4	0.1956899	max(0,x_1-25.3236)	0.064362	max(0,65.9905-x_2)
5	-0.0280089	max(0,x_1-53.133)	0.688915	max(0,x_2-65.9905)
6	-0.1765205	max(0,50.5905-x_2)	4.147025	max(0,8.37126-x_4)
7	0.0583893	max(0,x_2-61.6628)	-0.328439	max(0,x_4-8.37126)
8	0.2535048	max(0,7.13817-x_4)	-0.377685	max(0,x_5- -153.471)
9	-0.0304496	max(0,x_4-7.13817)	-0.142004	max(0,-56.5495-x_5)
10	0.0011136	max(0,-21.9842-x_5)	0.469004	max(0,x_5- -56.5495)
11	0.0012321	max(0,x_5- -21.9842)	0.202039	max(0,72.1-x_6)
12	0.0163136	max(0,64-x_6)	3.1205	max(0,x_6-72.1)
13	-0.0246747	max(0,x_6-64)	-0.144614	max(0,59-x_7)
14	-0.0088717	max(0,65.6-x_7)	-0.383335	max(0,x_7-59)
15	-0.0667027	max(0,x_7-65.6)	0.101161	max(0,53.4-x_8)
16	0.021989	max(0,52-x_9)	-0.471667	max(0,x_8-53.4)
17	0.0207513	max(0,x_9-52)	0.906536	max(0,x_8-62)
18	-0.0159023	max(0,77-x_{10})	-0.080821	max(0,145-x_{10})
19	-0.0007464	max(0,x_{10}-77)	-0.022994	max(0,x_{10}-145)
20	0.0105474	max(0,68-x_{11})	0.066911	max(0,236-x_{11})
21	0.0011178	max(0,x_{11}-68)	-0.031861	max(0,325-x_{12})
22	-	-	0.040382	max(0,x_{12}-325)
R^2	0.2078448		0.5677321	

Refer to Table 1 for the description of each index x_i

Figure 2.5 plots the comparison between observed and MARS-modelled NO_2 and $PM_{2.5}$ concentrations for both 60NR and 710NR. Similar with the MLR model, there is a small number of points which stand outside of the point cloud for $PM_{2.5}$. On the other hand, the

cluster of NO_2 points is tighter with less scattered points. The overall prediction performance of MARS is better than that of MLR.

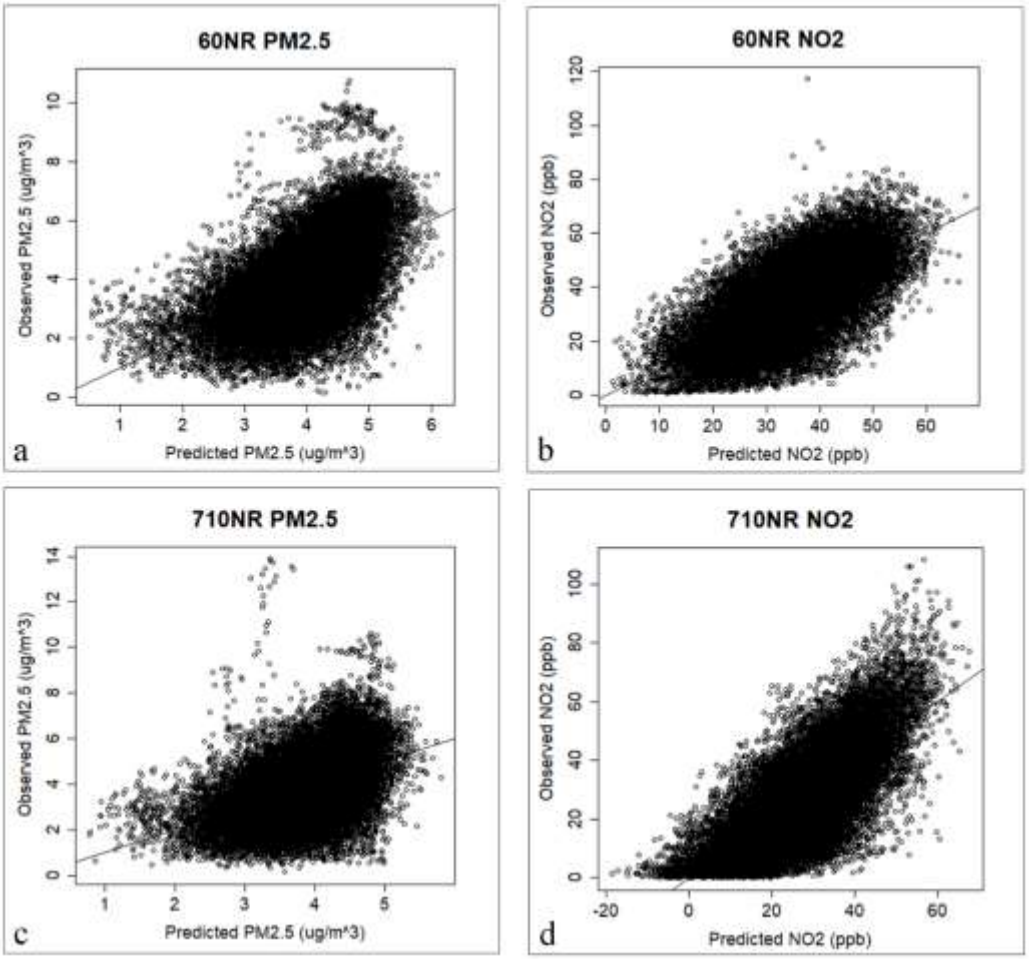

Figure 2.5: Predicted vs. observed graphs using the MARS model (a) 60NR $PM_{2.5}$ (b) 60NR NO_2 (c) 710NR $PM_{2.5}$ (d) 710NR NO_2. The axes for the $PM_{2.5}$ figures (a and c) are raised to the 0.5 due to the Box-cox transformation.

2.5 Conclusions and Future Work

In this study, 13 variables and more than 26,000 rows of data were collected, including weather parameters, traffic speed, and traffic volume near the AMS. The MLR and MARS models were applied to the data to examine the relationship among the weather parameters, traffic data, and near-freeway air pollutant concentration. Both MLR and

MARS shows that all weather parameters (e.g., relative humidity, pressure, temperature, wind) are significant variables. MLR coefficients indicates that for 710NR AMS, the traffic speed on the direction closest to the AMS had up to 13 times larger impact than the speed on the opposite direction. For 60NR AMS, MLR gives the adjusted R^2 as 0.18 and 0.27 for $PM_{2.5}$ and NO_2, respectively, and MARS gives the R^2 as 0.30 and 0.46, respectively. For 710NR AMS, MLR gives the adjusted R^2 as 0.14 and 0.36 for $PM_{2.5}$ and NO_2, respectively, and MARS gives the R^2 as 0.21 and 0.57. Generally, NO_2 concentration can be better explained by the selected variables than $PM_{2.5}$; this could be due to organic $PM_{2.5}$ undergoing gas-particle partitioning as it rapidly dilute and cools in the ambient atmosphere. Many studies have shown that the gas-particle partitioning of the organic $PM_{2.5}$ is important for modelling realistic atmospheric conditions and that a majority of the $PM_{2.5}$ emitted from on-road gasoline vehicles is organic [28,29,30,31].

Suggestions on how to improve the near-road prediction of $PM_{2.5}$ and NO_2 and future work is to include the following: heavy-duty diesel truck flow, near-road carbon dioxide measurements, near-road air quality measurements of $PM_{2.5}$ and other desired air pollutants up- and down-wind of the freeway to investigate the background ambient $PM_{2.5}$ into the models, and accounting for the gas-particle partitioning of the organic $PM_{2.5}$ emitted from on-road gasoline and diesel vehicles. With these suggestions and more near-road air quality data collected, it could help better explain the concentration variations and better predict the near-road air pollutant concentrations in the future.

2.6 Acknowledgements

The authors would like to acknowledge Center for Advancing Research in Transportation Emissions, Energy, and Health (CARTEEH) for funding this research, and SCAQMD for providing air pollution and meteorological data from the monitoring stations. The authors would also like to thank Prof. Heejung Jung for his valuable inputs. The contents of this paper reflect the views of the authors who are responsible for the facts and the accuracy of the data presented herein. The contents do not necessarily reflect the official views of or policy of the sponsor. This paper does not constitute a standard, specification, or regulation.

2.7 References

1. Smit, R., Ntziachristos, L., & Boulter, P. (2010). Validation of road vehicle and traffic emission models - A review and meta-analysis. Atmospheric Environment, 44(25), 2943–2953. https://doi.org/10.1016/j.atmosenv.2010.05.022
2. Zhang, K., Batterman, S., & Dion, F. (2011). Vehicle emissions in congestion: Comparison of work zone, rush hour and free-flow conditions. Atmospheric Environment, 45(11), 1929–1939. https://doi.org/10.1016/j.atmosenv.2011.01.030
3. McCreanor, J., P. Cullinan, M. J. Nieuwenhuijsen, J. Stewart-Evans, E. Malliarou, L. Jarup, R. Harrington, M. Svartengren, I.-K. Han, and P. Ohman-Strickland. Respiratory effects of exposure to diesel traffic in persons with asthma. New England Journal of Medicine, Vol. 357, No. 23, 2007, pp. 2348-2358.
4. McAuley, T. R., and M. Pedroso. Safe Routes to School and Traffic Pollution: Get Children Moving and Reduce Exposure to Unhealthy Air. 2012.

5. Weichenthal, S., M. Hatzopoulou, and M. S. Goldberg. Exposure to traffic-related air pollution during physical activity and acute changes in blood pressure, autonomic and micro-vascular function in women: a cross-over study. Particle and fibre toxicology, Vol. 11, No. 1, 2014, p. 70.
6. Sinharay, R., J. Gong, B. Barratt, P. Ohman-Strickland, S. Ernst, F. J. Kelly, J. J. Zhang, P. Collins, P. Cullinan, and K. F. Chung. Respiratory and cardiovascular responses to walking down a traffic-polluted road compared with walking in a traffic-free area in participants aged 60 years and older with chronic lung or heart disease and age-matched healthy controls: a randomised, crossover study. The Lancet, Vol. 391, No. 10118, 2018, pp. 339-349.
7. Atkinson, R. W., B. Barratt, B. Armstrong, H. R. Anderson, S. D. Beevers, I. S. Mudway, D. Green, R. G. Derwent, P. Wilkinson, and C. Tonne. The impact of the congestion charging scheme on ambient air pollution concentrations in London. Atmospheric environment, Vol. 43, No. 34, 2009, pp. 5493-5500.
8. Invernizzi, G., A. Ruprecht, R. Mazza, C. De Marco, G. Močnik, C. Sioutas, and D. Westerdahl. Measurement of black carbon concentration as an indicator of air quality benefits of traffic restriction policies within the ecopass zone in Milan, Italy. Atmospheric environment, Vol. 45, No. 21, 2011, pp. 3522-3527.
9. Boogaard, H., N. A. Janssen, P. H. Fischer, G. P. Kos, E. P. Weijers, F. R. Cassee, S. C. van der Zee, J. J. de Hartog, K. Meliefste, and M. Wang. Impact of low emission zones and local traffic policies on ambient air pollution concentrations. Science of the total environment, Vol. 435, 2012, pp. 132-140.

10. Karner, A. A., D. S. Eisinger, and D. A. Niemeier. Near-roadway air quality: synthesizing the findings from real-world data. Environmental science & technology, Vol. 44, No. 14, 2010, pp. 5334-5344.
11. Bigazzi, A. Y., and M. A. Figliozzi. Impacts of freeway traffic conditions on in-vehicle exposure to ultrafine particulate matter. Atmospheric environment, Vol. 60, 2012, pp. 495-503.
12. Wang, Y., Y. Zhu, R. Salinas, D. Ramirez, S. Karnae, and K. John. Roadside measurements of ultrafine particles at a busy urban intersection. Journal of the Air & Waste Management Association, Vol. 58, No. 11, 2008, pp. 1449-1457.
13. Kimbrough, S., R. W. Baldauf, G. S. Hagler, R. C. Shores, W. Mitchell, D. A. Whitaker, C. W. Croghan, and D. A. Vallero. Long-term continuous measurement of near-road air pollution in Las Vegas: seasonal variability in traffic emissions impact on local air quality. Air Quality, Atmosphere & Health, Vol. 6, No. 1, 2013, pp. 295-305.
14. Venkatram, A., V. Isakov, E. Thoma, and R. Baldauf. Analysis of air quality data near roadways using a dispersion model. Atmospheric environment, Vol. 41, No. 40, 2007, pp. 9481-9497.
15. Wu, G., P. Hao, L. Pham, H. Jung, and K. Boriboonsomsin. Prediction of real time particulate matter concentrations on highways using traffic information and emission model. 2017.

16. Choudhary, A., and S. Gokhale. Urban real-world driving traffic emissions during interruption and congestion. Transportation Research Part D: Transport and Environment, Vol. 43, 2016, pp. 59-70.
17. South Coast AQMD – Near-roadway Air Monitoring Stations. http://www.aqmd.gov/home/air-quality/air-quality-studies/air-quality-monitoring-studies/near-road-air-network. Accessed July 30, 2018.
18. South Coast AQMD – Annual Air quality monitoring network plan – Ontario SR-60. http://www.aqmd.gov/docs/default-source/clean-air-plans/air-quality-monitoring-network-plan/aaqmnp-ontario-route60-nearroad.pdf?sfvrsn=16. Accessed July 30, 2018.
19. South Coast AQMD – Annual Air quality monitoring network plan – Long Beach I-710. http://www.aqmd.gov/docs/default-source/clean-air-plans/air-quality-monitoring-network-plan/aaqmnp-longbeach710-nearroad.pdf?sfvrsn=16. Accessed July 30, 2018.
20. U.S. EPA, Meteorological Monitoring Guidance for Regulatory Modeling Applications, Feb, 2000. http://www.epa.gov/scram001/guidance/met/mmgrma.pdf. Accessed July 30, 2018.
21. California Department of Transportation Performance Measurement System (PeMS). http://pems.dot.ca.gov/. Accessed July 30, 2018.
22. California Department of Transportation Performance Measurement System (PeMS), Introduction to PeMS Manual & User Guide.

https://pems.ettp.energy.gov/pems/home/pems_user_guide.pdf. Accessed July 30, 2018.

23. Jia, Z., C. Chen, B. Coifman, and P. Varaiya. The PeMS algorithms for accurate, real-time estimates of g-factors and speeds from single-loop detectors. In Intelligent Transportation Systems, 2001. Proceedings. 2001 IEEE, IEEE, 2001. pp. 536-541.
24. Pearson, K. Note on regression and inheritance in the case of two parents. Proceedings of the Royal Society of London, Vol. 58, 1895, pp. 240-242.
25. R Development Core Team - "R: a language and environment for statistical computing". http://www.R-project.org. Accessed July 30, 2018.
26. Wu, G., K. Boriboonsomsin, M. Barth, and R. Tadi. Comparative Analysis of Empirical Capacities between Freeways with Different Types of High-Occupancy Vehicle (HOV) Access Control.
27. Friedman, J. H. Multivariate adaptive regression splines. The annals of statistics, 1991, pp. 1-67.
28. May, A. A., Presto, A. A., Hennigan, C. J., Nguyen, N. T., Gordon, T. D., & Robinson, A. L. (2013a). Gas-particle partitioning of primary organic aerosol emissions: (1) Gasoline vehicle exhaust. Atmospheric Environment, 77, 128–139. https://doi.org/10.1016/j.atmosenv.2013.04.060
29. May, A. A., Presto, A. A., Hennigan, C. J., Nguyen, N. T., Gordon, T. D., & Robinson, A. L. (2013b). Gas-particle partitioning of primary organic aerosol emissions: (2) diesel vehicles. Environmental Science & Technology, 47(15), 8288–8296.

30. Epstein, S. A., Riipinen, I., & Donahue, N. M. (2010). A semiempirical correlation between enthalpy of vaporization and saturation concentration for organic aerosol. Environmental Science and Technology, 44(2), 743–748. https://doi.org/10.1021/es902497z

31. Robinson, A. L., Grieshop, A. P., Donahue, N. M., & Hunt, S. W. (2010). Updating the Conceptual Model for Fine Particle Mass Emissions from Combustion Systems. Journal of the Air & Waste Management Association, 60(10), 1204–1222. https://doi.org/10.3155/1047-3289.60.10.1204

Chapter 3. Improved Prediction of Near-Road Vehicle Emissions for Gasoline and Diesel On-Road Vehicles Between Emission Simulators and Measured Data from PEMS and Laboratory Measurements

Ayla Moretti[1,2], David Cocker III[1,2], Matthew Barth[1,3]

1. Bourns College of Engineering, Center for Environmental Research and Technology (CE-CERT), University of California, 1084 Columbia Avenue, Riverside, California 92507, United States
2. Department of Chemical and Environmental Engineering, Bourns College of Engineering, University of California, Riverside, California 92521, United States
3. Department of Electrical and Computer Engineering, Bourns College of Engineering, University of California, Riverside, California 92521, United States

3.1 Abstract

The gas-particle partitioning of the organic particulate matter ($PM_{2.5}$) is important for modeling realistic atmospheric conditions, with a majority of the $PM_{2.5}$ emitted from on-road gasoline vehicles being volatile organic $PM_{2.5}$. Despite this, emission simulators continue to treat the $PM_{2.5}$ as non-volatile and do not adjust the $PM_{2.5}$ based on the gas-particle partitioning. This leads to emission simulators and atmospheric dispersion models being unable to account for the gas-particle partitioning that occurs to the organic $PM_{2.5}$ emitted from on-road vehicles as emissions rapidly dilute and cool in the ambient atmosphere. A model was developed using published volatility basis set (VBS) data to improve the prediction of near-road $PM_{2.5}$ from on-road gasoline and diesel vehicles. Using the VBS method (method developed in this research), the gas-particle partitioning of OA from on-road gasoline and diesel vehicles were modeled using Python to create a correction factor (CF) that helps bridge the gap between regulatory model estimations and what is measured near-road. Results indicate that, the CF is sensitive to the sampling dilution and temperature (from the PEMS and dynamometers), ambient temperature and background PM, distance from the vehicle, and the vehicles EC/TC ratio, and shows that there is a bias in predicted roadside $PM_{2.5}$ using the current transportation models. Including a correction factor for G/P partitioning will help emission simulators better predict near-road $PM_{2.5}$ as the tailpipe emissions rapidly dilute and cool in the ambient atmosphere.

3.2 Introduction

On-road gasoline and diesel vehicle emissions are a major source of particulate matter ($PM_{2.5}$) in urban areas, with emissions from on-road vehicles having a significant impact on human health and the environment. Many epidemiological studies have shown risk of illness and mortality for drivers and individuals living near busy roadways due to these emissions [1,2], with $PM_{2.5}$ being strongly associated with illness and mortality [3,4]. Two of the main methods researchers currently use to measure vehicle emissions are a dynamometer in series with a constant volume sampler (dilution tunnel) and/or a portable emissions measurement system (PEMS). Dilution tunnels measure vehicle exhaust in the laboratory using a set driving cycle under controlled conditions, whereas the PEMS can either measures on-road emissions under real-world driving conditions or in the laboratory. Using the emission factors (EF) from the PEMS and dilution tunnels, emission simulators can be used to predict near-roadway $PM_{2.5}$ due to on-road vehicles. However, the PEMS and dilution tunnel operate at temperatures and dilution ratios that are not representative of the ambient atmosphere, this can lead to emission simulators being unable to account for the gas-particle partitioning (G/P partitioning) that occurs as the emissions rapidly dilute and cool in the ambient atmosphere.

Many studies have shown that the G/P partitioning of the organic aerosol (OA) is important for modeling realistic atmospheric conditions, and that a majority of the $PM_{2.5}$ emitted from on-road gasoline vehicles (LDGV) is volatile [5,6,7]. For example, May et al. 2013a tested 51 LDGV from the California in-use fleet spanning model years 1987-2012 and found that none of the POA should be considered non-volatile and that the

primary OA (POA) EF measured using the dilution tunnel was often biased high relative to typical atmospheric conditions [5]. May et al. 2013b also found that a majority of the POA from medium-duty and heavy-duty diesel vehicles (HDDV) should not be considered non-volatile [3]. Lastly, Li et al. 2018 used a thermodenuder to determine the volatility of vehicle emitted primary particles, and concluded that ~72% of the particle mass is composed of volatile material that evaporates at 250°C and that the total particle number decreased by 69% in the thermodenuder [6]. Despite these findings, emission simulators such as the U.S. Environmental Protection Agency's Motor Vehicle Emission Simulator (MOVES) continues to treat OA as non-volatile and does not adjust the $PM_{2.5}$ based on the G/P partitioning [8].

G/P partitioning can be predicted through thermodynamic models [7]. Absorption is assumed to be the dominate G/P partitioning mechanism in the atmosphere [5,7], with adsorptive partitioning possibly being important in source-dominated cases such as dilution tunnels [7]. The POA EF (EF_{OA}) can be expressed as (Robinson et al. 2010 & May et al. 2013):

$$EF_{OA} = EF_{tot} \sum_i f_i \left(1 + \frac{C_i^*(T)}{C_{OA}}\right) \quad (3.1)$$

Where EF_{tot} is the total emissions (vapors + particles), f_i is the mass fraction of species i in EF_{tot}, C_i^* is the effective saturation concentration of species i, and C_{OA} is the mass concentration of OA. Equation 3.1 can be used to predict the contribution of organic emissions to ambient $PM_{2.5}$ [7]. A challenge to applying this to vehicle emissions is that the thermodynamic properties of all the emissions must be known. Therefore, the G/P partitioning of the bulk POA can be estimated using a surrogate set of compounds and the

volatility basis set (VBS) [9,10,11,5,7]. The VBS [9,10,11] approach provides a framework for the G/P partitioning: the organic species are organized according to their volatility to investigate the G/P partitioning of the organic vehicle emissions. A detailed explanation of the VBS can be found in Donahue et at. [9,10,11].

Current emission simulators treat all $PM_{2.5}$ as non-volatile and do not account for the additional vehicle emitted $PM_{2.5}$ due to G/P partitioning. This manuscript utilizes the VBS to improve the prediction of EF_{OA} as a function of temperature and dilution ratio, while also accounting for the varying measurement strategies (PEMS vs. dilution tunnel), to provide a correction factor (CF) that can be directly applied to emission simulators to better predict near-road $PM_{2.5}$. The volatility distribution of the organic LDGV and HDDV emissions were used to account for G/P partitioning due to temperature and dilution ratio (DR) changed, enabling the estimation of the CF.

3.3 Methodology

The volatility distribution of the organic aerosol from LDGV and HDDV were obtained using data from May et al 2013ab, respectfully [5,3]. This work used the median volatility distribution corresponding to each $\log(C^*)$ bin. The experimental distribution used here represents the mass fraction of organics from the vehicle exhaust derived from TD-GC-MS analyses of bare-quartz filters [5,3]. An additional set amount was added to the mass fraction corresponding to log(C*) greater than one to account for gases that may also be present in those bins. The addition to the log(C*) bins greater than one were done to make sure that there was enough room for the G/P partitioning, especially at the higher temperatures as seen in the PEMS.

The Clausius Clapeyron equation estimates saturation concentration (C*) as a function of temperature and enthalpy of vaporization (ΔH_v) [12].

$$C^*(T_2) = C^*(T_1) * \exp\left(-\frac{\Delta H_v}{R} * \left(\frac{1}{T_2} - \frac{1}{T_1}\right)\right) \quad (3.2)$$

ΔH_v varies between the different C^* bins, with the lower volatility compounds having higher ΔH_v. ΔH_v was estimated by assuming that all the compounds from the LDGV and HDDV could be represented as n-alkanes ranging from carbon number 10 to 30 to span the $\log_{10}(C^*)$ range of 6 to -2 µg/m^3 at 25°C [9]. Therefore, the ΔH_v was estimated to range from 40 to 160kJ/mole at 25°C [13,14], assuming adequate viscosity such that the gas-particle equilibrium is reached instantly [15]. Using the VBS method and previously published volatility distributions, Python version 3.9 [16] code is created to estimate the CF accounting for the G/P partitioning between the traditional approach used by emission simulators to that of a VBS approach using the EF from the PEMS and dilution tunnel.

3.3.1 Modelled Parameters

The VBS $PM_{2.5}$ loading is a function of temperature and dilution ratio (DR), with DR being defined as the amount of dilute exhaust per amount of undiluted exhaust [17]. For example, if there was two parts of clean air and one part vehicle exhaust that would be a ratio of 2:1 and a DR of 3. The DR and sampling temperature (T_{samp}) for the PEMS was allowed to vary between 2 to 10 and 50°C to 70°C, respectfully for both the LDGV and HDDV, representing operating conditions typical for PEMS measurements [18,19]. The dilution tunnel used a T_{samp} that varied between 42°C to 52°C, since federal regulations

requires that samples be collected at 47±5°C [7,20]; and a DR that varied between 7 to 30 and 6 to 30 for LDGV and HDDV, respectfully.

Tailpipe elemental carbon varied between 0 μg/m^3 to 1,000,000 μg/m^3, to capture a range of organic carbon to elemental carbon (OC:EC) ratios from 1:0 to 0:1. The OC was obtained through the VBS modeled Python code, and total carbon (TC) is the sum of the EC and OC. An EC/TC value of zero describes $PM_{2.5}$ that is entirely OC whereas an EC/TC value of one describes $PM_{2.5}$ that is entirely EC. The ambient temperature (T_{amb}) and background ambient $PM_{2.5}$ were also varied; T_{amb} was varied from 0°C to 40°C and ambient background OC (OC_{amb}) and EC (EC_{amb}) varied between 0 μg/m^3 to 10 μg/m^3 and 0 μg/m^3 to 1 μg/m^3, respectively, to simulate a pristine to polluted urban environment.

To assist current emission simulators in accurately accounting for the G/P partitioning of the OA emitted from on-road vehicles, a correction factor (CF) was developed by taking the ratio of the predicted near-road $PM_{2.5}$ from the method developed in this manuscript (accounting for G/P partitioning using VBS method) to the traditional methods used by emission simulators assuming all species are conservative (traditional approach). The CF was calculated by using Equation 3.3:

$$CF = \frac{TC_{VBS}}{TC_{DRsamp}} * \frac{DR_{samp}}{DR_{tot}} \quad (3.3)$$

Where TC_{VBS} is the predict-near road total carbon (TC) from the method developed in this manuscript, TC_{DRsamp} is the TC predicted by the PEMS or dilution tunnel at the sampling DR, DR_{tot} is the total DR, and DR_{samp} is the sampling DR of the PEMS or dilution tunnel.

3.4 Results & Discussion

A sample correction factor heat map showing the ratio in estimated $PM_{2.5}$ when accounting for G/P partitioning to not accounting for G/P partitioning, is shown (Figure 3.1) for a LDGV whose emissions were sampled using a PEMS with a T_{samp} of 60ºC and at DR varying between 2 to 10.

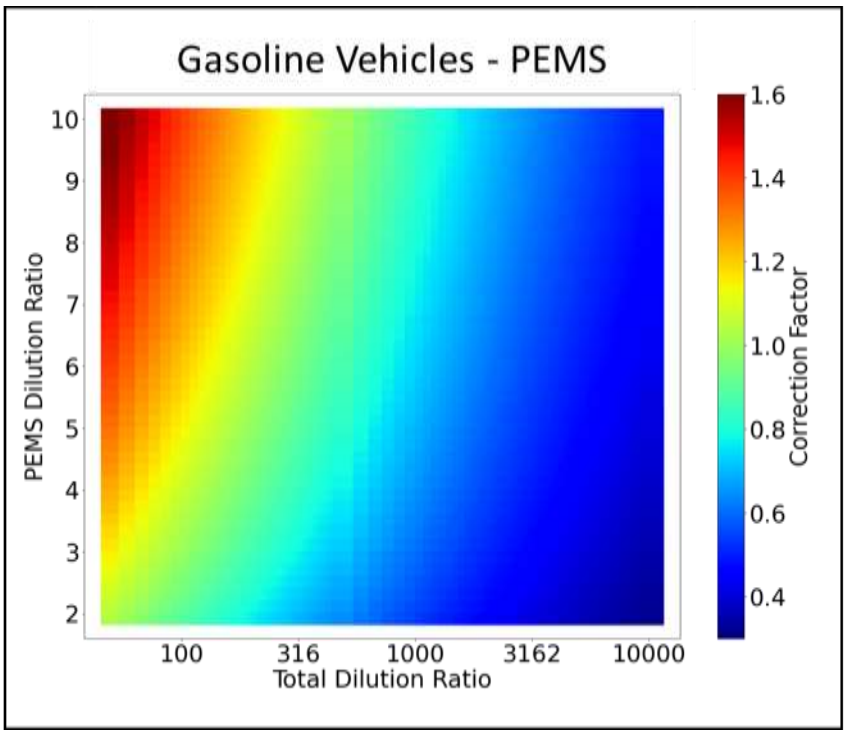

Figure 3.1: Correction factor sensitivity for a LDGV emission captured using a PEMS at a sampling temperature of 60ºC with a varying sampling DR assuming an ambient temperature of 25ºC.

In this (Figure 3.1) and the following heat maps (Figure 3.2-Figure 3.5), a correction factor (color bar value) greater than one means that the traditional approach underestimates predicted near-road $PM_{2.5}$; a value of one means the traditional approach and VBS method agree; and a CF value less than one means that the traditional approach overestimates predicted near-road $PM_{2.5}$.

The following sections explore G/P partitioning corrections as a function of sampling conditions, environmental parameters, and EC-OC composition.

3.4.1 Sampling Conditions

G/P partitioning is a function of measurement and ambient temperature (equation 2). To explore the sensitivity of CF to measurement temperature, the CF with varying T_{samp} were investigated (Figure 3.2). Figure 3.2a shows CF for a LDGV sampled with a PEMS with a DR_{samp} of 3 and T_{amb} of 25°C when the T_{samp} varies between 60°C $\pm$ 10°C. In Figure 3.2a at lowest DR_{tot} and the highest T_{samp} the CF tends to be above 1, however, as the T_{samp} is lowered and the DR_{tot} increases the CF drops below 1. Increasing the DR_{samp} to 10 (Figure 3.2b) and holding all other simulation conditions constant the CF followed a similar trend with the main differences between the two figures being the CF scale. In Figure 3.2b the CF increases to 2.25 (compared to 1.6 in Figure 3.2a) indicating that the higher DR_{samp} the larger the required CF; however, the CF decreases to 0.5 (compared to 0.4 in Figure 3.2a). In Figure 3.2b the effect of the vapor pressure (P^{vap}) is greater than that of the dilution with respect to CF.

Similar trends are observed for the dilution tunnel varying the T_{samp} between 47°C $\pm$ 5°C (Figure 3.1c-Figure 3.1d) with the CF closer to 1 for the dilution tunnel compared with the PEMS. The dilution tunnel has CF closer to 1 due to the lower T_{samp} and higher DR_{samp} that the dilution tunnel is generally operated at. Comparing Figure 3.2b and Figure 3.2c both are at a DR_{samp} of 10 but have different T_{samp}, the CF ranges from 1.2 to 0.4 in Figure 3.2c (compared to 2.25 to 0.5 in Figure 3.2b). This again shows the effect of P^{vap}, and how decreasing the T_{samp} decreases the P^{vap} leading to a CF closer to 1. Increasing the

dilution tunnel DR_{samp} increases the CF (compared to Figure 3.2c) also consistent with the fact that the effect of P^{vap} is greater than that of the dilution. However, when comparing Figure 3.2b and Figure 3.2d, Figure 3.2d shows how increasing the DR_{samp} while also decreasing the T_{samp} results in evaporation starting to overcome condensation resulting in a CF closer to 1.

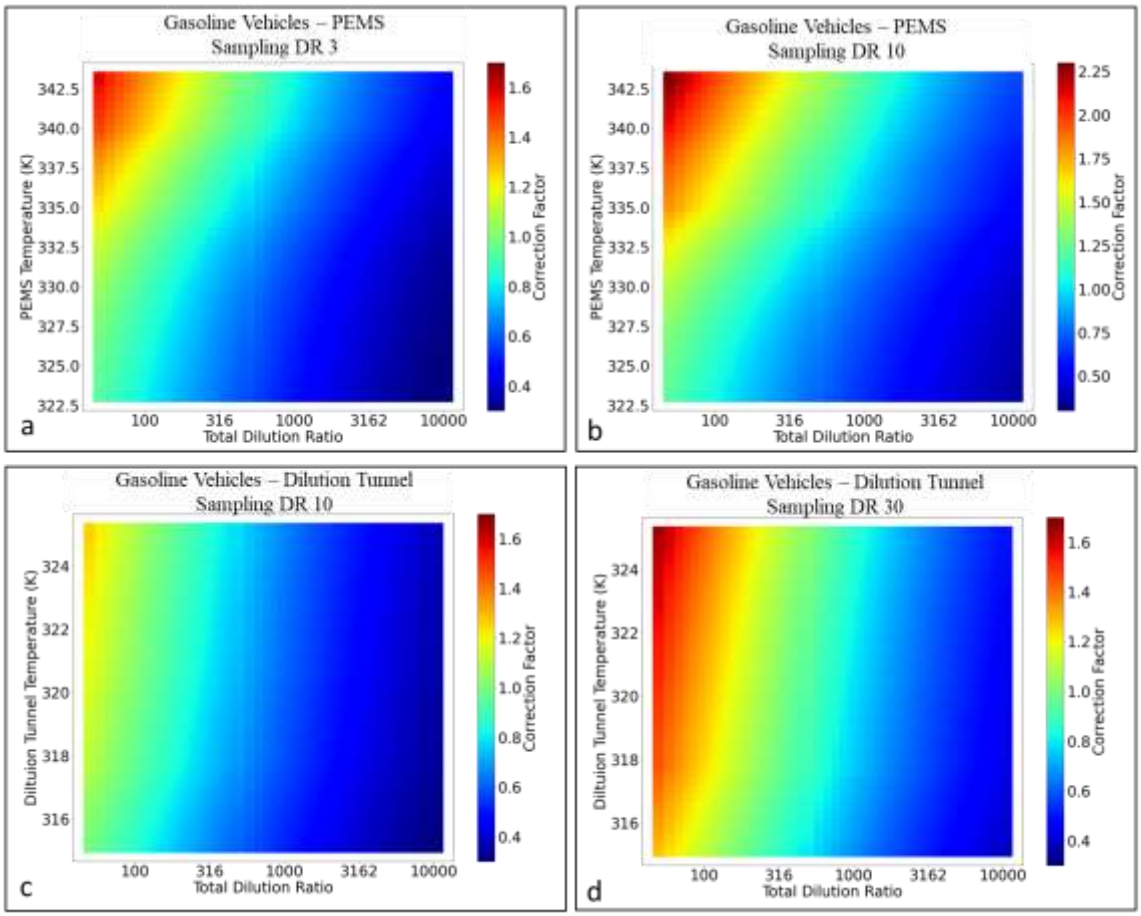

Figure 3.2: Correction factor (CF) sensitivity to varying the sampling temperatures for a LDGV sampled from a PEMS and dilution tunnel obtained from a modelling VBS method, assuming an ambient temperature of 25ºC. a) CF for PEMS results with a sampling DR of 3; b) CF for PEMS results with a sampling DR of 10; c) CF for dilution tunnel results with a sampling DR of 10; d) CF for dilution tunnel results with a sampling DR of 30.

The HDDVs, when all things are held equal, have the same general trends for CF; the heat maps showing the sensitivity of the CF with varying T_{samp} are found in SI Figure

3.1. The initial hypothesis was that the HDDV would have a CF closer to 1 due to HDDV typically having a higher EC/TC ratio resulting in less volatile PM. A comparison between the HDDV and LDGV to investigate the CF sensitivity (holding all sampling conditions constant, including the initial reactive organic gases emitted from the vehicle) and varying only the EC/TC ratio was performed (SI Figure 3.2-3.3). The HDDV was found to have CFs further away from one, when compared to the LDGV. This is attrinted to the HDDV, when compared to the LDGV, having a larger mass fraction in the 0 to 2 log(C*) bins (May et al. 2013ab). These are the bins most sensitive to G/P partitioning for the ambient conditions studied. The DR_{samp} also impacts CF and will be vetted in the following section.

3.4.2 Environmental parameters

G/P partitioning is a function of suspended organic aerosol mass concentration, which is dictated by the plume dilution and ambient background OC (OC_{amb}). Further, ambient background EC (EC_{amb}) affects the CF by averaging the CF towards 1 since the traditional approach predicts total $PM_{2.5}$ and correctly accounts for emitted EC. Therefore, it is needed to quantify the CF for a variety of ambient conditions from pristine to polluted. The sensitivity of the CF with and without OC_{amb} and EC_{amb} concentrations is explored (Figure 3.3).

Figure 3.3a shows the CF needed for a LDGV whose emissions were captured using a PEMS at a T_{samp} of 60^{o}C and DR varying between 2 to 10, T_{amb} of 25°C, and no OC_{amb} and EC_{amb}. In Figure 3.3a at the lowest DR_{tot} the CF is above 1; however, as the DR_{tot} increases past 100 to 360 (depending on DR_{samp}) the CF drops below 1. The CF below 1 is a result of the OA concentration becoming sufficiently low resulting in the evaporation of

the OA dominating over condensation. Simulations of the CF for more polluted atmospheres, with background OC_{amb} (10 µg/m3) and EC_{amb} (1 µg/m^3) concentrations (Figure 3.3b), holding all other simulation conditions the same followed similar trends to pristine ambient atmosphere. The CF is above 1 for the at the lowest DR_{tot} then drops below 1 as the DR_{tot} increases (Figure 3.3b). The difference between the pristine and polluted atmospheres is in the CF in the more polluted atmosphere only approaches 1 at the highest DR_{tot}, whereas in the pristine atmosphere the CF continues to drop. This is due to the background $PM_{2.5}$ concentrations starting to dominate the OC pool available for G/P partitioning making the difference between the VBS method and traditional approach negligible. Similar trends are observed for the dilution tunnel (Figure 3.3c-Figure 3.3d) with the CF closer to 1 for emissions developed from dilution tunnels than developed from PEMS. The CF is closer to 1, in these scenarios, due to the dilution tunnel operating at lower temperatures and generally higher DR than the PEMS, explained in detail in the Sampling Conditions section above.

The blue "parabolic" coloration with background $PM_{2.5}$ (Figure 3.3b and Figure 3.3d) highlights the non-linearity of the response of P^{vap} versus DR. This coloration occurs when the effects of P^{vap} is much greater than those of dilution and shows why it is important to account for the G/P partitioning when predicting near-road $PM_{2.5}$.

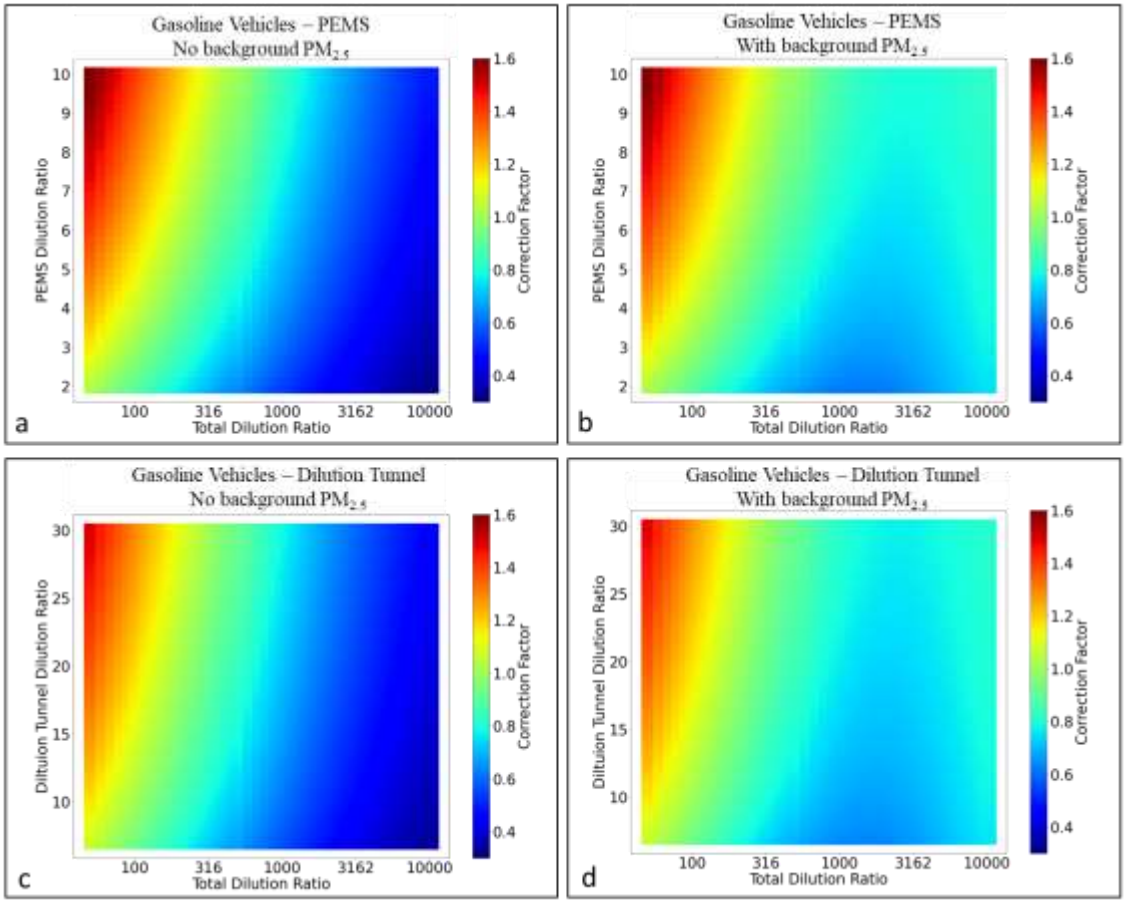

Figure 3.3: Correction factor (CF) sensitivity looking at with and without OC_{amb} and EC_{amb} concentrations for a LDGV sampled from a PEMS and dilution tunnel obtained from a modelling VBS method, assuming an ambient temperature of 25ºC and sampling temperature for the PEMS and dilution tunnel at 60ºC and 47ºC, respectfully. a) CF for PEMS results assuming no OC_{amb} and EC_{amb} concentrations; b) CF for PEMS results assuming background OC_{amb} (10 µg/m3) and EC_{amb} (1 µg/m3) concentrations; c) CF for dilution tunnel results assuming no OC_{amb} and EC_{amb} concentrations; d) CF for dilution tunnel results assuming background OC_{amb} (10 µg/m3) and EC_{amb} (1 µg/m3) concentrations.

G/P partitioning is also a strong function of T_{amb} (equation 2). To explore this, the effects of varying the T_{amb} on CF were investigated (Figure 3.4). The CF for T_{amb} of 0ºC (Figure 3.4a), 25ºC (Figure 3.4b), and 40ºC (Figure 3.4c) for a LDGV emissions sampled using a PEMS at a T_{samp} of 60ºC and a background OC_{amb} (10 µg/m3) and EC_{amb} (1 µg/m^3) concentrations, indicate a large range of CF (0.4 to 4.0) for changes in T_{amb} (0ºC to 40ºC). For colder T_{amb}, the CF ranges from 1.4 to 4.0; but, as T_{amb} increases the CF begins to lower

past 1. This is due to greater evaporation, which leads to lower OC concentration with increasing T_{amb}.

Similar results (Figure 3.4d-Figure 3.4f) are observed for the dilution tunnel with a T_{samp} of 47°C assuming background OC_{amb} (10 µg/m3) and EC_{amb} (1 µg/m^3) concentrations, with the CF closer to 1 for EF developed from dilution tunnel measurements than PEMS based measurements. This difference is due to the DR_{samp} and T_{samp} differences between the PEMS and dilution tunnel, explained in detail in the Sampling Conditions section above.

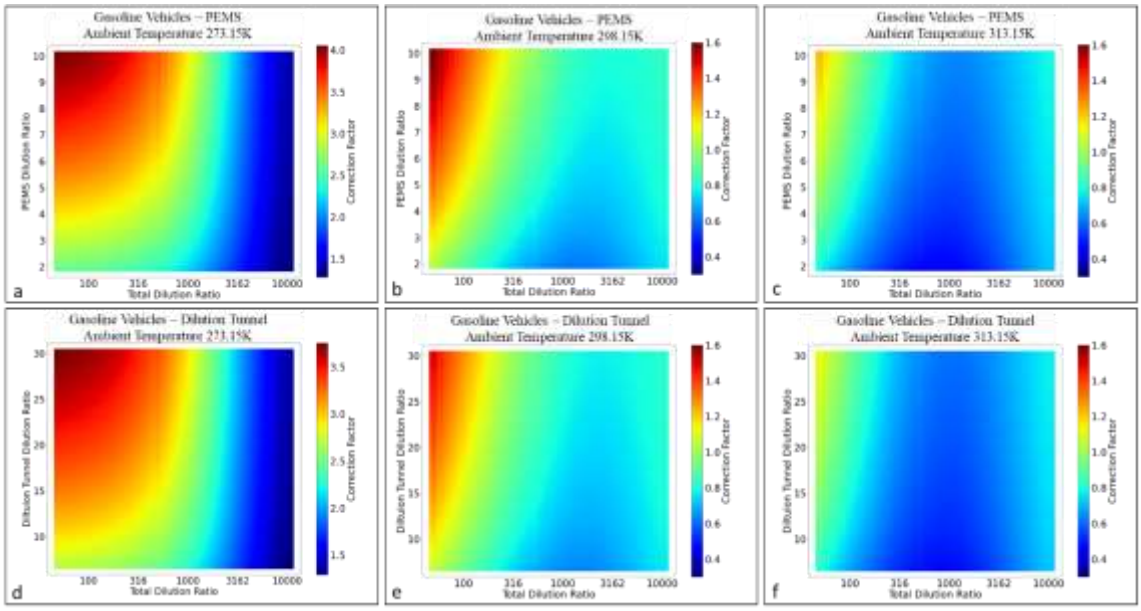

Figure 3.4: Correction factor (CF) sensitivity to ambient temperatures with background OC_{amb} (10 µg/m3) and EC_{amb} (1 µg/m3) concentrations for a LDGV sampled from a PEMS and dilution tunnel obtained from a modelling VBS method, assuming sampling temperature for the PEMS and dilution tunnel at 60°C and 47°C, respectfully. a) CF for a PEMS at 0°C; b) CF for PEMS at 25°C; c) CF for PEMS at 40°C; d) CF for dilution tunnel at 0°C; e) CF for dilution tunnel at 25°C; f) CF for dilution tunnel at 40°C.

HDDV have similar trends with the heat maps showing the sensitivity to the diesel CF to background ambient $PM_{2.5}$ and varying T_{amb} (SI Figures 3.4-3.5).

3.4.3 Composition

With changing vehicle technology, aftertreatments, engine ages, and fuel blends the relative amount of the vehicle's EC/OC will vary. To explore this, the effects of the vehicle's EC/TC ratio on the sensitivity of the CF was investigated (Figure 3.5). EC is a non-volatile conservative species, therefore closer to pure EC (EC/TC = 1) the less important G/P partitioning is.

Figure 3.5a shows the sensitivity of the CF for a LDGV sampled using a PEMS with a T_{samp} of 60°C and a DR_{samp} of 3 assuming an T_{amb} of 25°C and a background OC_{amb} (10 µg/m3) and EC_{amb} (1 µg/m^3) while varying the vehicle's EC/TC ratio from 0 to 1. At the lowest EC/TC ratios and when the DR_{tot} is below ~100 the CF is above 1; however, as the DR_{tot} increases further the CF starts to drop below 1. For all DR_{tot} when the EC/TC ratio is greater than ~0.6 the CF is at or around 1. This is due to $PM_{2.5}$ having a larger EC/TC ratio, with EC being a non-volatile species the effect of the G/P partitioning is less important than when the EC/TC ratio is lower.

Increasing the DR_{samp} to 10 (Figure 3.5b) and holding all other simulation conditions constant, similar results are observed as for the DR_{samp} of 10. The CF has the largest deviation from 1 at the lowest EC/TC ratios and approaches 1 as the EC/TC ratio approaches 1. When the DR_{samp} is increased to 10, the CF is only above 1 when closest to the vehicle (DR_{tot} less than ~300) with almost all DR_{tot} greater than ~300 leading to a CF below 1.The dilution tunnel also has similar trends as the PEMS (Figure 3.5c-Figure 3.5d), with the CF generally being closer to 1, especially when the DR_{samp} is highest. The

difference, between the PEMS and dilution tunnel, is due to the DR_{samp} and T_{samp} differences, which is explained in detail in the Sampling Conditions section above.

The initial amount of hydrocarbon (HC_i) can affect which species can be present in the particle-phase. The sensitivity of the CF to HC_i is shown in SI Figure 3.6; holding all sampling conditions the same as in Figure 3.5 with just the HC_i reduced by a factor of 10. Decreasing the HC_i by a factor of 10 impacts the realtive ratio of the emitted OC to the OC_{amb} resulting in the OC_{amb} having a larger relative impact. This results in a smaller amount of OC available for the G/P partitioining resuling in the CF generally being closer to 1 for these LDGV scenarios (SI Figure 3.6).

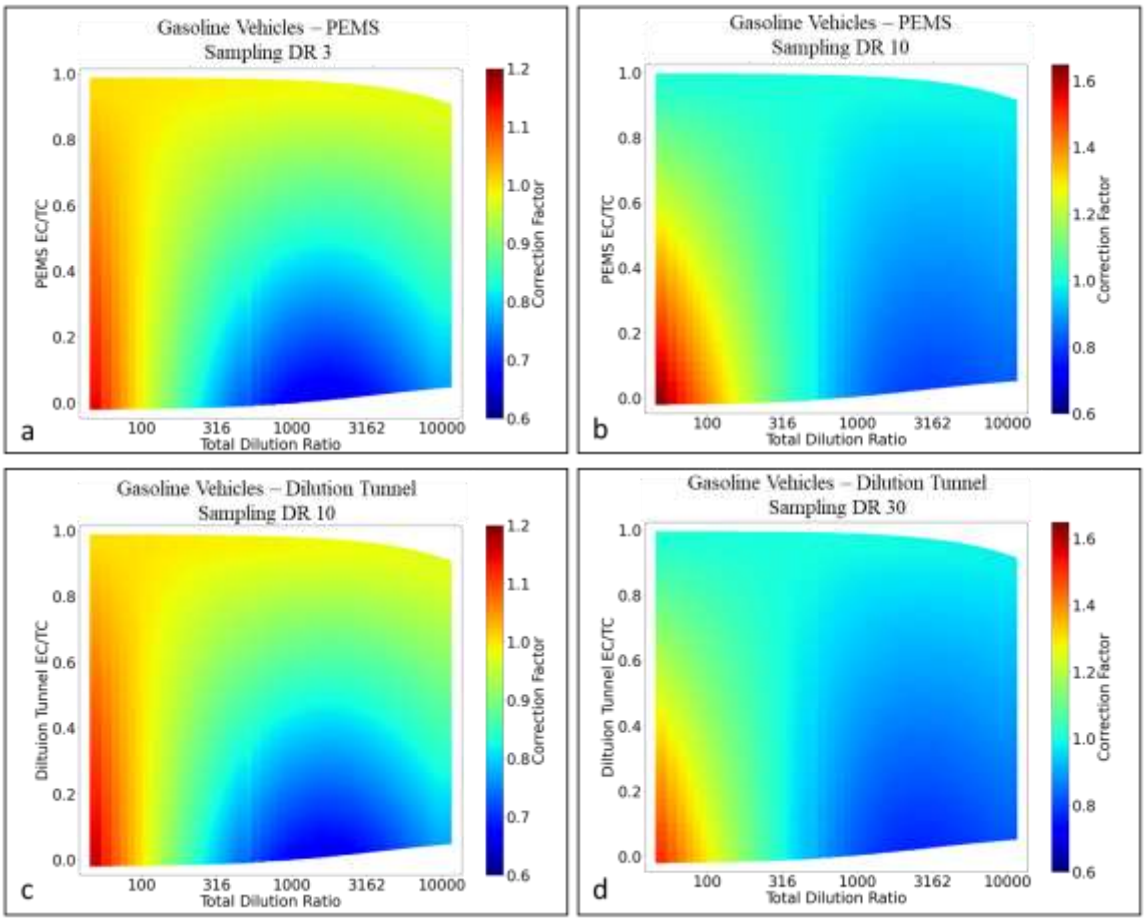

Figure 3.5: Correction factor (CF) sensitivity to a vehicle's EC/TC ratio with background OC_{amb} (10 µg/m3) and EC_{amb} (1 µg/m3) concentrations for a LDGV sampled from a PEMS and dilution tunnel obtained from a modelling VBS method, assuming an ambient temperature of 25ºC and sampling temperature for the PEMS and dilution tunnel at 60ºC and 47ºC, respectfully. a) CF for a PEMS at a DR_{samp} of 3; b) CF for PEMS a DR_{samp} of 10; c) CF for dilution tunnel a DR_{samp} of 10; d) CF for dilution tunnel at a DR_{samp} of 30.

3.4.3.1 Percentage of Organic Carbon evaporated

The percentage of OC evaporated (%OC evaporated) is a function of dilution and suspended OA mass concentration (emitted OA + OC_{amb}). As the %OC evaporated changes so does the composition and species of the $PM_{2.5}$ present. The composition is important because it may dictate the potential toxicity per gram as well as affect the light refraction, hygroscapicity of the particles and more. The additional %OC evaporated

between the VBS method and traditional approach shows how the G/P partitioning could affect the composition of the particles (Figure 3.6).

Figure 3.6a show the additional %OC evaporated for LDGV sampled from a PEMS with a T_{samp} of 60^{o}C and a background OC_{amb} (10 µg/m3) and EC_{amb} (1 µg/m^3) concentrations assuming an T_{amb} of 25^{o}C. At the lowest DR_{tot} the traditional approach is overestimating the amount of %OC evaporated (negative color bar values) and as the DR_{tot} increases the traditional approach starts to underestimate the %OC evaporated (positive values); these results are in agreement with what were observed in Figure 3.3b. Similar results are observed for a dilution tunnel with a T_{samp} of 47^{o}C holding all ambient parameters constant (Figure 3.6b), with the %OC evaporated being closer to zero for the dilution tunnel. The differences observed between the PEMS, and dilution tunnel is explained in detail in the Sampling Conditions section.

The additional vehicle %OC evaporated due to the VBS method were also investigated (SI Figure 3.7) by subtracting out the background $PM_{2.5}$ and holding all other sampling conditions the same as in Figure 3.6. SI Figure 3.7 shows similar trends to Figure 3.6; however, when only considering the additional vehicle %OC evaporated the %OC evaporated ranges from -60% to 60% (compared to -60% to 30% in Figure 3.6). The higher upper bound (60%) in SI Figure 3.7 implies that when only accounting for the additional vehicle %OC evaporated the traditional approach will have a larger overestimation of the predicted near-road $PM_{2.5}$ at the largest DR_{tot}. This is due to inaccuracies in accounting for the additional evaporated OA (dilution) and not considering the OC_{amb}, both of which are parameters in G/P partitioning.

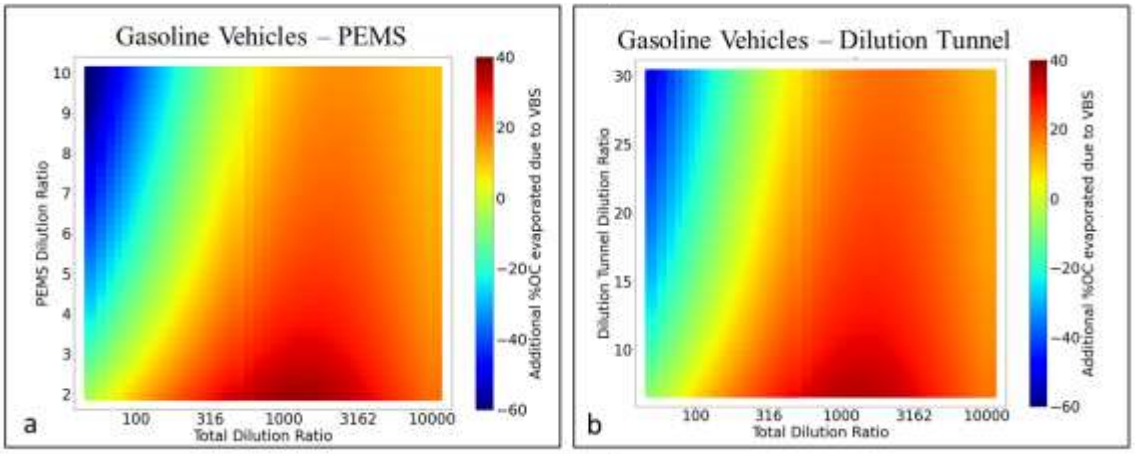

Figure 3.6: Additional %OC evaporated between the VBS method and traditional approach sensitivity to the sampling DR with background OC_{amb} (10 µg/m3) and EC_{amb} (1 µg/m3) concentrations for a LDGV sampled from a PEMS and dilution tunnel obtained from a modelling VBS method, assuming an ambient temperature of 25ºC and sampling temperature for the PEMS and dilution tunnel at 60ºC and 47ºC, respectfully. a) additional %OC evaporated for a PEMS; b) additional %OC evaporated for a dilution tunnel

As the temperature and dilution changes the species present can also change leading to potential health implications. To explore this, the emitted EC/TC ratio based on DR_{samp} was investigated (Figure 3.7). Predicted near-road $PM_{2.5}$ for a LDGV whose emissions were sampled using a PEMS (Figure 3.7a) assuming a T_{samp} of 60ºC, near-road ambient (Figure 3.7b) and dilution tunnel (Figure 3.7c) assuming a T_{samp} of 47ºC. All subfigures assumed an initial undiluted tailpipe EC of 1,000 µg/m^3, an T_{amb} of 25ºC, and a background OC_{amb} (10 µg/m3) and EC_{amb} (1 µg/m^3) concentrations. Figure 3.7 shows that the $PM_{2.5}$ collected on filters from the PEMS, and dilution tunnel have different EC/TC ratio than that of ambient. The different EC/TC ratios have different species present in the PEMS, dilution tunnel and ambient conditions. This could imply that the $PM_{2.5}$ toxicity per mass, a function of organic content, increases with the decreasing EC/TC ratio resulting in health implications--future works needs to be done to look more into this.

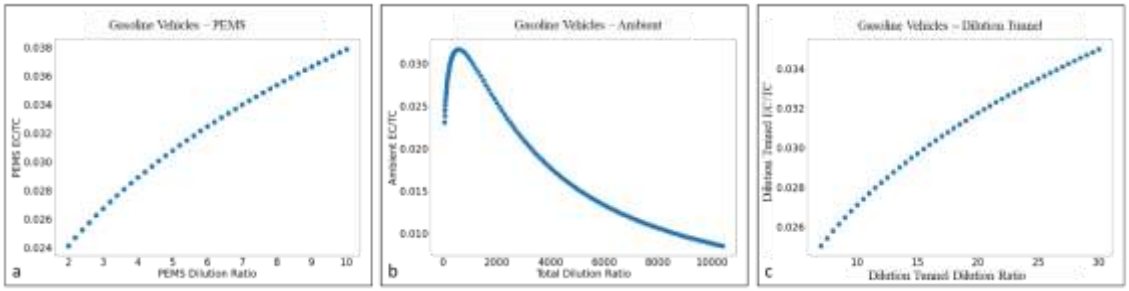

Figure 3.7: EC/TC variation between the VBS method and traditional approach sensitivity to the sampling DR with background OC_{amb} (10 µg/m3) and EC_{amb} (1 µg/m3) concentrations for a LDGV sampled from a PEMS and dilution tunnel obtained from a modelling VBS method, assuming an ambient temperature of 25ºC and sampling temperature for the PEMS and dilution tunnel at 60ºC and 47ºC, respectfully. a) PEMS using the traditional approach; b) near-road using the VBS method; c) dilution tunnel using the traditional approach.

HDDVs exhibited similar trends when looking at how composition affects the CF, %OC evaporated and the EC/TC variation between the PEMS, dilution tunnel and ambient, the diesel figures can be seen in SI Figures 3.8-3.11.

3.5 Conclusion

Many studies have shown that the G/P partitioning of the OA is important for modeling realistic atmospheric conditions and that a majority of the $PM_{2.5}$ emitted from LDGV and HDDV is volatile OA [3,5,6,7]. G/P partitioning is a function of temperature, dilution ratio, and suspended organic aerosol mass concentration.

The T_{amb} and DR_{tot} had the largest impact on the correction factor. When T_{amb} is at 0ºC the CF is always above 1 with a maximum around 4, and when the T_{amb} is at 40ºC the CF is always below 1. Generally, the CF is above 1 at the lowest DRtot and drops below 1 as the DRtot increases. However, when assuming a background OC_{amb} (10 µg/m3) and EC_{amb} (1 µg/m3) concentrations the CF approaches 1 at the highest DR_{tot}, as the background $PM_{2.5}$ concentrations start to dominate and making the difference between the VBS method and traditional approach negligible.

The vehicle's EC/TC ratio also impacts the CF. When the EC/TC ratio is closest to 0 the CF has the largest divergence from 1 whereas when the EC/TC ratio approaches 1 so does the CF. This is due to the traditional approach inaccurately accounting for OC evaporated as the emissions dilute and cool in the ambient atmosphere. The CF is also sensitive to the sampling temperature with the CF greater than 1 at the highest T_{samp}.

When comparing the results from emission factors developed using PEMS measurements to that of the dilution tunnel, the results indicate that generally the emission factors developed using dilution tunnel had CF values closer to one. This manuscript provides a range of these variations and can be used to better estimate the near-road PM estimation. HDDV, when environmental and sampling parameters are held constant, were observed to have similar trends with the CF typically be further from 1 for the PEMS and dilution tunnel, when compared to LDGV, SI Figures 3.1–3.7. This was due to the HDDV having a larger mass fraction in the 0 to 2 log(C*) bins, which are the bin sin the VBS which are most affected by the G/P partitioning for the ambient $PM_{2.5}$ loadings studied.

Overall, these results show that there is a bias in predicted roadside $PM_{2.5}$ using current transportation models. Including a correction factor would help emission simulators better predict near-road $PM_{2.5}$ by accounting for the G/P partitioning that occurs as the emissions rapidly dilute and cool in the ambient atmosphere.

3.6 Acknowledgments

This study was funded, by a grant from the National Center for Sustainable Transportation (NCST), supported by the U.S. Department of Transportation (USDOT) through the University Transportation Centers program. The authors would like to thank

the NCST and the USDOT for their support of university-based research in transportation, and especially for the funding provided in support of this project.

3.7 Appendix 3A. Supporting Information

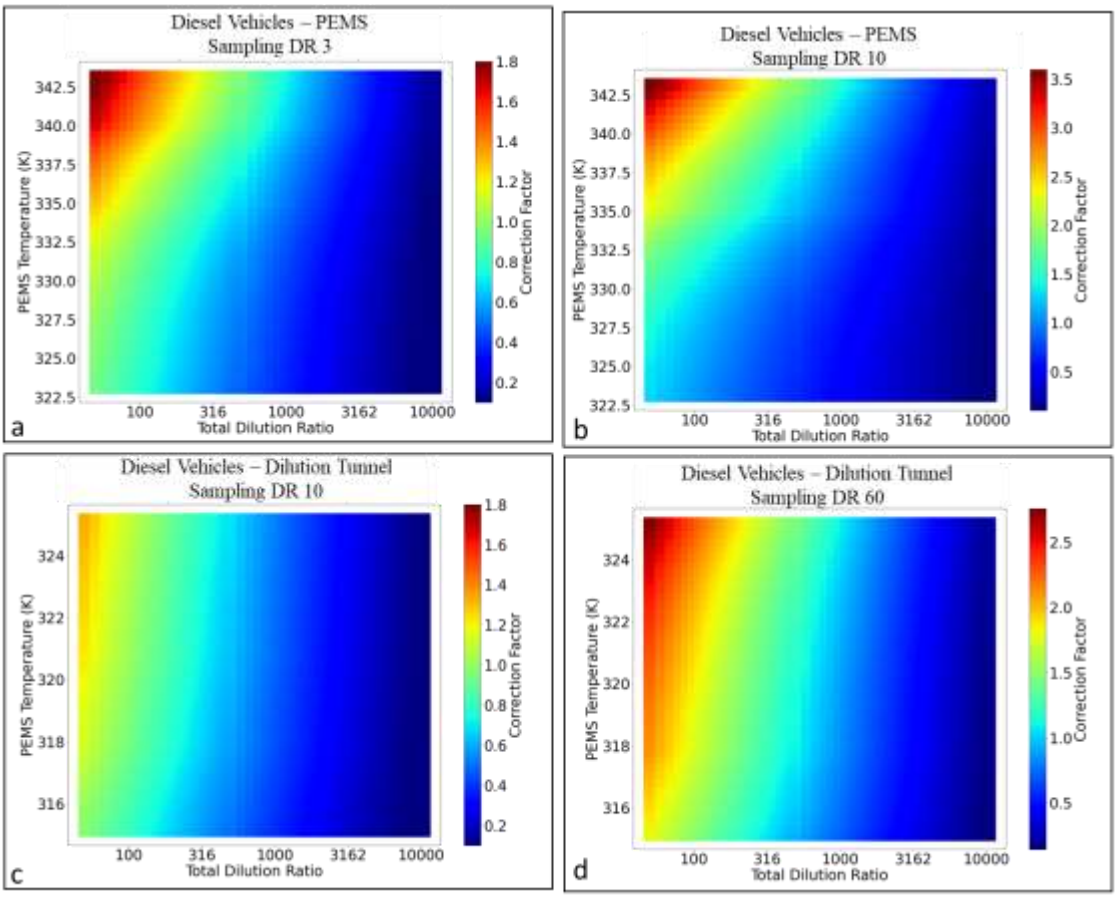

SI Figure 3.1: Correction factor (CF) sensitivity to varying the sampling temperatures for a diesel vehicle sampled from a PEMS and dilution tunnel obtained from a modelling VBS method, assuming an ambient temperature of 25ºC. a) CF for PEMS results with a sampling DR of 3; b) CF for PEMS results with a sampling DR of 10; c) CF for dilution tunnel results with a sampling DR of 10; d) CF for dilution tunnel results with a sampling DR of 60.

The comparison between the correction factor (CF) between the Light-Duty Gasoline Vehicle (LDGV) and Heavy-Duty Diesel Vehicle (HDDV) holding all simulation conditions constant are shown for emissions captured from a PEMS and dilution tunnel, SI Figure 3.2 and SI Figure 3.3, respectfully. The PEMS was operated at a DR_{samp} of 3 and

T_{samp} of 60ºC with an ambient temperature of 21ºC and background OC_{amb} (10µg/m^3) and EC_{amb} (1µg/m^3) concentrations (SI Figure 3.2). The dilution tunnel was operated at a DR_{samp} of 11 and T_{samp} of 47ºC with an ambient temperature of 21ºC and background OC_{amb} (10µg/m^3) and EC_{amb} (1µg/m^3) concentrations (SI Figure 3.3).

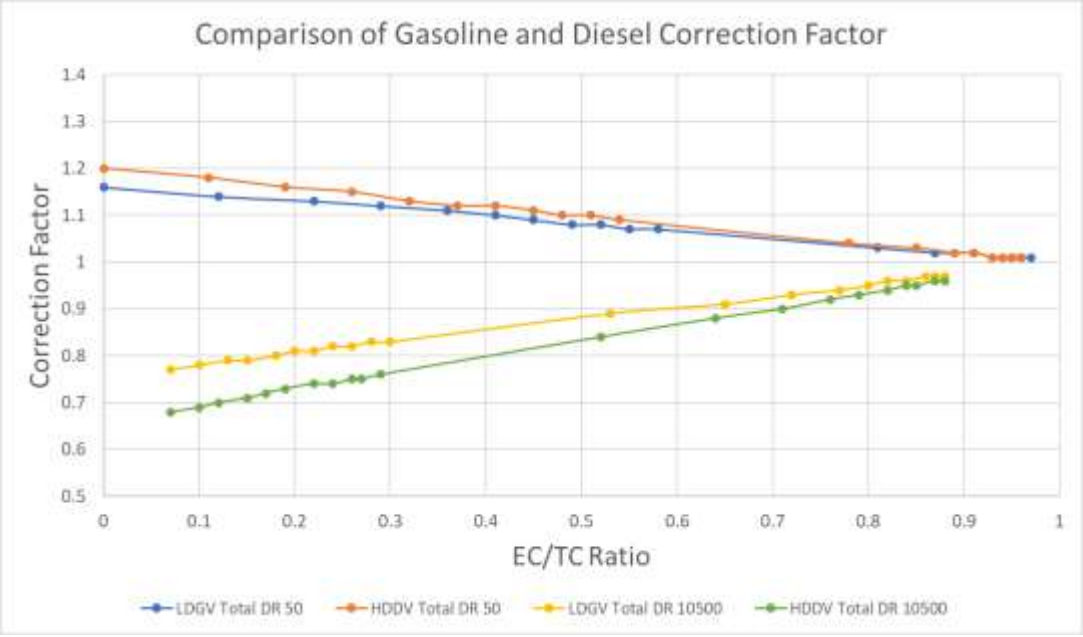

SI Figure 3.2: Correction factor (CF) comparison between a gasoline and diesel vehicle at two different DR_{tot}. Sampled from a PEMS with a DR of 3 and T_{samp} of 60C. Assuming an T_{amb} of 21C and background OC_{amb} (10 µg/m3) and EC_{amb} (1 µg/m3) concentrations and same initial HC in µg/m^3.

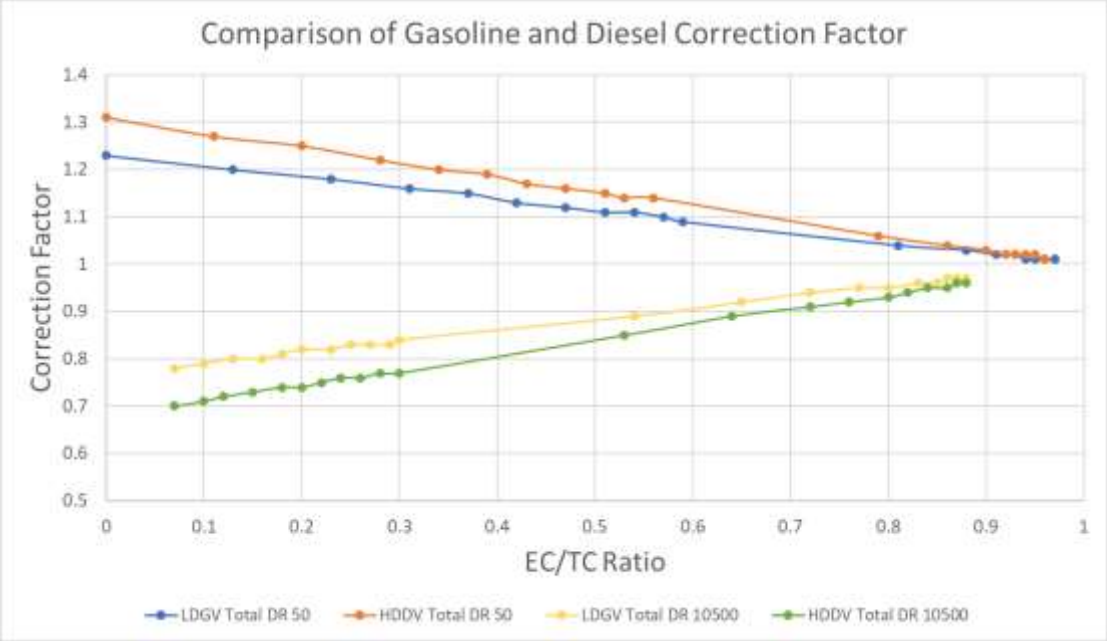

SI Figure 3.3: Correction factor (CF) comparison between a gasoline and diesel vehicle at two different DR_{tot}. Sampled from a dilution tunnel with a DR of 11 and T_{samp} of 47C. Assuming an T_{amb} of 21C and background OC_{amb} (10 µg/m3) and EC_{amb} (1 µg/m3) concentrations and same initial HC in µg/m^3.

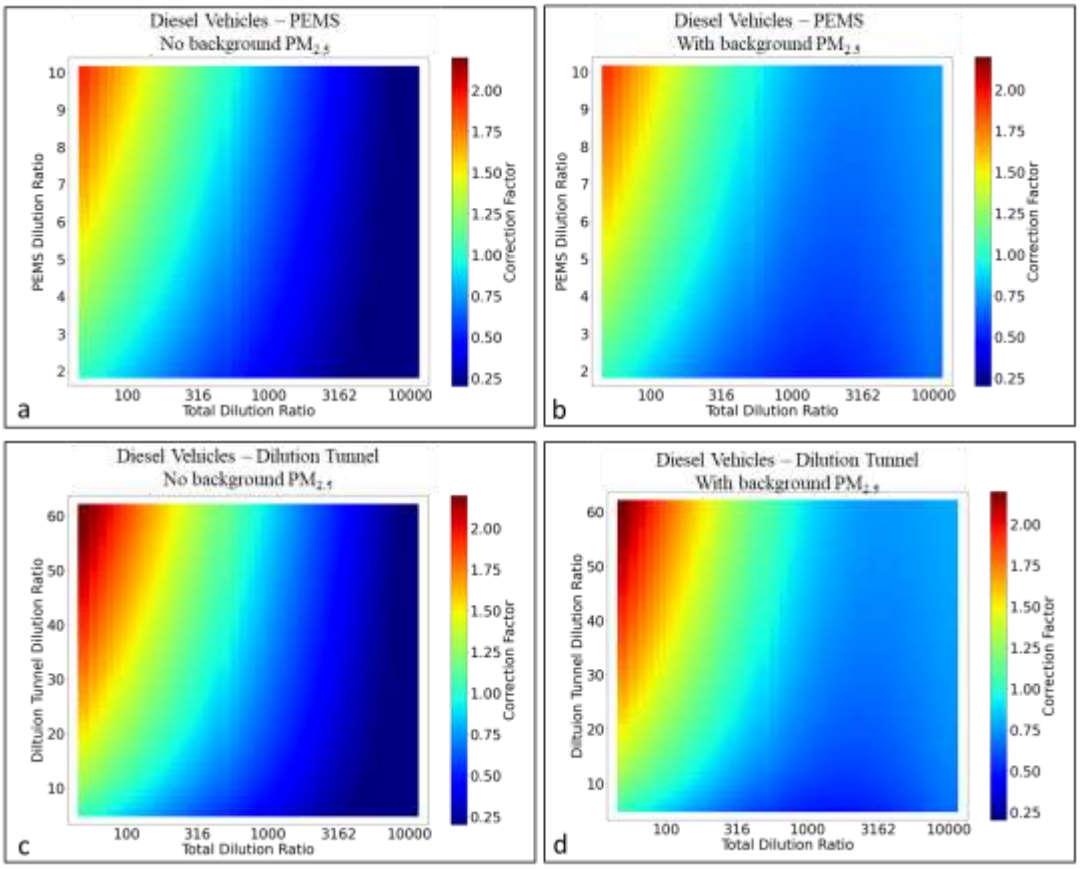

SI Figure 3.4: Correction factor (CF) sensitivity looking at with and without OC_{amb} and EC_{amb} concentrations for a diesel vehicle sampled from a PEMS and dilution tunnel obtained from a modelling VBS method, assuming an ambient temperature of 25ºC and sampling temperature for the PEMS and dilution tunnel at 60ºC and 47ºC, respectfully. a) CF for PEMS results assuming no OC_{amb} and EC_{amb} concentrations; b) CF for PEMS results assuming background OC_{amb} (10 µg/m3) and EC_{amb} (1 µg/m3) concentrations; c) CF for dilution tunnel results assuming no OC_{amb} and EC_{amb} concentrations; d) CF for dilution tunnel results assuming background OC_{amb} (10 µg/m3) and EC_{amb} (1 µg/m3) concentrations.

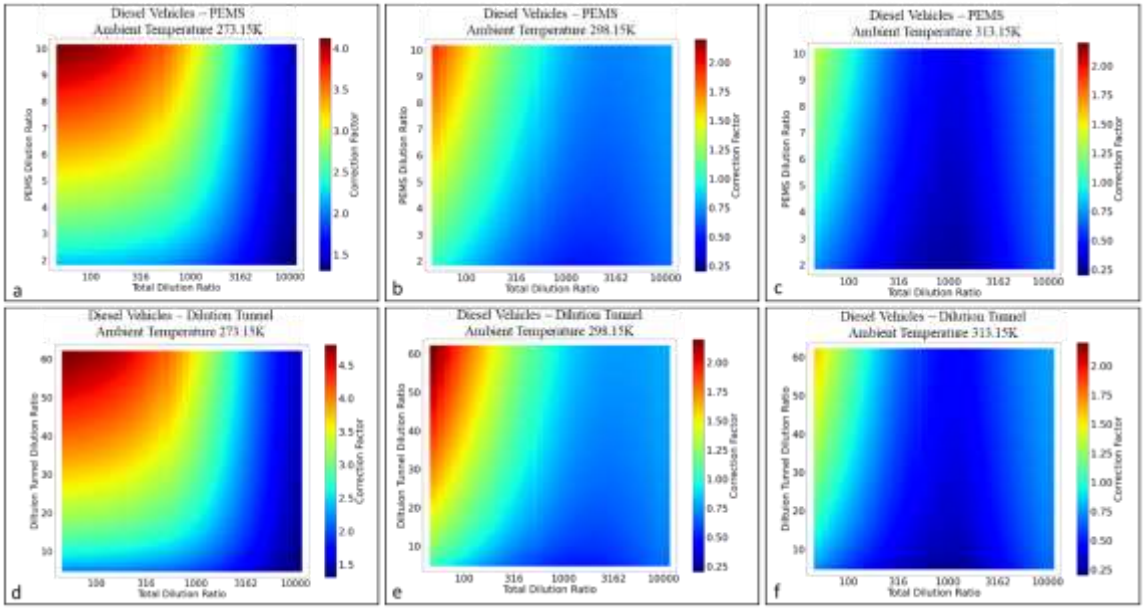

SI Figure 3.5: Correction factor (CF) sensitivity to ambient temperatures with background OC_{amb} (10 µg/m3) and EC_{amb} (1 µg/m3) concentrations for a diesel vehicle sampled from a PEMS and dilution tunnel obtained from a modelling VBS method, assuming sampling temperature for the PEMS and dilution tunnel at 60ºC and 47ºC, respectfully. a) CF for a PEMS at 0ºC; b) CF for PEMS at 25ºC; c) CF for PEMS at 40ºC; d) CF for dilution tunnel at 0ºC; e) CF for dilution tunnel at 25ºC; f) CF for dilution tunnel at 40ºC.

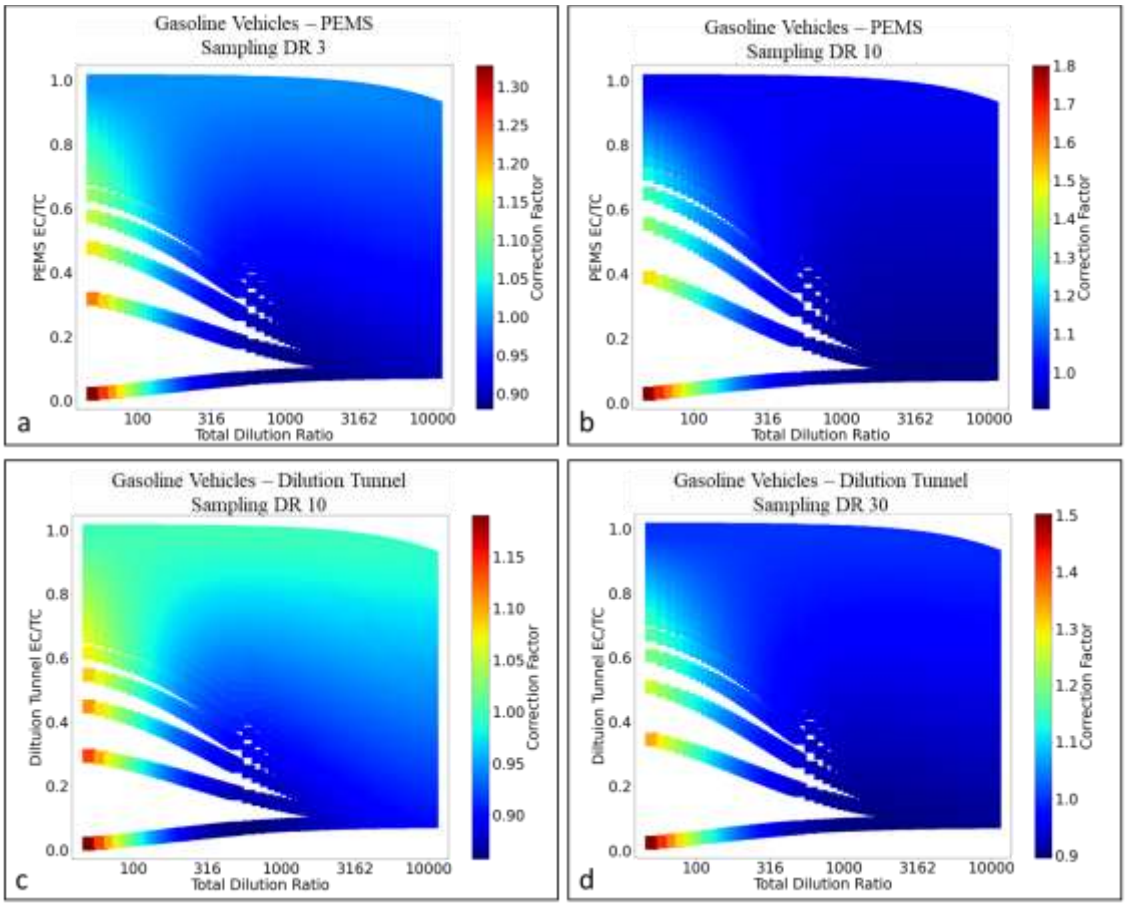

SI Figure 3.6: Correction factor (CF) sensitivity to a vehicle's EC/TC ratio with the initial HC cut by a factor of 10, a background OC_{amb} (10 µg/m3) and EC_{amb} (1 µg/m3) concentrations for a gasoline vehicle sampled from a PEMS and dilution tunnel obtained from a modelling VBS method, assuming an ambient temperature of 25ºC and sampling temperature for the PEMS and dilution tunnel at 60ºC and 47ºC, respectfully. a) CF for a PEMS at a DR_{samp} of 3; b) CF for PEMS a DR_{samp} of 10; c) CF for dilution tunnel a DR_{samp} of 10; d) CF for dilution tunnel at a DR_{samp} of 60.

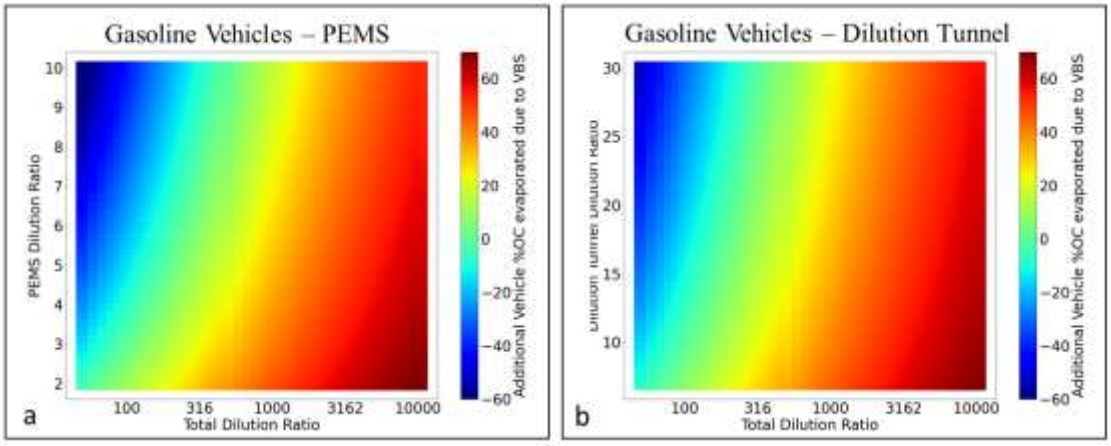

SI Figure 3.7: Additional vehicle %OC evaporated between the VBS method and traditional approach sensitivity to the sampling DR with background OC_{amb} (10 µg/m3) and EC_{amb} (1 µg/m3) concentrations subtracted out for a gasoline vehicle sampled from a PEMS and dilution tunnel obtained from a modelling VBS method, assuming an ambient temperature of 25ºC and sampling temperature for the PEMS and dilution tunnel at 60ºC and 47ºC, respectfully. a) additional %OC evaporated for a PEMS; b) additional %OC evaporated for a dilution tunnel.

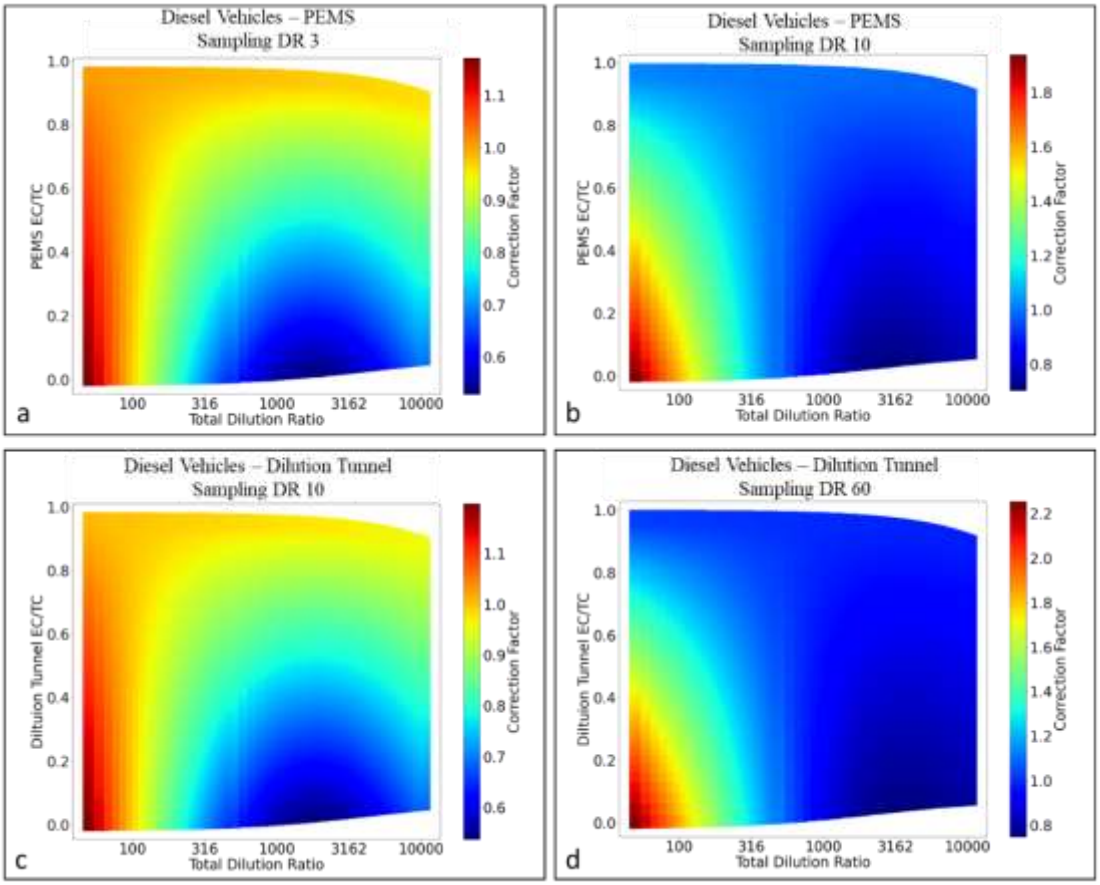

SI Figure 3.8: Correction factor (CF) sensitivity to a vehicle's EC/TC ratio with background OC_{amb} (10 µg/m3) and EC_{amb} (1 µg/m3) concentrations for a diesel vehicle sampled from a PEMS and dilution tunnel obtained from a modelling VBS method, assuming an ambient temperature of 25ºC and sampling temperature for the PEMS and dilution tunnel at 60ºC and 47ºC, respectfully. a) CF for a PEMS at a DR_{samp} of 3; b) CF for PEMS a DR_{samp} of 10; c) CF for dilution tunnel a DR_{samp} of 10; d) CF for dilution tunnel at a DR_{samp} of 60.

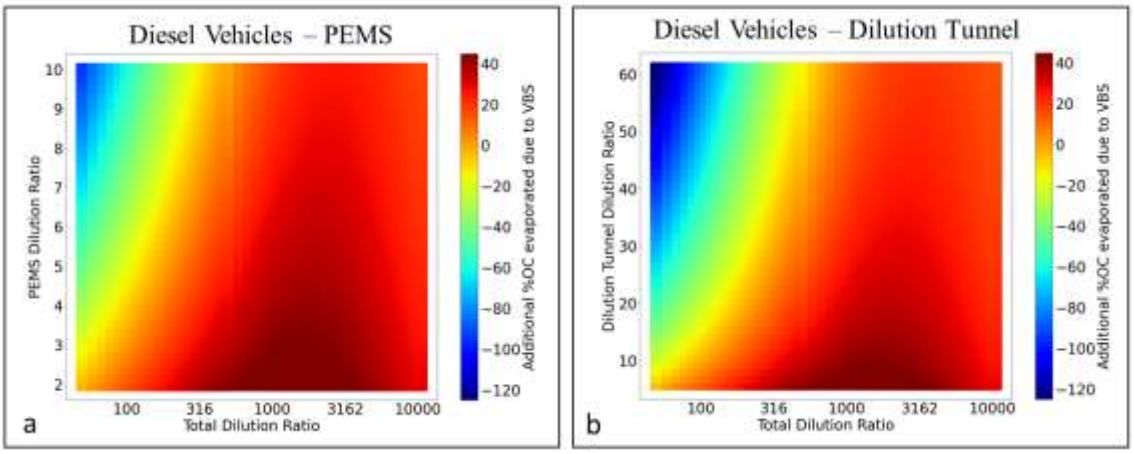

SI Figure 3.9: Additional %OC evaporated between the VBS method and traditional approach sensitivity to the sampling DR with background OC_{amb} (10 µg/m3) and EC_{amb} (1 µg/m3) concentrations for a diesel vehicle sampled from a PEMS and dilution tunnel obtained from a modelling VBS method, assuming an ambient temperature of 25ºC and sampling temperature for the PEMS and dilution tunnel at 60ºC and 47ºC, respectfully. a) additional %OC evaporated for a PEMS; b) additional %OC evaporated for a dilution tunnel

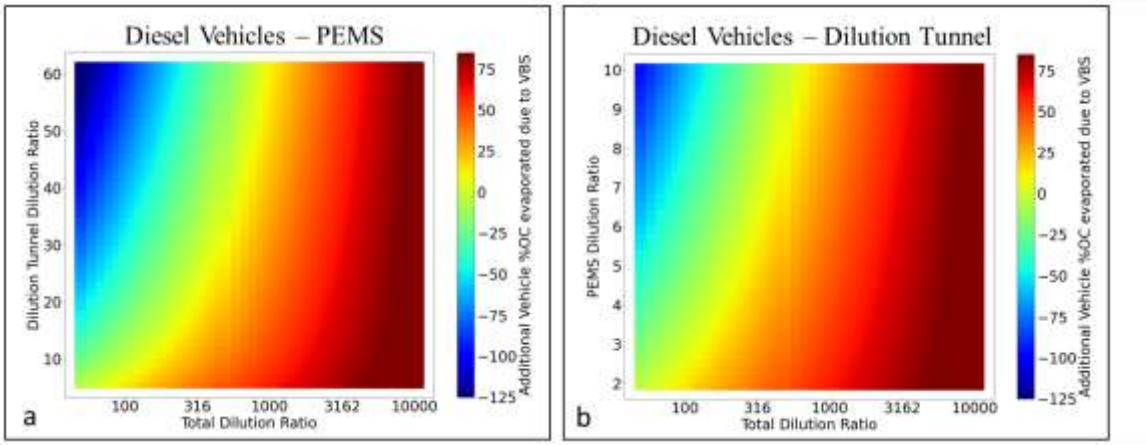

SI Figure 3.10: Additional vehicle %OC evaporated between the VBS method and traditional approach sensitivity to the sampling DR with background OC_{amb} (10 µg/m3) and EC_{amb} (1 µg/m3) concentrations subtracted out for a diesel vehicle sampled from a PEMS and dilution tunnel obtained from a modelling VBS method, assuming an ambient temperature of 25ºC and sampling temperature for the PEMS and dilution tunnel at 60ºC and 47ºC, respectfully. a) additional %OC evaporated for a PEMS; b) additional %OC evaporated for a dilution tunnel.

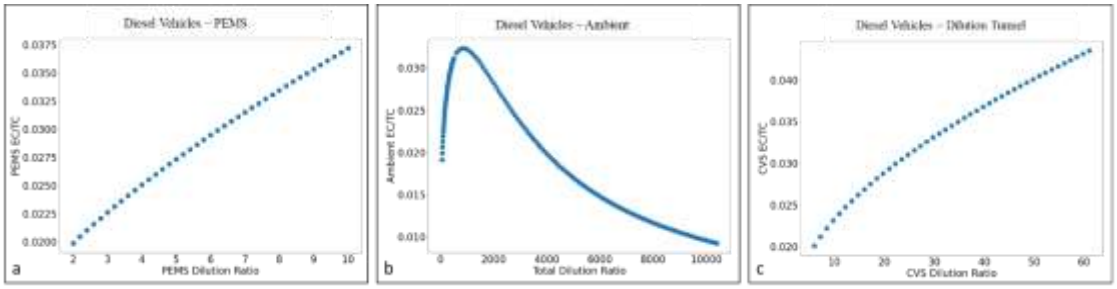

SI Figure 3.11: EC/TC variation between the VBS method and traditional approach sensitivity to the sampling DR with background OC_{amb} (10 µg/m3) and EC_{amb} (1 µg/m3) concentrations for a diesel vehicle sampled from a PEMS and dilution tunnel obtained from a modelling VBS method, assuming an ambient temperature of 25ºC and sampling temperature for the PEMS and dilution tunnel at 60ºC and 47ºC, respectfully. a) PEMS using the traditional approach; b) near-road using the VBS method; c) dilution tunnel using the traditional approach.

3.8 References

1. Wang, X., Ho, K. F., Chow, J. C., Kohl, S. D., Chan, C. S., Cui, L., … Watson, J. G. (2018). Hong Kong vehicle emission changes from 2003 to 2015 in the Shing Mun Tunnel. Aerosol Science and Technology, 6826, 1–14. https://doi.org/10.1080/02786826.2018.1456650.
2. Zhang, K., & Batterman, S. (2013). Air pollution and health risks due to vehicle traffic. Science of the Total Environment, 450–451, 307–316, http://doi.org/10.1016/j.scitotenv. 2013.01.074.
3. May, A. A., Presto, A. A., Hennigan, C. J., Nguyen, N. T., Gordon, T. D., & Robinson, A. L. (2013b). Gas-particle partitioning of primary organic aerosol emissions: (2) diesel vehicles. Environmental Science & Technology, 47(15), 8288–8296.
4. Wu, G., Pham, L., Hao, P., Jung, H., & Boriboonsomsin, K. (2017). Prediction of real-time particulate matter concentrations on highways using traffic information and emission model. Transportation Research Board, 96th Annual Meeting.

5. May, A. A., Presto, A. A., Hennigan, C. J., Nguyen, N. T., Gordon, T. D., & Robinson, A. L. (2013a). Gas-particle partitioning of primary organic aerosol emissions: (1) Gasoline vehicle exhaust. Atmospheric Environment, 77, 128–139. https://doi.org/10.1016/j.atmosenv.2013.04.060
6. Li, X., Dallmann, T. R., May, A. A., Stanier, C. O., Grieshop, A. P., Lipsky, E. M., Robinson, A. L., & Presto, A. A. (2018). Size distribution of vehicle emitted primary particles measured in a traffic tunnel. In Atmospheric Environment (Vol. 191, pp. 9–18). https://doi.org/10.1016/j.atmosenv.2018.07.052
7. Robinson, A. L., Grieshop, A. P., Donahue, N. M., & Hunt, S. W. (2010). Updating the Conceptual Model for Fine Particle Mass Emissions from Combustion Systems. Journal of the Air & Waste Management Association, 60(10), 1204–1222. https://doi.org/10.3155/1047-3289.60.10.1204
8. U.S. Environmental Protection Agency. (2015). Speciation of Total Organic Gas and Particulate Matter Emissions from On - road Vehicles in MOVES2014 Speciation of Total Organic Gas and Particulate Matter Emissions from On - road Vehicles in MOVES2014. Assessment and Standards Division Office of Transportation and Air Quality U.S. Environmental Protection Agency.
9. Donahue, N. M., Epstein, S. A., Pandis, S. N., & Robinson, A. L. (2011). A two-dimensional volatility basis set: 1. organic-aerosol mixing thermodynamics. Atmospheric Chemistry and Physics, 11(7), 3303–3318. https://doi.org/10.5194/acp-11-3303-2011

10. Donahue, N. M., Kroll, J. H., Pandis, S. N., and Robinson, A. L.: A two-dimensional volatility basis set – Part 2: Diagnostics of organic-aerosol evolution, Atmos. Chem. Phys., 12, 615-634, doi:10.5194/acp-12-615-2012, 2012.
11. Donahue, N. M., Robinson, A. L., Stanier, C. O., & Pandis, S. N. (2006). Coupled partitioning, dilution, and chemical aging of semivolatile organics. Environmental Science & Technology, 40(8), 2635–2643. https://doi.org/10.1021/es052297c
12. Epstein, S. A., Riipinen, I., & Donahue, N. M. (2010). A semiempirical correlation between enthalpy of vaporization and saturation concentration for organic aerosol. Environmental Science and Technology, 44(2), 743–748. https://doi.org/10.1021/es902497z
13. Chickos, J. S., & Hanshaw, W. (2004). Vapor pressures and vaporization enthalpies of the n-alkanes from C 31 to C 38 at T = 298.15 K by correlation gas chromatography. Journal of Chemical and Engineering Data, 49(3), 620–630. https://doi.org/10.1021/je030236t
14. R´žika, K., & Majer, V. (1994). Simultaneous Treatment of Vapor Pressures and Related Thermal Data Between the Triple and Normal Boiling Temperatures for n-Alkanes C5–C20. Journal of Physical and Chemical Reference Data, 23(1), 1–39. https://doi.org/10.1063/1.555942
15. Marshall, F. H., Berkemeier, T., Shiraiwa, M., Nandy, L., Ohm, P. B., Dutcher, C. S., & Reid, J. P. (2018). Influence of particle viscosity on mass transfer and heterogeneous ozonolysis kinetics in aqueous-sucrose-maleic acid aerosol.

Physical Chemistry Chemical Physics, 20(22), 15560–15573. https://doi.org/10.1039/c8cp01666f

16. Python [online]. Available: https://www.python.org/ [Accessed: 24-June-2020].
17. Definitions. 40 CFR § 1065.1001.
18. AVL. (2018). Application Guide - AVL M.O.V.E PM-PEMS iX 494.
19. AVL. (2018). Product Guide - AVL M.O.V.E PM-PEMS iX 494.
20. Engine Testing Regulations. CFR, Part 1065, Title 40, 2008.

Chapter 4. Bridging the Gap Between Near-Road Ambient $PM_{2.5}$ Studies and Emission Simulators

Ayla Moretti[1,2], David Cocker III[1,2], Matthew Barth[1,3]

1. Bourns College of Engineering, Center for Environmental Research and Technology (CE-CERT), University of California, 1084 Columbia Avenue, Riverside, California 92507, United States
2. Department of Chemical and Environmental Engineering, Bourns College of Engineering, University of California, Riverside, California 92521, United States
3. Department of Electrical and Computer Engineering, Bourns College of Engineering, University of California, Riverside, California 92521, United States

4.1 Abstract

This work bridges ambient $PM_{2.5}$ estimated from emission simulators to ambient $PM_{2.5}$ concentrations by developing a correction factor (CF) method that accounts for gas-particle partitioning of organic gases and particulate. The CF is developed to account for gas-particle partitioning of organics using the volatility basis set (a thermodynamic based model). A look-up table is created for a user to easily look up the CF with CF ranging from 0 to 29.95 for the conditions studied. Cases with CF greater than 1 imply traditional emission simulators underestimate predicted near-road $PM_{2.5}$ and vice-versa for CF less than 1. The CF is dependent on a few key variables: fuel and vehicle type, sampling temperature and dilution ratio (DR), vehicle tailpipe elemental carbon to organic carbon (EC:OC) and initial reactive organic gas (ROG_i) concentration, total DR, ambient temperature and background $PM_{2.5}$. In lieu of the look-up table or for values not listed within the lookup table, a Random Forest (RF) approach is also developed to ascertain the CF as well. The two most important variables when predicting CF using RF is ambient temperature and tailpipe EC:OC followed by the vehicle's ROG_i. The look-up table and RF developed in this work can be used with emission simulators and/or dispersion models to improve ambient $PM_{2.5}$ estimates from tailpipe emissions.

4.2 Introduction

Vehicle emissions are a major source of particulate matter (PM) in urban areas, with emissions from on-road gasoline and diesel vehicles significantly impacting human health and the environment. Many epidemiological studies have shown a link between $PM_{2.5}$ and adverse health effects such as asthma, Alzheimer's, autism, heart attacks, and premature death [1,2,3]. currently diesel and gasoline vehicle emissions are commonly measured either in the laboratory using a dynamometer in series with a constant volume sampler (dilution tunnel) or on-road with a portable emissions measurement system (PEMS). Emission simulators, such as the U.S. Environmental Protection Agency (EPA) Motor Vehicle Emission Simulator (MOVES), uses the emission factors derived from these systems to predict the on-road vehicle emitted $PM_{2.5}$. However, studies have found that emission simulators are substantially underestimating the vehicles $PM_{2.5}$ emissions [4]. This underestimation could be due to the PEMS and dilution tunnels measuring $PM_{2.5}$ emissions operating at temperatures and DRs not representative of the atmosphere. Differences in temperature and DR leads to inaccuracy in ambient estimates from current emission simulators that do not currently account for gas-particle (G/P) partitioning processes of organic gas and particulate emissions as they cool and dilute.

$PM_{2.5}$ can either be inorganic or organic, with organic $PM_{2.5}$ often referred to as organic aerosol (OA). Figure 4.1 shows an illustration of possible gas-particle partitioning processes as the exhaust cools and dilutes in the atmosphere; this figure is for illustration purposes only as the actual condensation or evaporation is a function of actual DR and temperature. As exhaust is emitted into the atmosphere, the plume rapidly dilutes, which

drives evaporation of OA into organic gases; however, the plume also rapidly cools which drives condensation of organic gases into OA.

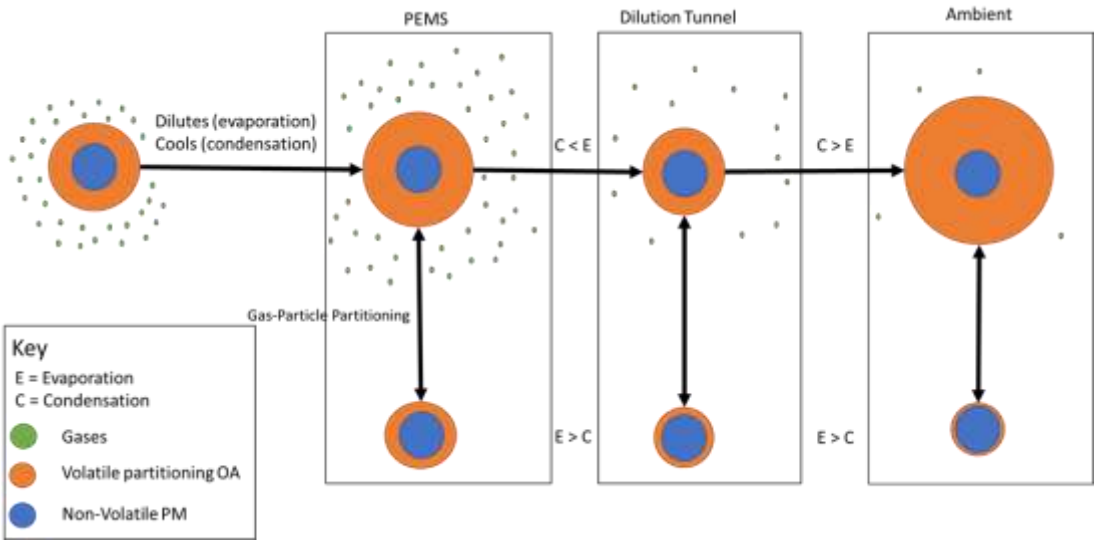

Figure 4.1: Illustration of gas-particle partitioing. Actual condenstation and evaporation is determined by the actual diltuion ratio and temperarue

Many studies have shown that the gas-particle partitioning of OA is important for modeling realistic atmospheric conditions and that a majority of the $PM_{2.5}$ emitted from on-road gasoline and diesel vehicles is volatile [5,6,15,31]. For example, May et al. 2013a tested 51 light-duty gasoline vehicles from the California in-use fleet spanning model years 1987-2012 and found that none of the primary OA (POA) should be considered non-volatile and that the POA emission factor measured from using the dilution tunnel was often biased high relative to typical atmospheric conditions [5]. Looking at diesel vehicles, May et al. 2013b also found that a majority of the POA from diesel vehicles should not be considered non-volatile [6]. Despite these findings, emission models such as the EPA's MOVES continue to treat OA as non-volatile and do not adjusting the $PM_{2.5}$ based on the gas-particle partitioning [9].

This paper describes a correction factor (CF) developed using the volatility basis set (VBS) to account for the varying measurement strategies (PEMS vs. dilution tunnel) and OA emission factor as a function of temperature and dilution ratio. There are two main goals of this work: 1) present a look-up table so that the CF can be looked up based on six variables and 2) present a model which can be used in place of the look-up table when extrapolation is needed to determine the CF.

4.3 Methodology

The VBS is a thermodynamic based model used to predict gas-particle partitioning of organics. The VBS [10,11,12] approach provides a framework for understanding and quantifying G/P partitioning; organic compounds are organized according to their volatility to investigate the G/P partitioning of the organic gasoline and diesel vehicle emissions. A full explanation of the VBS is found in Donahue et at. [10,11,12]. The volatility distribution of the organic aerosol from gasoline and diesel vehicles emissions was obtained using data from May et al 2013 ab, respectively [5,6]. The May et al 2013 ab [5,6] work provided the median volatility distribution corresponding to each bin. The VBS uses the volatility distribution, temperature changes and changes in dilution to account for the gas-particle partitioning of the volatile OA. Within the VBS, compounds are distributed according to their mass-equivalent effective saturation concentration (C*,μg/m3). As the temperature decreases, from the tailpipe, PEMS and/or dilution tunnel to ambient, individual organic compounds shift towards lower C* allowing for some of these compounds to further partition from the gas-phase to the aerosol-phase. A full explanation of the methodology

used in creating the correction factor and the thermodynamics and G/P partitioning observed through the development of the model can be found in Chapter 3.

To assist current emission simulators account for the G/P partitioning of organics emitted from on-road vehicles, a correction factor (CF) was developed. The CF was calculated by taking the ratio of the predicted near-road $PM_{2.5}$ (VBS approach) to the traditional method used by emission simulators (traditional approach). The VBS approach accounts for the G/P partitioning of the organic $PM_{2.5}$ and organic gases whereas the traditional approach assumes all PM species are conservative and therefore do not undergo gas-particle partitioning. The correction factor was calculated using the following equation:

$$CF = \frac{TC_{VBS}}{TC_{sampling\ DR}} * \frac{DR_{samp}}{DR_{tot}} \quad (4.1)$$

Where TC_{VBS} is the predicted near-road total carbon (TC) using the method developed in this manuscript, $TC_{sampling\ DR}$ is the TC predicted by the PEMS or dilution tunnel at the sampling DR, DR_{tot} is the total DR, and DR_{samp} is the sampling DR of the PEMS or dilution tunnel. The CF is a function of the variables listed in Table 4.1 as well as the fuel type (gasoline or diesel).

Table 4.1: description of the explanatory variables

i	x_i	**Unit**
1	Initial Reactive Organic Gases	$\mu g/m^3$
2	Sampling Dilution Ratio	-
3	Total Dilution Ratio	-
4	Sampling Temperature	K
5	Ambient Temperature	K
6	Vehicle's EC:OC	-
7	Ambient Background Organic Aerosol	$\mu g/m^3$

CF is evaluated for a range of environmental and sampling conditions: sampling (PEMS or dilution tunnel) temperature and dilution ratio (DR), tailpipe elemental carbon to organic carbon (EC:OC), ambient temperature, background PM and distance from the vehicle. The DR is defined as the amount of dilute exhaust per amount of undiluted exhaust [13]. The sampling DR and the temperature for the PEMS varied between 2 to 10 and 50^{o}C to 70^{o}C, for both gasoline and diesel vehicles [14,15]. The dilution tunnel sampling temperature was evaluated for temperature ranging between 42^{o}C to 52^{o}C based on federal regulations requiring that sample be collected at 47$\pm$5^{o}C [8,16]; and a DR that varied between 7 to 30 and 6 to 60 for gasoline and diesel vehicles, respectfully. The initial concentration of undiluted Reactive Organic Gases (ROG_i) from the vehicle was obtained from California Air Resources Board EMission FACtor (EMFAC) [17] and the following equation:

$$ROG_i = \frac{ROG_{run}}{CO_{2\,run}} * \%CO_2 \quad (4.2)$$

where ROG_i is the initial un-diluted ROG emitted from the vehicle, ROG_{run} is the ROG EMFAC running emission, $CO_{2\,run}$ is the CO_2 EMFAC running emission, and $\%CO_2$ is the percent of CO_2 in the un-diluted exhaust. The ROG_{run} and $CO_{2\,run}$ were obtained through EMFAC assuming the light-duty gasoline vehicle (LDGV) was the EMFAC LDA and the heavy-duty diesel vehicle (HDDV) was the EMFAC T7 tractor. Both values were estimated for California statewide levels and using aggregated speed over all model years. The $\%CO_2$ was calculated by using the ideal stoichiometric air-fuel ratio of 14.7:1 for gasoline and 14.5:1 for diesel [18]. ROG_i ranged from 2,000 µg/m^3 to 300,000 µg/m^3 and

3,500 μg/m^3 to 26,000 μg/m^3 for LDGV and HDDV, respectively. Tailpipe elemental carbon varied between 0 μg/m^3 to 1,000,000 μg/m^3, to capture a range the vehicle's EC:OC.

The ambient temperature and background ambient PM were also varied; ambient temperature was varied from 0°C to 40°C and the ambient background OC (OC_{amb}) and EC (EC_{amb}) was varied between 0μg/m^3 to 10μg/m^3 and 0μg/m^3 to 1μg/m^3, respectively, to simulate a range of pristine to polluted urban environments. Lastly, the total DR ranged from 0 to 10,500 to capture a range of distances away from the vehicle. The total DR can be correlated to distance from the vehicle through dispersion modeling. For example, if a dispersion model is solved assuming: a line source, stability class "C", wind speed of 1m/s, source height of 2.5 meters (~8.2ft), and a receptor height (average adult female) of 1.65 meter (~5.5ft), then total DR of 1,500 and 10,500 would correspond to 13m and 104m from the vehicle, respectfully.

4.4 Results & Discussion

The CF can be used by either using a look-up table or through a Random Forest (RF), both of which are described below. The look-up table uses MySQL [19] while the RF was created using the look-up table, Python version 3.9 [20], and the package scikit-learn version 0.24 [21].

4.4.1 Look-up Table

Table 4.2 and Table 4.3 shows a snippet of the look-up table generated for a LDGV and a HDDV, respectively. The look-up table was built based on the variables in Table 4.1 and can be used to manually look-up the CF for specific conditions. For example, an CF factor of 2.10 and 2.03 is obtained for a LDGV and HDDV, respectively, when both

sampled from a PEMS at an ambient temperature of 0°C and with a total DR of 1,500 while assuming a background $PM_{2.5}$ concentrations of 11µg/m^3 (10µg/m^3 OC_{amb} and 1µg/m^3 EC_{amb}). The CF, including LDGV and HDDV vehicles for the PEMS and dilution tunnel, ranged from 0 (complete evaporation) to 29.95. A CF greater than one implies that the traditional approach underestimates the predicted near-road $PM_{2.5}$. Since most emission simulators are currently treating all $PM_{2.5}$ emitted from on-road vehicles as non-volatile (CF=1), using CF through the look-up table allows for correction for G/P partitioning.

Table 4.2: Snippet of the look-up table for a light-duty gasoline vehicle.

Sampling Type	ROG_i	Sampling DR	Total DR	Sampling Temperature (K)	Ambient Temperature (K)	EC:OC	Background $PM_{2.5}$ (µg/m^3)	Correction Factor
PEMS	2084.32	3	1500	333.15	273.15	0.7	11	1.16
	34488.73	3	1500	333.15	273.15	0.17	11	2.1
	34488.73	3	1500	333.15	273.15	0.18	0	2.41
	34488.73	3	1500	333.15	273.15	0.67	11	1.77
	34488.73	3	10500	333.15	273.15	0.16	11	1.37
	34488.73	3	10500	333.15	273.15	0.18	0	2.21
	34488.73	3	1500	333.15	298.15	0.17	11	0.67
Dilution Tunnel	2084.32	11	1500	320.15	273.15	0.69	11	1.16
	34488.73	11	1500	320.15	273.15	0.17	11	2.17
	34488.73	11	1500	320.15	273.15	0.19	0	2.51
	34488.73	11	1500	320.15	273.15	0.69	11	1.81
	34488.73	11	10500	320.15	273.15	0.16	11	1.38
	34488.73	11	10500	320.15	273.15	0.19	0	2.3
	34488.73	11	1500	320.15	298.15	0.17	11	0.69

Table 4.3: Snippet of the look-up table for a heavy-duty diesel vehicle.

Sampling Type	ROG_i	Sampling DR	Total DR	Sampling Temperature (K)	Ambient Temperature (K)	EC:OC	Background $PM_{2.5}$ (µg/m^3)	Correction Factor
PEMS	3584.43	3	1500	333.15	273.15	0.66	11	1.41
	25502.51	3	1500	333.15	273.15	0.11	11	2.03
	25502.51	3	1500	333.15	273.15	0.11	0	2.4
	25502.51	3	1500	333.15	273.15	0.61	11	1.7
	25502.51	3	10500	333.15	273.15	0.1	11	1.34
	25502.51	3	10500	333.15	273.15	0.11	0	2.35
	25502.51	3	1500	333.15	298.15	0.11	11	0.57
Dilution Tunnel	2084.32	11	1500	320.15	273.15	0.69	11	1.16
	25502.51	11	1500	320.15	273.15	0.11	11	2.11
	25502.51	11	1500	320.15	273.15	0.12	0	2.53
	25502.51	11	1500	320.15	273.15	0.64	11	1.75
	25502.51	11	10500	320.15	273.15	0.11	11	1.36
	25502.51	11	10500	320.15	273.15	0.12	0	2.48
	25502.51	11	1500	320.15	298.15	0.11	11	0.59

The look-up table can be used when the variables from Table 4.1 are known and similar to those used in the look-up table, the SI contains a link to be able to use the look-

up table. In lieu of look-up tables or for values not listed within the lookup tables, a RF approach is developed to ascertain CF as well.

4.4.2 Random Forest

Due to the non-linearity of the response of vapor pressure versus dilution when modeling the gas-particle partitioning, a regression tree (RT) and random forest (RF) were used to provide an alternate method to estimate CF. A RT captures the non-linearity of a dataset by partitioning the data into smaller groups and then fitting a model for each subgroup [22]. The RF is then created by growing many RT; the RF predicts the CF by having each RT give a predicted CF and then the trees "vote" on a CF and the RF chooses the CF having the most votes [23]. The variables used to create the RT and grow the RF are shown in Table 4.1. In order to have the most accurate prediction of the CF four different RF were developed: 1) a LDGV with the emissions sampled from a PEMS (LDGV PEMS); 2) a LDGV with emissions sampled from a dilution tunnel (LDGV DT); 3) a HDDV with the emissions sampled from a PEMS (HDDV PEMS); and 4) a HDDV with the emissions sampled from a dilution tunnel (HDDV DT).

Within each RF the feature importance [24] was used to assist in determining which variables are the most and least relevant when building the RF and in making a CF prediction (Table 4.4). For each RF, the feature importance sums up to 1 and the higher the importance score (maximum = 1) the more relevant that variable is in creating the RF and predicting the CF. Overall, the ambient temperature, ROG_i and the vehicle's EC:OC were the most relevant variables. It was found that the ambient background elemental carbon

(EC_{amb}) had a feature importance of zero and is excluded from the results and the RF. Excluding the EC_{amb} from the RF also reduces computational costs.

Table 4.4: Feature importance for each model and variable

Random Forest Models	Initial ROG	Sampling Dilution Ratio	Total Dilution Ratio	Sampling Temperature	Ambient Temperature	Vehicle's EC:OC	Ambient Background Organic Aerosol
LDGV PEMS	0.138	0.035	0.042	0.063	0.429	0.293	0
LDGV DT	0.164	0.023	0.048	0.013	0.503	0.25	0
HDDV PEMS	0.129	0.109	0.027	0.182	0.241	0.312	0
HDDV DT	0.101	0.098	0.031	0.03	0.34	0.4	0

The RT fit training data very well (high R^2 and low mean squared error), but they tend to fail to generalize new input data, which is commonly referred to as overfitting. One solution to prevent overfitting is to prune each of the RT in a RF to optimize the number of trees within the RF. Pruning the tree depth is important because the deeper the tree the higher the accuracy of the prediction and the more complex the model; however, if the tree depth is too high the RT could overfit the data leading to increases in the testing error. The number of trees in the RF correlates to computational cost; generally, the greater number of trees in a RF improves the model but also increases the computational cost. In order to find the ideal tree depth and number of trees within the RF, a hyperparameter [25] and k-fold cross-validation [26] were used. Figure 4.2 shows the hyperparameter tuning used to optimize the number of trees (Figure 4.2a) and tree depth (Figure 4.2b) for the LDGV PEMS model.

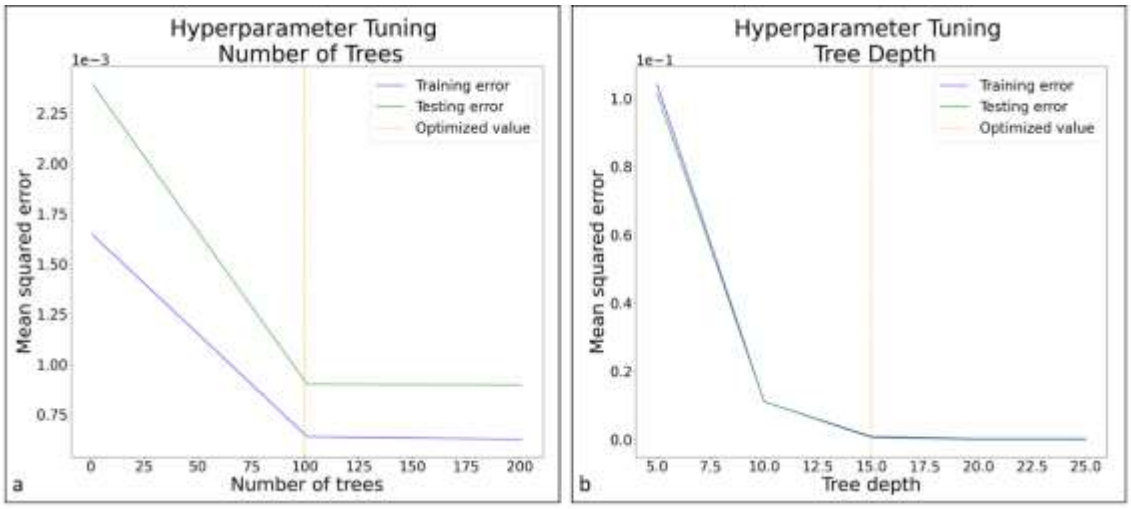

Figure 4.2: LDGV PEMS Hyperparameter tuning based on mean squared error for the testing and training data to find the optimized values for a. the number of trees in the random forest and b. the depth of each tree.

The number of trees in the RF was selected by finding the number of trees that yielded the lowest mean squared error, before improvement became negligible, resulting in 100 trees in the RF (yellow line in Figure 4.2a). Tree depth was found using the same method and yielded an optimized tree depth of 15 (yellow line in Figure 4.2b). Finding the optimized number of trees and max depth were repeated for each model. Resulting in the same tree depth and number of trees for each model, 15 and 100, respectfully.

80% of the data was used to train the RF leave 20% to test. The SI show a small snippet of one of the RT within the LDGV PEMS RF and contains a link to be able to download and run the RF to predict the CF or use the look-up table.

4.4.3 Applications

The CF derived in this research accounts for the evaporation and condensation compared to measured emission factors (CVS or PEMS) due to the temperature and dilution of organics emitted from on-road gasoline and diesel vehicles. The CF could either

be applied before or after a dispersion model is applied to the emission simulators. Applying the CF after the emission simulator output data but before the dispersion model could allow for correction between $PM_{2.5}$ results for CVS and PEMS due to differences in dilution and temperature. Applying the CF after dispersion modeling could improve ambient $PM_{2.5}$ estimates.

The user will get the most accurate correction factor if specific sampling, environmental and composition variables are known; however, if the values are not known the nominal range could be used as a starting point (Table 4.5). For example, the HDDV has two nominal ranges for the EC:OC for model years 2009 and newer. The first being 0.05 to 0.25 for a HDDV sampled with a Diesel Particulate Filter (DPF) and Selective Catalytic Reduction (SCR) with the vehicle sampled with a hot start cycle having an EC:OC of 0.05 to 0.08 and a cold start having an EC:OC of 0.1 to 0.25. The second is for HDDV with no SCR and a broken or damaged DPF (such that it is not working properly) the EC:OC ratio for this scenario is 10-13.

Table 4.5: Nominal values to use to calculate CF if specific parameters are unknown assuming a typical LDGV and HDDV (not gross emitter).

x		PEMS	Dilution Tunnel	Unit
ROG	LDGV	2,000 – 300,000		µg/m^3
	HDDV	3,500 – 26,000		
Sampling Dilution Ratio	LDGV	2 - 10	7 - 30	-
	HDDV		7 - 60	
Total Dilution Ratio	LDGV & HDDV	0 - 10,500		-
Sampling Temperature	LDGV & HDDV	60±10	47±5	^{o}C
Ambient Temperature	LDGV & HDDV	0 - 40		^{o}C
Ambient Background Organic Aerosol	LDGV & HDDV	0 - 10		µg/m^3
EC:OC	LDGV	0.2 to 0.5 [27]		-
	HDDV	With DPF and SCR – Cold start: 0.1 to 0.25 [28]		
		With DPF and SCR – Hot start: 0.05 to 0.08 [28]		
		Without SCR and broken/damaged DPF: 10-13 [28]		

4.5 Conclusion

G/P partitioning of the organics is important for modeling realistic atmospheric conditions. Many studies have shown that a majority of the PM emitted from on-road gasoline and diesel vehicles is volatile organic PM. Despite these observations, current emission simulators treat all $PM_{2.5}$ as non-volatile not accounting for the additional (or lesser) vehicle emitted $PM_{2.5}$ due to G/P partitioning. G/P partitioning is a function of temperature, dilution, and suspended OA mass concentrations, which are dictated by the vehicle emissions and ambient $PM_{2.5}$.

This paper provides a look-up table, for the CF, that can be used to easily lookup the CF without running any code. The CF was developed based on changes in temperature, dilution, and suspended OA mass concentrations. The rapid changes in temperature and dilution, as a plume is emitted, affects the G/P partitioning in different ways. The decrease in temperature drives condensation of organic gases into OA, which can increase the CF past 1; however, the increasing dilution drives evaporation of OA into organic gases, which can then decrease the CF closer to or below 1. Whether the condensation or evaporation dominates then depends on the ambient temperatures and suspended OA mass concentrations, which is dictated by the plume's EC:OC and ambient background OC. Changes in technology, aftertreatments, engine ages, and fuel blends all affect the vehicle's EC:OC and therefore G/P partitioning. With EC being a conservative species, the closer the emitted $PM_{2.5}$ is to pure EC (without any organics) the less important G/P partitioning is. A detailed description on how each parameter affects the CF.

Further, an optimized RF is developed and provided that can be used in lieu the look-up table. Sensitivity analysis from the RF indicates that ambient temperature, ROG_i, and vehicle's EC:OC were the most important parameters. The look-up table and the RF models developed in manuscript can be used with emission simulators and/or dispersion models to better predict the near-road $PM_{2.5}$ concentrations by accounting for the G/P partitioning that occurs after emissions dilute and cool in the atmosphere.

4.6 Acknowledgments

This study was funded by a grant from the National Center for Sustainable Transportation (NCST), supported by the U.S. Department of Transportation (USDOT)

through the University Transportation Centers program. The authors would like to thank the NCST and the USDOT for their support of university-based research in transportation, and especially for the funding provided in support of this project.

4.7 Appendix 4A. Supporting Information

The look-up table and the Random Forest models are available at https://gitlab.com/ayla.moretti/Vehicle-PM-CF.

4.8 References

1. Volk HE, Lurmann F, Penfold B, Hertz-Picciotto I, McConnell R. (2013). Traffic-Related Air Pollution, Particulate Matter, and Autism. JAMA Psychiatry. 2013;70(1):71–77. doi:10.1001/jamapsychiatry.2013.266
2. Yegambaram, M., Manivannan, B., Beach, T. G., Halden, R. U. (2015). Role of Environmental Contaminants in the Etiology of Alzheimer's Disease: A Review. Current Alzheimer Research, 12(2), 116-146, 2015.
3. United States Environmental Protection Agency. Health and Environmental Effects of Particulate Matter (PM). https://www.epa.gov/pm-pollution/health-and-environmental-effects-particulate-matter-pm
4. Smit, R., Ntziachristos, L., & Boulter, P. (2010). Validation of road vehicle and traffic emission models - A review and meta-analysis. Atmospheric Environment, 44(25), 2943–2953. https://doi.org/10.1016/j.atmosenv.2010.05.022
5. May, A. A., Presto, A. A., Hennigan, C. J., Nguyen, N. T., Gordon, T. D., & Robinson, A. L. (2013a). Gas-particle partitioning of primary organic aerosol

emissions: (1) Gasoline vehicle exhaust. Atmospheric Environment, 77, 128–139. https://doi.org/10.1016/j.atmosenv.2013.04.060

6. May, A. A., Presto, A. A., Hennigan, C. J., Nguyen, N. T., Gordon, T. D., & Robinson, A. L. (2013b). Gas-particle partitioning of primary organic aerosol emissions: (2) diesel vehicles. Environmental Science & Technology, 47(15), 8288–8296. https://doi.org/10.1021/es400782j
7. Li, X., Dallmann, T. R., May, A. A., Stanier, C. O., Grieshop, A. P., Lipsky, E. M., Robinson, A. L., & Presto, A. A. (2018). Size distribution of vehicle emitted primary particles measured in a traffic tunnel. In Atmospheric Environment (Vol. 191, pp. 9–18). https://doi.org/10.1016/j.atmosenv.2018.07.052
8. Robinson, A. L., Grieshop, A. P., Donahue, N. M., & Hunt, S. W. (2010). Updating the Conceptual Model for Fine Particle Mass Emissions from Combustion Systems. Journal of the Air & Waste Management Association, 60(10), 1204–1222. https://doi.org/10.3155/1047-3289.60.10.1204
9. U.S. Environmental Protection Agency. (2015). Speciation of Total Organic Gas and Particulate Matter Emissions from On - road Vehicles in MOVES2014 Speciation of Total Organic Gas and Particulate Matter Emissions from On - road Vehicles in MOVES2014. Assessment and Standards Division Office of Transportation and Air Quality U.S. Environmental Protection Agency.
10. Donahue, N. M., Kroll, J. H., Pandis, S. N., and Robinson, A. L.: A two-dimensional volatility basis set – Part 2: Diagnostics of organic-aerosol evolution, Atmos. Chem. Phys., 12, 615-634, doi:10.5194/acp-12-615-2012, 2012.

11. Donahue, N. M., Robinson, A. L., Stanier, C. O., & Pandis, S. N. (2006). Coupled partitioning, dilution, and chemical aging of semivolatile organics. Environmental Science & Technology, 40(8), 2635–2643. https://doi.org/10.1021/es052297c
12. Donahue, N. M., Epstein, S. A., Pandis, S. N., & Robinson, A. L. (2011). A two-dimensional volatility basis set: 1. organic-aerosol mixing thermodynamics. Atmospheric Chemistry and Physics, 11(7), 3303–3318. https://doi.org/10.5194/acp-11-3303-2011
13. https://www.law.cornell.edu/cfr/text/40/1065.1001
14. AVL. (2018). Product Guide - AVL M.O.V.E PM-PEMS iX 494.
15. AVL. (2018). Application Guide - AVL M.O.V.E PM-PEMS iX 494.
16. Engine Testing Regulations. CFR, Part 1065, Title 40, 2008.
17. California Air Resources Board. EMFAC2014 Web Database. https://arb.ca.gov/emfac/2014/.
18. X-Engineer. Air-fuel Ratio. https://x-engineer.org/automotive-engineering/internal-combustion-engines/performance/air-fuel-ratio-lambda-engine-performance/
19. MySQL. https://www.mysql.com/
20. Python [online]. Available: https://www.python.org/ [Accessed: 24-June-2020].
21. Scikit-learn. Machine Learning in Python. https://scikit-learn.org/stable/
22. UC Business Analytics R Programming Guide. https://uc-r.github.io/regression_trees.

23. Leo Breiman and Adele Cutler. Random Forest. https://www.stat.berkeley.edu/~breiman/RandomForests/cc_home.htm
24. Machine Learning Mastery. How to Calculate Feature Importance With Python. https://machinelearningmastery.com/calculate-feature-importance-with-python/
25. DeepAI. Hyperparameter. https://deepai.org/machine-learning-glossary-and-terms/hyperparameter
26. Machine Learning Mastery. A introduction to k-fold Cross-Validation. https://machinelearningmastery.com/k-fold-cross-validation/
27. Lough, G. C., Christensen, C. G., Schauer, J. J., Tortorelli, J., Mani, E., Lawson, D. R., Clark, N. N., & Gabele, P. A. (2007). Development of molecular marker source profiles for emissions from on-road gasoline and diesel vehicle fleets. Journal of the Air and Waste Management Association, 57(10), 1190–1199. https://doi.org/10.3155/1047-3289.57.10.1190
28. University of California, Riverside. 200 Vehicle Study. https://www.cert.ucr.edu/200-vehicle-study

Chapter 5. Reducing Community Exposure to Freight-related Air Pollution through Exposure-Based Truck Routing

Ayla Moretti[1,2], Ji Luo[1], Kanok Boriboonsomsin[1], Matthew Barth[1,3]

1. Bourns College of Engineering, Center for Environmental Research and Technology (CE-CERT), University of California, 1084 Columbia Avenue, Riverside, California 92507, United States
2. Department of Chemical and Environmental Engineering, Bourns College of Engineering, University of California, Riverside, California 92521, United States
3. Department of Electrical and Computer Engineering, Bourns College of Engineering, University of California, Riverside, California 92521, United States

5.1 Abstract

This research utilizes a chain of vehicle emission modelling, dispersion modelling and exposure assessment to assess how much of the fine particulate matter ($PM_{2.5}$) and nitrogen oxides (NO_x) emissions from heavy-duty diesel trucks (HDDT) were inhaled by the nearby population when these trucks travel in disadvantaged communities. Specific HDDT routes were calculate from the four corners of the study area in San Bernardino, California, to and from the San Bernardino Airport to calculate the impact of pollutant inhalation on the surrounding neighborhoods as well as HDDT travel time and distance. "Low-exposure routes" (LER) were calculated and compared to the traditional routes at 10 A.M. and 3 P.M. On average, these LER resulted in lower pollutant inhalation for the 3 P.M. scenario compared to that of the 10 A.M. scenario, illustrating that traffic and meteorological conditions can play an important role in determining the inhalation values. The effects of breathing rate were also investigated, comparing between a population averaged and an age-group specific breathing rate. Results indicated that the breathing rate slightly affects the inhalation, with the NO_x inhalation affected more than the $PM_{2.5}$ inhalation. Lastly, a $PM_{2.5}$ correction factor was applied to predict near-road $PM_{2.5}$ concentration by accounting for the gas-particle partitioning that affects the organic $PM_{2.5}$ emitted from the HDDT. Results suggest that rerouting the HDDT at least 10m away from the sensitive receptors would reduce the $PM_{2.5}$ inhalation by an additional 50% or more after accounting for the $PM_{2.5}$ correction factor.

5.2 Introduction

Heavy-Duty diesel trucks emit a complex mix of pollutants including fine particulate matter ($PM_{2.5}$) and nitrogen oxides (NO_x). Diesel exhaust contains more than 40 cancer-causing substance and is estimated to be responsible for about 70% of California's toxic air contaminants cancer risk [1] with exposure to diesel $PM_{2.5}$ expected to increase in urban environments over the next decade [2]. The highest levels of diesel related air pollution often occur at ports, distribution centers and freeways leading to an increased exposure for the people living in communities nearby. Typically, low income and minority communities experience the highest vehicle emitted $PM_{2.5}$ and NO_x concentrations leading to increased pollutant exposure and adverse health effects [3].

There has been an increased level of awareness to these environmental justice issues leading to the designation of disadvantaged communities in California per Senate Bill 535 (SB 535) [4]. Disadvantaged communities are now receiving additional funds aimed at improving public heath, quality of life and economic opportunities per Assembly Bill 1550 (AB 1550) [4,5]. Additionally, in response to Assembly Bill 617 (AB 317) the California Air Resources Board is focusing on reducing exposure in communities that are most impacted by air pollution [6].

As a particular case study area, the San Bernardino International Airport is a public airport located two miles southeast of San Bernardino City in San Bernardino County, California. The airport mainly supports air cargo operations, and it is recently approved to undergo a major expansion as an Amazon regional air hub [7]. Residents, communities, and organizations have been expressing concerns about future employment opportunities

and environmental impacts [8]. This community is largely part of a SB 535 Disadvantaged Communities area [9], and it is located east to Muscoy, which is one of the AB 617 community designated [10] in 2018 (red shaded area in Figure 5.1). To help reduce the adverse effects of heavy-duty trucks, exposure-based routing can navigate a heavy-duty-diesel-truck (HDDT) through a disadvantaged community in a way that lowers the total exposure of community members to the pollutant emissions from the truck without significantly increasing travel time [11].

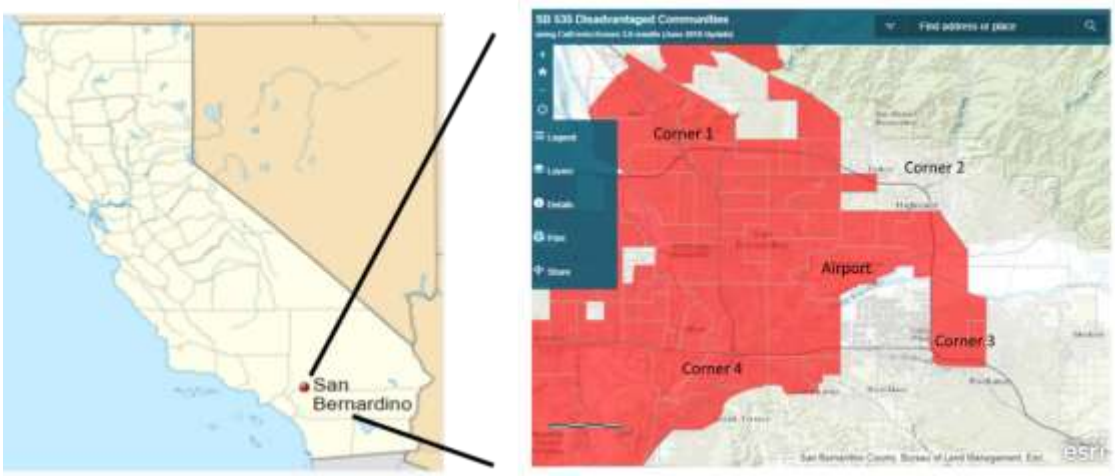

Figure 5.1: Map of study area. Red shading shows the disadvantaged communities in the study area [4].

One objective of this research is to evaluate the exposure-based routing in the San Bernardino Airport case study area. This area is bounded by Freeway I-215 in the west, I-10 in the south, and I-210 curving from south to north then connecting the east to west side. The potential HDDT trips from the four corners to and from the airport and the travel time, distance, and inhalation values are evaluated in detail in this study. Another objective, and novel contribution, of this research is to examine the impact of breathing rate assumption and near-road $PM_{2.5}$ prediction on the effects of low exposure route.

5.3 Modelling Method

Figure 5.2 presents the methodological framework of exposure-based routing that has been applied in previous studies [12]. It involved a modelling chain that started with vehicle emission modelling to air dispersion modelling, human exposure assessment, and finally a vehicle route calculation. In addition, the key inputs at each step are listed in the orange boxes in Figure 5.2.

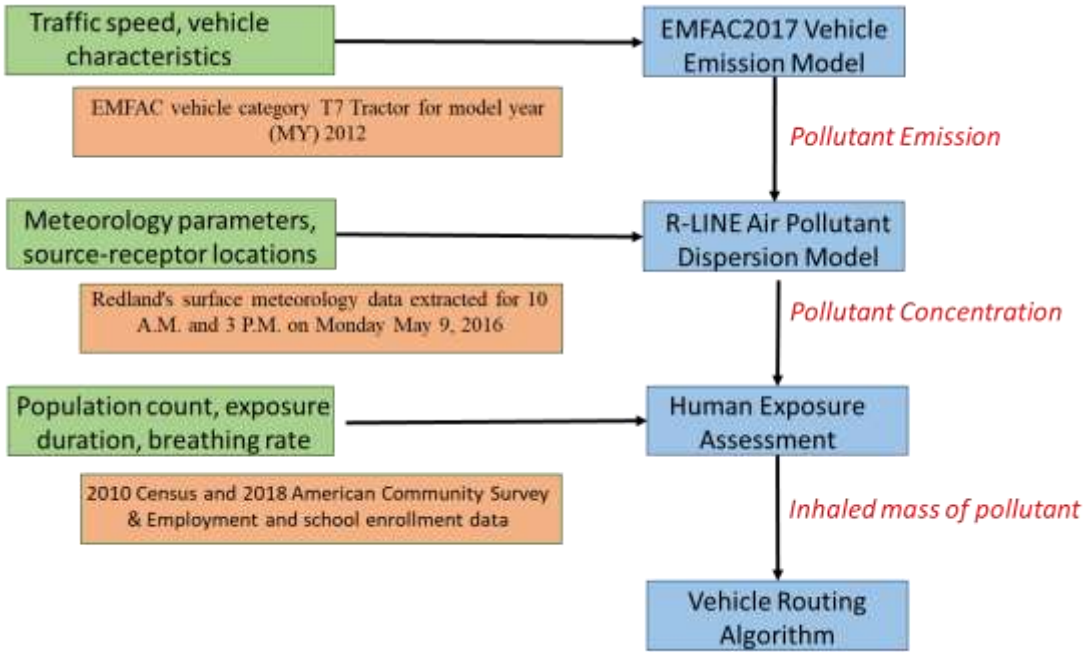

Figure 5.2: Methodological framework of exposure-based routing

5.3.1 Vehicle Emission Modelling

To determine vehicle emission factors (in the unit of *gram/mile*), link-based traffic activities (e.g., average traffic speed) and vehicle characteristics (e.g., vehicle type and model year) are needed as inputs. The link-level emissions were calculated using equation below.

$$E_{i,j} = V_{i,k} \times L_i \times EF_{j,k} \quad (5.1)$$

where $E_{i,j}$ is mass emission of pollutant j on link i; $V_{i,k}$ is HHDT volume on link i with link speed k; L_i is length of link i; and $EF_{j,k}$ is emission factor of pollutant j at speed k.

The emission factors for heavy-duty diesel trucks were obtained from CARB's EMFAC2017 emission model for the following model run specifications:

- *Source* – EMFAC2017 (v1.0.2) Emission Rates [13,14]
- *Region Type* – County
- *Region* – Los Angeles, assuming trucks come from LA County.
- *Calendar Year* – 2018
- *Season* – Annual
- *Vehicle Classification* – EMFAC2011 Categories
- *Model Year* – 2012

For this study, the modelling of vehicle emissions was performed for a heavy-duty diesel truck of model year 2012, and the calculation of its tailpipe emissions were done for all the roadway links in the modelling area. It was assumed that this truck would be traveling at the speed equal to the average speed at each roadway link. The data regarding average speed on roadway links were obtained from a commercial digital roadway map. Running exhaust $PM_{2.5}$, NO_x, and CO_2 emissions factors of the truck were obtained from EMFAC2017 [13,14], which was the latest version of EMFAC at the time of study.

5.3.2 Dispersion Modelling

An atmospheric dispersion model is needed to estimate the concentration of air pollutants emitted from vehicular sources at specific receptor locations. In this study, R-LINE, a research grade dispersion model for near-roadway assessment was used [15,16].

Micrometeorology data inputs for R-LINE such as temperature, wind speed, wind direction, surface friction velocity, and Monin-Obukhov length were obtained for Redlands Station from a South Coast Air Quality Management District website [17]. As part of the case study time period, the data for Monday May 9, 2016 was used. Source height was assumed to be 2.5 meters (~8.2 ft), which represents a typical height of exhaust stacks of heavy-duty diesel trucks. Receptor height was assumed to be 1 meter (~3.3 ft), which represents an average height of 5 years old children.

5.3.3 Exposure Assessment

In this research, pollutant exposure is referred to the amount of pollutant inhaled by a group of subjects. Therefore, inhaled mass (IM) was used to represent the pollutant exposure, which is calculated as:

$$IM = \mathrm{C} * \mathrm{Pop} * \mathrm{t} * \mathrm{BR} \quad (5.2)$$

where C is pollutant concentration ($\mu g/m^3$) in a given microenvironment; Pop is number of subjects in the microenvironment; t is truck travel time on the road link (hour); and BR is breathing rate (m^3/hour/capita) of the subjects exposed to the pollutant.

Breathing rates of population in different age groups were based on the U.S. EPA's Exposure Factors Handbook [18]. In addition, the California Office of Environmental Health Hazard Assessment's Technical Support Document of Exposure Assessment and Stochastic Analysis included detailed breathing rate scenarios [19]. It is desirable to reduce population exposure to traffic-related air pollutants because tailpipe emissions, such as $PM_{2.5}$ and NO_x, are associated with health risks in young children, older adults, patients,

and even healthy adults [20,21,22,23]. Thus, in this research both population-wide average breathing rate of 15 m^3/day and population-specific breathing rate were applied.

5.3.4 Vehicle Routing Calculation

In previous studies, a weighting method that transformed the multi-objective Vehicle Routing Problem (VRP) [24] into a single-objective VRP was used. The specific methods can be found in a companion study [12]; since there are only four OD pairs, the freeway routes were compared to manually selected alternative routes that have similar travel time.

5.4 Results

5.4.1 Network-Wide Inhalation Values

To model the HDDT running emission, the EMFAC T7 Tractor for model year (MY) 2012 was selected for the modelling scenarios since they were the most common HDDT used for goods transportation in 2018 in the Los Angeles and inland region. $PM_{2.5}$ and NO_x were selected for the primary pollutants for evaluation due to their adverse health and environmental effects; CO_2 emissions were also presented. All scenarios were modelled for a typical workday, with meteorological parameters extracted for 10 A.M. and 3 P.M. on Monday May 9, 2016. Four entry/exit points along the major freeway intersections were selected and one truck stop located near the airport is marked in yellow star in Figure 5.3; it was assumed that a HDDT would enter or exit the study area through one of these four corners. Corner one, two, three and four corresponds to the Northwest, Northeast, Southeast, and Southwest corners of the San Bernardino city area, respectively.

The sensitive receptors for this study include daycares, schools (elementary to high schools), assisted living homes, and public parks. The population data was projected to calendar year 2018 at census block level based on 2010 Census and 2018 American Community Survey. Population at sensitive receptors were estimated based on school enrollment data and census population. Population at residential blocks were estimated based on several sources including population by age groups [12,25], employment data [26,27,28], and school enrollment rate [29,30].

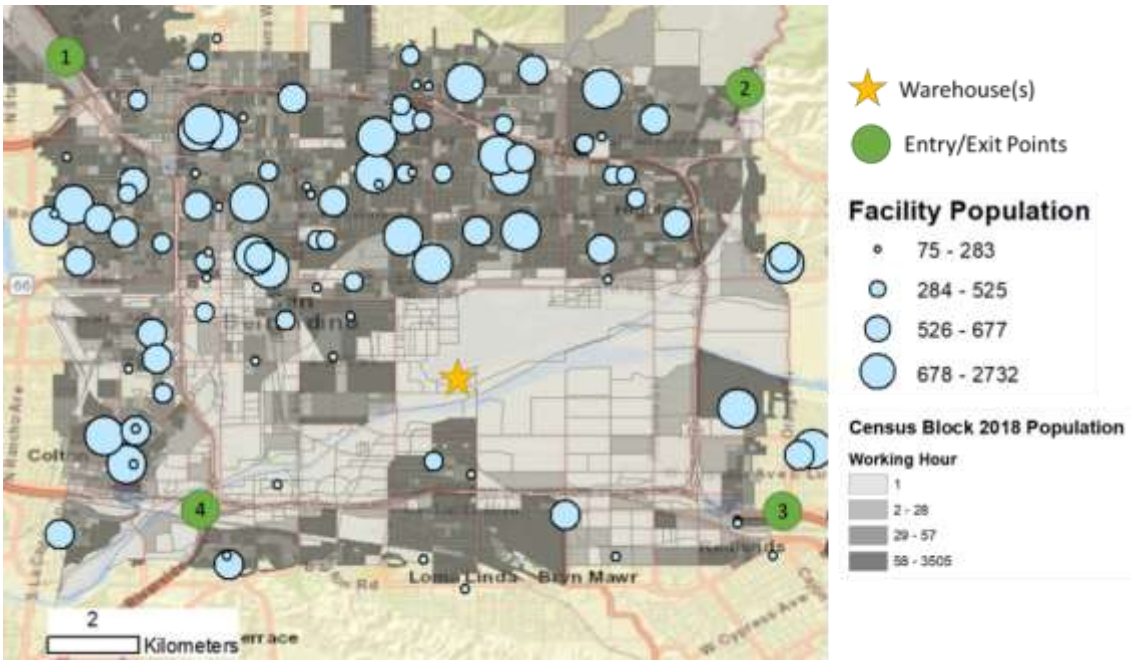

Figure 5.3: Map of population, sensitive receptors, and truck trip attractions in San Bernardino City

Figure 5.4 shows the colored map of modelled $PM_{2.5}$ *IM* values at sensitive receptors and census blocks based on the meteorological conditions at 10 A.M. on May 9, 2016, assuming a population-averaged breathing rate of 15 m^3/day. For instance, a $PM_{2.5}$ *IM* value of 0.23 µg/link means that there would be 0.23 µg of $PM_{2.5}$ inhaled by the nearby population after the truck traversed this roadway link in the given scenario. As air

pollutants from one roadway link can reach multiple facilities/blocks within 1,500 meters, the *IM* values of roadway links are generally higher for those near large sensitive receptors and densely populated census blocks. Figure 5.4 also shows the wind direction, and it can be observed that roadway links upwind of large sensitive receptors and densely populated census blocks generally have higher *IM* values than those downwind.

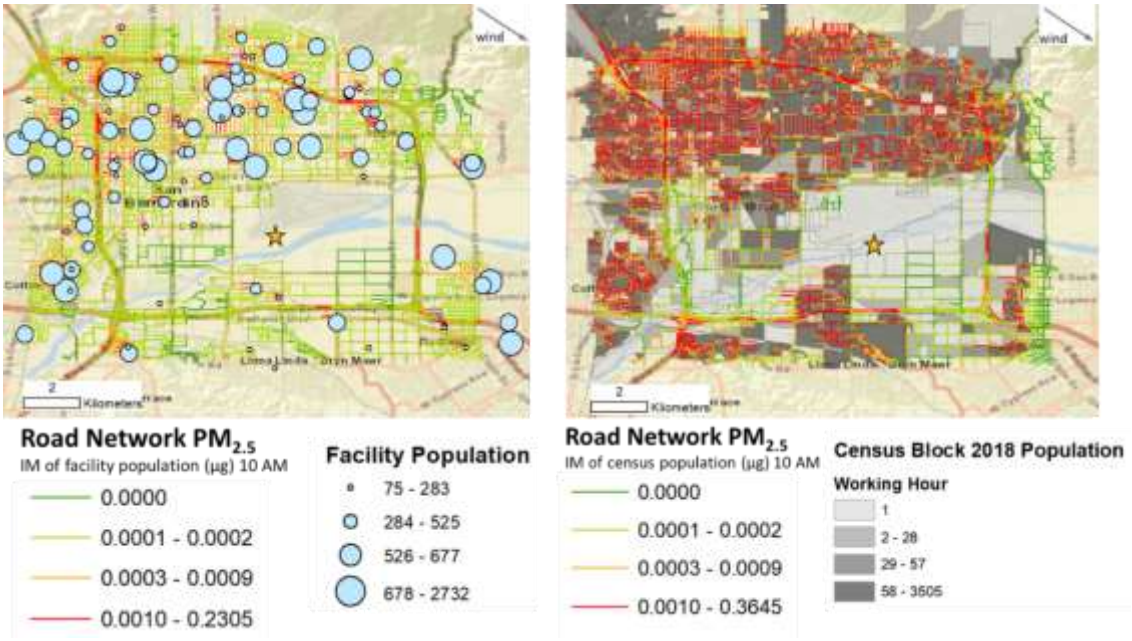

Figure 5.4: Inhaled mass of $PM_{2.5}$ (µg/link) at (left) sensitive receptors and (right) census blocks at 10 A.M. assuming a population-averaged breathing rate of 15 m^3/day.

Figure 5.5 shows the aggregated $PM_{2.5}$ *IM* values from both sensitive receptors and census blocks based on the meteorological conditions at 10 A.M. and 3 P.M. on May 9, 2016, assuming a population-averaged breathing rate of 15 m^3/day. The aggregated $PM_{2.5}$ *IM* values are generally higher at 10 A.M., when compared to that of 3 P.M., due to the more turbulent condition in the afternoon contributes to faster dispersion of air pollutants. The comparison shows how the meteorological conditions can affect the *IM* values.

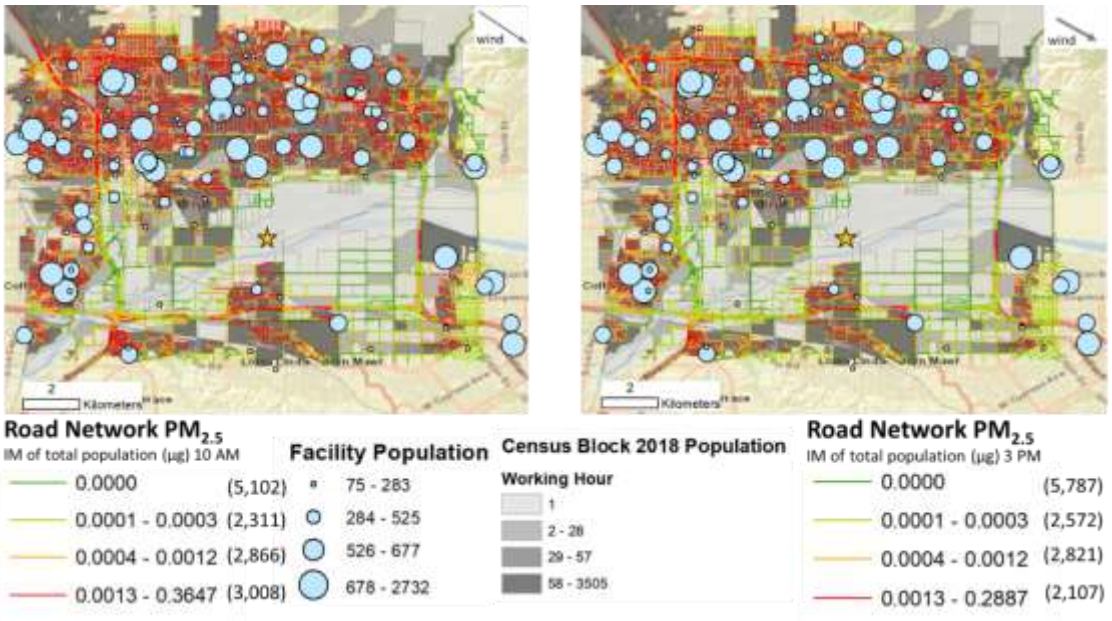

Figure 5.5: Total inhaled mass of $PM_{2.5}$ (µg/link) at 10 A.M. (left) and 3 P.M. (right) assuming a population-averaged breathing rate of 15 m^3/day. The numbers in the parentheses show how many links fall into the corresponding $PM_{2.5}$ IM range.

5.4.2 Low Exposure Routes Comparison

For trips that connect four corners and the warehouse, both a freeway route (FR) and a low exposure route (LER) were determined. The selection methods were based on freeway routes and local street routes that have similar travel time.

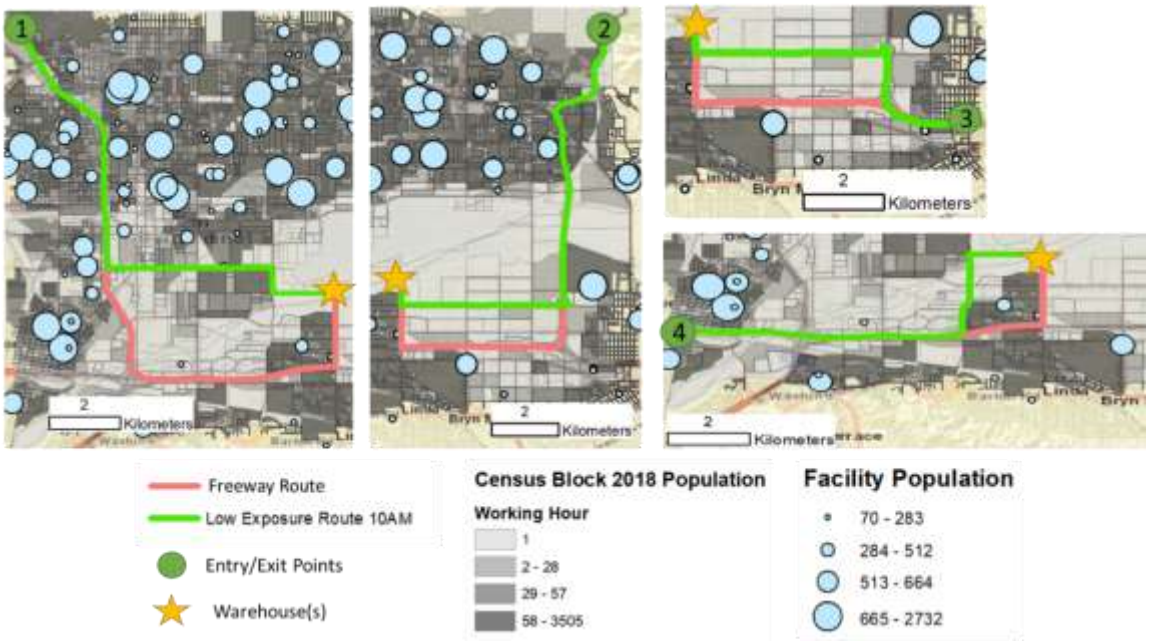

Figure 5.6: FR and LER for an example trip in San Bernardino City for all four corners. Corner 1 (left); Corner 2 (center); Corner 3 (top right); and Corner 4 (bottom right).

Figure 5.6 illustrates an example trip from each of the four corners; the coral routes show the FR, and the green routes show LER. Originating from corner one, the LER selected took Mill Street (left) to the warehouse area. Corner two (center) and three (top right) both took an LER that traveled along San Bernardino Ave to the warehouse area. Lastly, corner four (bottom right) the LER took Tippecanoe Ave to the warehouse area. The comparison of route attributes is summarized in Table 5.1, assuming a population-averaged breathing rate of 15 m^3/day. Generally, the driving distance decreased when choosing the LER over the FR; however, the driving duration only decreased for corners one and four. The largest decrease in CO_2 emissions occurred at corner one's LER, the reduction in CO_2 emissions was 26%; this could be due to the LER diverting the HDDT away from the I-215 and I-10 interchange which consist of bridges and typically higher levels of stop-and-go traffic. The $PM_{2.5}$ inhalation was reduced in every scenario, when

comparing the LER to the FR, by 14%, 29%, 48% and 40% for corner one, corner two, corner three and corner four, respectfully.

NO_x inhalation only reduced in the LER for corners two and three by 28% and 43%, respectfully, with corner one and four seeing an increase in NO_x by 9% and 16%, respectfully. The increase in NO_x inhalation could be due to HDDT being heavy emitters of NO_x with slow stop-and-go driving on arterial roads, increasing the NO_x emission. One possible way to help reduce the NO_x emissions on the LER would be signal controls which could decrease the number of stop-and-go scenarios; future work is needed to investigate this further.

Table 5.1: Comparison of route attributes for an example trip in San Bernardino City at all four corners at 10 A.M., assuming a population-averaged breathing rate of 15 m^3/day.

May 9th 2016, 10 A.M.		Driving Distance (miles)	Driving duration (minutes)	$PM_{2.5}$ IM (µg)	NO_x IM (µg)	CO_2 (kg)
Freeway Route (FR)	Corner 1	11.45	12.99	0.22	21.27	18.65
Low Exposure Route (LER)		8.16	11.32	0.19	23.27	13.73
Freeway Route (FR)	Corner 2	9.36	13.00	0.09	10.14	14.31
Low Exposure Route(LER)		7.99	13.30	0.06	7.34	12.81
Freeway Route (FR)	Corner 3	4.74	7.27	0.05	6.73	8.33
Low Exposure Route(LER)		4.96	9.54	0.03	3.85	8.60
Freeway Route (FR)	Corner 4	5.72	8.13	0.05	6.55	9.95
Low Exposure Route(LER)		5.21	7.94	0.03	7.57	9.08
Percent Difference (LER vs. FR)	Corner 1	-29%	-13%	-14%	9%	-26%
	Corner 2	-15%	2%	-29%	-28%	-10%
	Corner 3	5%	31%	-48%	-43%	3%
	Corner 4	-9%	-2%	-40%	16%	-9%

5.4.2.1 Varying breathing rates

Influence of varying breathing rate were also examined. Two different breathing rate scenarios were applied: an averaged breathing rate of 15 m^3/day, and an age-group specific breathing rates (in m^3/day) as shown in Table 5.2.

Table 5.2: Recommended Mean Point Estimates for Long-Term Daily Breathing Rates [19].

Age group	**0-2**	**2-9**	**2-16**	**16-30**	**16-70**
m^3/day	6.2	10.7	13.3	15	13.9

Table 5.3 shows the inhaled $PM_{2.5}$ and NO_x weighted change for the LER for all four corners at 10 A.M. for the different breathing rate scenarios. Similar to the population averaged breathing rate, the age-group specific breathing rate showed a decrease in $PM_{2.5}$ inhalation for all four corners, and the NO_x inhalation decreased by over 25% for corners two and tree, when compared to the FR. When comparing the population averaged and the age-group specific breathing rates, the $PM_{2.5}$ and NO_x inhalations (in μg) were typically 7% to 15% higher and 8% to 18% higher, respectfully, when using the population averaged breathing rate. However, comparing the percent difference for each corner the two breathing rates only vary by $\pm$ 2% for the $PM_{2.5}$ inhalation with the NO_x inhalation has a slighter larger variation of 7%, -2%, -3% and -2% for corners one, two, three and four, respectfully.

Table 5.3: Comparison of $PM_{2.5}$ and NO_x inhalation based on a population-averaged and age-group specific breathing rates for an example trip in San Bernardino City at all four corners at 10 A.M.

May 9th 2016, 10 A.M.		Population-averaged breathing rate of 15 m^3/day		Age-group specific breathing rates (m^3/day)	
		$PM_{2.5}$ IM (µg)	NO_x IM (µg)	$PM_{2.5}$ IM (µg)	NO_x IM (µg)
Freeway Route (FR)	Corner 1	0.22	21.27	0.19	18.51
Low Exposure Route (LER)		0.19	23.27	0.16	19.02
Freeway Route (FR)	Corner 2	0.09	10.14	0.08	8.92
Low Exposure Route(LER)		0.06	7.34	0.06	6.64
Freeway Route (FR)	Corner 3	0.05	6.73	0.05	5.90
Low Exposure Route(LER)		0.03	3.85	0.03	3.54
Freeway Route (FR)	Corner 4	0.05	6.55	0.04	5.75
Low Exposure Route(LER)		0.03	7.57	0.03	6.76
Percent Difference (LER vs. FR)	Corner 1	-14%	9%	-16%	3%
	Corner 2	-29%	-28%	-28%	-26%
	Corner 3	-48%	-43%	-46%	-40%
	Corner 4	-40%	16%	-40%	18%

Table 5.4 shows the inhaled $PM_{2.5}$ and NO_x weighted change for the LER for all four corners at 3 P.M. for the different breathing rate scenarios. Comparing the 10 A.M. and the 3 P.M. scenarios, at 3 P.M. the $PM_{2.5}$ and NO_x inhalation (in µg) decreased for all four corners. However, the percent difference (LER vs FR) only has noticeable changes for $PM_{2.5}$ inhalation for corners one and two and NO_x inhalation for corners one, two and four.

The comparison between the two breathing rates at 3 P.M. is almost identical to the comparison at 10 A.M. with the only a few differences in the NO_x inhalation. When looking at the inhalations (in µg) the NO_x inhalation is 9% to 19% higher for the population-averaged breathing rate, when compared to the age-group specific breathing rates. Additionally, the percent difference for the NO_x inhalation decreased by 3%, compared to the 2% decrease at 10 A.M., for corner four when comparing the population averaged to the age-group specific breathing rates.

Table 5.4: Comparison of $PM_{2.5}$ and NO_x inhalation based on a population-averaged and age-group specific breathing rates for an example trip in San Bernardino City at all four corners at 3 P.M.

May 9th 2016, 3 P.M.		Population-averaged breathing rate of 15 m^3/day		Age-group specific breathing rates (m^3/day)	
		$PM_{2.5}$ IM (µg)	NO_x IM (µg)	$PM_{2.5}$ IM (µg)	NO_x IM (µg)
Freeway Route (FR)	Corner 1	0.14	13.96	0.13	12.12
Low Exposure Route (LER)		0.13	16.35	0.11	13.29
Freeway Route (FR)	Corner 2	0.06	6.47	0.05	5.68
Low Exposure Route(LER)		0.04	4.88	0.04	4.41
Freeway Route (FR)	Corner 3	0.03	3.87	0.03	3.36
Low Exposure Route(LER)		0.02	2.19	0.01	2.00
Freeway Route (FR)	Corner 4	0.03	3.89	0.02	3.39
Low Exposure Route(LER)		0.02	4.68	0.01	4.18
Percent Difference (LER vs. FR)	Corner 1	-11%	17%	-13%	10%
	Corner 2	-26%	-25%	-25%	-22%
	Corner 3	-48%	-43%	-46%	-40%
	Corner 4	-40%	20%	-40%	23%

Overall, the scenarios suggest that the different breathing rates affect the NO_x inhalation slightly more than the $PM_{2.5}$ inhalation; with the time-of-day variation (10 A.M. vs. 3 P.M.) having a slightly larger impact on the inhalation for both pollutants.

5.4.2.2 $PM_{2.5}$ Correction Factor

Many studies have shown that the gas-particle (G/P) partitioning of the organic $PM_{2.5}$ is important for modelling realistic atmospheric conditions and that a majority of the $PM_{2.5}$ emitted from on-road vehicles is organic $PM_{2.5}$ [28,29,31]. G/P partitioning is a function of temperature, dilution and suspended organic PM mass concentrations, which is dictated by the vehicle emissions and ambient PM. Elemental carbon (EC) is a conservative species, therefore the closer the emitted $PM_{2.5}$ is to pure EC (without any organics) the less important G/P partitioning is; however, organic carbon (OC) behaves differently than the EC and undergoes G/P partitioning. The EC relative to the OC is reported as the elemental carbon to organic carbon (EC:OC) ratio, with the smaller the EC:OC ratio being the more OC, relative to EC, emitted from the HDDT and therefore the more important the G/P partitioning.

As the HDDT exhaust is emitted the plume rapidly dilutes, which leads to the evaporation of the organic $PM_{2.5}$ into organic gases; however, the plume also rapidly cools which leads to the condensation of organic gases into organic $PM_{2.5}$. As part of our research, a correction factor is being developed to help emission and dispersion models better predict near-road $PM_{2.5}$ by accounting for the G/P partitioning that occurs as the vehicle emissions rapidly dilute and cool in the ambient atmosphere [34].

Using the 10 A.M. scenario assuming an ambient temperature of 20°C and that the initial emissions from the HDDT was captured using a dynamometer in series with a constant volume sampler (dilution tunnel) at a sampling temperature of 47°C and sampling dilution ratio of 10. The correction factor was applied to investigate how much the $PM_{2.5}$ would vary accounting for the G/P partitioning that occurred as the exhausted diluted and cooled in the ambient atmosphere (Table 5.5). Based on results from the 200-vehicle study it was assumed the HDDT was a the EMFAC T7 Tractor MY 2014 certified diesel vehicle with a diesel particulate filter and selective catalytic reduction with an EC:OC ratio ranging from 0.05 to 0.25 [35] with the distance from the roadway varying between 1m to 600m.

Table 5.5: $PM_{2.5}$ percent change based on a correction factor accounting for the gas-particle portioning of the volatile organic $PM_{2.5}$ emitted from the HDDT [34].

	Distance (m)	1	5	10	50	100	600
$PM_{2.5}$ Percent Change	**EC:OC of 0.05**	+7%	-44%	-85%	-97%	-100%	-100%
	EC:OC of 0.25	+7%	-31%	-48%	-68%	-75%	-75%

The $PM_{2.5}$ percent change results in Table 5.5 indicate how much EMFAC and RLINE are over- or underestimating the predicted near-road $PM_{2.5}$. For example, at 1m EMFAC and RLINE are underestimating the near-road $PM_{2.5}$ by 8% whereas at 600m they are overestimating between 75% to 100%, depending on the HDDT EC:OC ratio. This is due to EMFAC and RLINE assuming the $PM_{2.5}$ is non-volatile conservative species and therefore are not accounting for the G/P partitioning the volatile organic $PM_{2.5}$ undergoes. At the 1m distance the temperature change between the tailpipe and ambient is dominating resulting in condensation of organic gases into organic $PM_{2.5}$ and the positive $PM_{2.5}$ percent

change. However, as the distance from the roadway increases the effect of dilution starts to dominate, resulting in the organic $PM_{2.5}$ evaporating into organic gases and, consequently, the negative $PM_{2.5}$ percent change. While the $PM_{2.5}$ percent change seems to indicate that evaporation of the organic $PM_{2.5}$ is complete (100m to 600m distances in Table 5.5), over longer timescales the organic $PM_{2.5}$ is expected to age, oxidize and recondense [36]. These results suggest that rerouting trucks at least 10m away from the sensitive receptors and dense populations would reduce the $PM_{2.5}$ inhalation by an additional 50% or more.

5.4.2.3 Travel Delay on a Signalized Corridor

With the proposed LERs on a signalized local corridor, the travel time delay due to stoplights along Mill St. were also investigated. Using Google Maps [37], it was discovered that from corner one to the warehouses the FR had approximately two stops, whereas the LER along Mill St. had approximately twelve possible stops.

To estimate the travel time of a heavy-duty vehicle driving on Mill Street, this study referred to a real-world measurement study [38] during which the local transit bus's emission and trajectory were measured. The bus services San Bernardino City area and the trajectory referenced is on Baseline Street, which is approximately two miles north of Mill Street.

The driving duration between exiting the freeway and arriving at the warehouse were compared. In the original scenario, the HDDT had a driving duration 5.72 minutes on Mill Street. The synthesized speed trajectory scenario estimated that the HDDT had a driving duration of 9.87 minutes, leading to a 4-minute (67%) delay in driving duration.

This delay in driving duration, due to the increased stop-and-go driving at the stoplights, could also increase the fuel usage, the CO_2 emitted, and the NO_x inhalation to the surrounding area. In the future, the goal is to leverage in-use measurement and up-to-date microscopic emission model to evaluate the emission changes. To mitigate the increasing driving time and the emissions from stop-and-go events, the use of vehicle and signal control technologies have shown promising results [39,40].

5.4.2.4 Safety

When redirecting heavy duty trucks to other streets, safety concerns always arise if it will increase the number of collisions on the streets. Historical collision data [41] from 2009 through 2019 on Mill were collected and is shown in Figure 5.7.

Figure 5.7: Historical vehicle collision map in Corner 1 LER, Mill Street.

The number of collisions by involved party is summarized in Figure 5.8. Looking at Figure 5.8, it showed that after 2013 and 2014, the number of total collisions increased significantly, and the trend continued to 2019. It can also be seen that most of the collisions are passenger vehicle related. From 2009 to 2019, 13 out of the 120 collisions involved a truck. In order to improve both safety and mobility, there needs to be a combination of

technology improvements, such as improved visibility as well as signal controls, and education to reduce collisions.

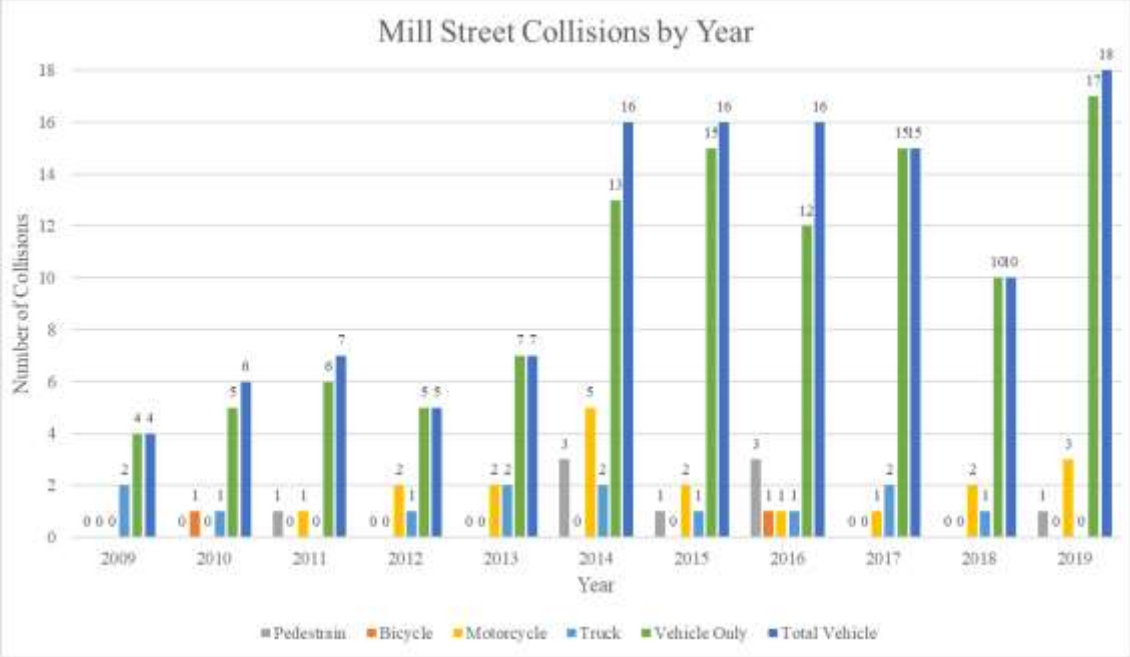

Figure 5.8: Summary the number of collisions by involved party type on Mill Street.

5.4.3 Weighted Results based on Truck Flow Analysis

Truck flow between each corner and the warehouse were estimated so that a truck flow weighted comparison of the route attributes between the freeway route and low exposure routes in the San Bernardino City could be analyzed. The truck flow data was obtained by using the Caltrans Performance Measurement System (PeMS) truck flow at mainline loop detector stations (LDS) [42] for June 2020. To find the number of trucks entering and exiting from the four corners was estimated using a proportional truck flow as well as the truck flow from the corresponding corner. Figure 5.9 shows the number of trucks coming inbound from the corresponding corner and going to the warehouse and the

number of trucks going outbound from the warehouse to the corresponding corner at both 10 A.M and 3 P.M.

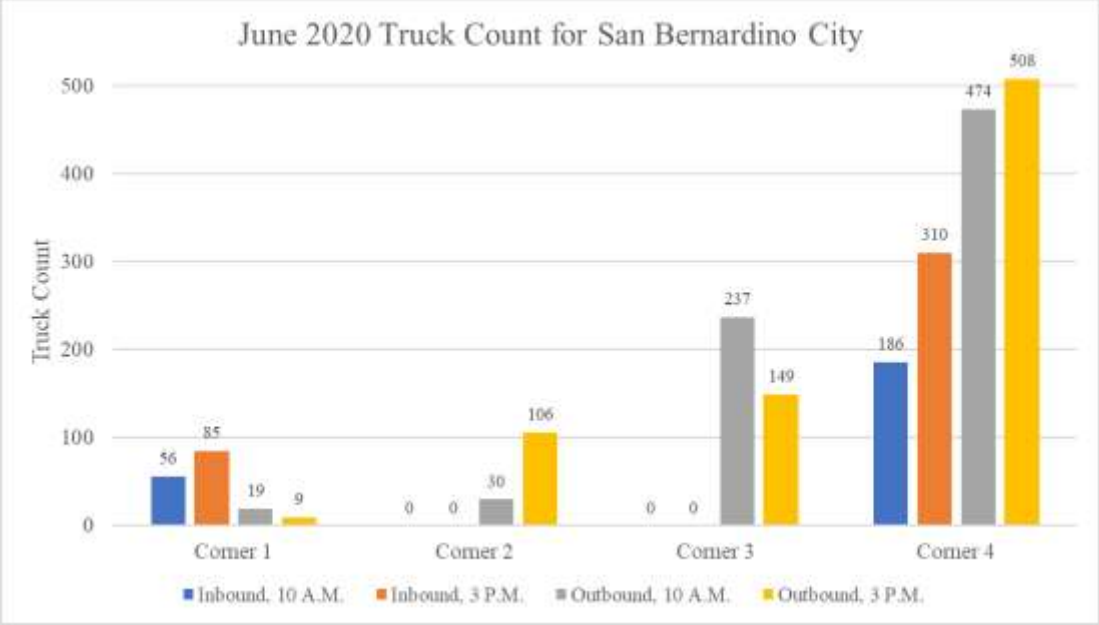

Figure 5.9: Summary of inbound and outbound truck count for all for corners in June 2020

Table **5.6** shows the weighted change of the LER for all four corners at 10 A.M. (top) and 3 P.M. (bottom), including the trucks heading outbound from all four corners and inbound from corners one and four. The overall, as compared with the FR at 10 A.M., the LER would be 5% longer in travel time, but would reduce distance by 7%, $PM_{2.5}$ inhalation by 54%, NO_x inhalation by 43%, and CO_2 by 7%. Whereas at 3 P.M. the overall, as compared with the FR, the LER would be 1% longer in travel time, but would reduce distance by 9%, $PM_{2.5}$ inhalation by 47%, NO_x inhalation by 32%, and CO_2 by 9%. The $PM_{2.5}$ values presented in Table 5.6 does not account for the $PM_{2.5}$ correction factor, future work will look at implementing the correction factor over the whole network.

Table 5.6: Summary of route attributes based on truck flow at 10 A.M. (top) and 3 P.M. (bottom), assuming an averaged breathing rate of 15 m^3/day

June 2020 Truck Flow at 10AM

MY 2012 10am		Freeway Route					Low Exposure Route					Difference (v.s. Freeway Route)				
Corner #	No. of Trucks	Driving Distance (miles)	Driving duration (min)	$PM_{2.5}$ IM (ug)	NOx IM (ug)	CO_2 (kg)	Driving Distance (miles)	Driving duration (min)	$PM_{2.5}$ IM (ug)	NOx IM (ug)	CO_2 (kg)	Driving Distance (miles)	Driving duration (min)	$PM_{2.5}$ IM (ug)	NOx IM (ug)	CO_2 (kg)
1 Inbound	56	641.34	727.51	12.14	1191.23	1044.42	456.90	633.66	10.48	1303.18	769.03	-184.44	-93.86	-1.66	111.95	-275.39
1 Outbound	19	202.16	233.29	4.38	430.55	330.89	143.80	203.47	3.97	478.26	242.90	-58.36	-29.82	-0.41	47.71	-87.99
2 Outbound	30	280.68	389.99	2.64	304.25	429.17	239.64	399.15	1.88	220.22	384.31	-41.05	9.15	-0.76	-84.03	-44.86
3 Outbound	237	1122.50	1722.28	12.65	1594.75	1973.66	1174.77	2260.36	6.64	912.72	2038.62	52.28	538.07	-6.01	-682.03	64.96
4 Inbound	186	1064.18	1511.84	8.76	1218.59	1851.44	969.34	1476.62	5.24	1408.27	1688.25	-94.84	-35.22	-3.53	189.68	-163.19
4 Outbound	474	2528.72	3387.33	20.56	2909.19	4328.83	2436.82	3369.99	0.20	49.80	4131.14	-91.90	-17.34	-20.35	-2859.39	-197.69
Total	1002	5840	7972	61	7649	9958	5421	8343	28	4372	9254	-418.31	370.99	-32.72	-3276.11	-704.17
												-7%	5%	-54%	-43%	-7%

June 2020 Truck Flow at 3PM

MY 2012 3pm		Freeway Route					Low Exposure Route					Difference (v.s. Freeway Route)				
Corner #	No. of Trucks	Driving Distance (miles)	Driving duration (min)	$PM_{2.5}$ IM (ug)	NOx IM (ug)	CO_2 (kg)	Driving Distance (miles)	Driving duration (min)	$PM_{2.5}$ IM (ug)	NOx IM (ug)	CO_2 (kg)	Driving Distance (miles)	Driving duration (min)	$PM_{2.5}$ IM (ug)	NOx IM (ug)	CO_2 (kg)
1 Inbound	85	973.47	1104.26	12.24	1186.68	1585.29	693.51	961.80	10.94	1389.86	1167.28	-279.95	-142.46	-1.29	203.18	-418.01
1 Outbound	9	95.76	110.51	1.39	135.33	156.74	68.11	96.38	1.29	158.80	115.06	-27.65	-14.12	-0.10	23.47	-41.68
2 Outbound	106	991.74	1377.98	5.96	685.56	1516.41	846.71	1410.32	4.41	516.85	1357.90	-145.03	32.34	-1.55	-168.72	-158.51
3 Outbound	149	705.70	1082.79	4.41	577.00	1240.82	738.57	1421.07	2.30	326.22	1281.66	32.87	338.28	-2.11	-250.78	40.84
4 Inbound	310	1773.63	2519.74	8.66	1205.19	3085.73	1615.56	2461.04	5.18	1450.64	2813.75	-158.06	-58.70	-3.49	245.45	-271.98
4 Outbound	508	2710.10	3630.31	13.27	1883.63	4639.34	2611.61	3611.72	0.13	33.37	4427.46	-98.49	-18.59	-13.14	-1850.26	-211.87
Total	1167	7250.40	9825.58	45.93	5673.39	12224.32	6574.09	9962.33	24.25	3875.73	11163.11	-676.32	136.76	-21.68	-1797.66	-1061.21
												-9%	1%	-47%	-32%	-9%

When comparing the 10 A.M. (Table 5.6 top) to 3 P.M. (Table 5.6 bottom), the 10 A.M. scenarios had a greater $PM_{2.5}$ and NO_x inhalation reduction. The higher reduction in $PM_{2.5}$ and NO_x inhalation at 10 A.M. could be due to the atmosphere being more static in the morning allowing for a higher pollutant build-up (Figure 5.5), therefore a bigger impact on the reduction, when compared to 3 P.M. This time-of-day effect can also be applied to reduce population inhalation as fleet operations.

5.5 Discussion & Conclusions

The main objective of this research was to evaluate the exposure-based routing in the San Bernardino Airport area. This research evaluated the potential HDDT trips from the major freeway junctions to and from the airport and compared the travel time, distance, and inhalation values. The following summarizes the finding in this work:

1) At 10 A.M. the LERs, for all four corners, showed a decrease in the $PM_{2.5}$ inhalation and corners two and three see a decrease in NO_x inhalation.

The LER for corner one (11.32 minutes) takes less time than the freeway route (12.99 minutes) and was significantly more fuel efficient than the freeway route (26% decrease in CO_2 emissions), given the assumption of constant speed on signalized street. The $PM_{2.5}$ inhalation was also reduced by 14% when taking the LER over the FR for corner one. This reduction in $PM_{2.5}$ inhalation could increase by an additional 50+% by selecting LERs that are over 10m from the sensitive receptors, and when accounting for the $PM_{2.5}$ correction factor and therefore the G/P partitioning of the organic $PM_{2.5}$. Furthermore, the latest Google Maps and land use data show that there are few residential houses but mostly commercial zone directly adjacent to Mill Street, making it appropriate for truck route. However, for LER, when considering stop-and-go activities on Mill Street, it was estimated that the HDDT would have approximately 4-minutes delay in driving duration, which also means increased fuel and pollutant emissions. It requires microscopic emission model to analyze the speed trajectories on both signalized street and freeway to determine the emissions, which is highly dynamic in real world. In future work, a portable emission measurement system can be used to assess in-use emissions. In addition, the stop-and-go activities on signalized street can be minimized with smart technologies such as Freight Signal Priority [39,40] and Eco Approach and Departure [43].

2) The comparison between the population-averaged breathing rate of 15μg/m^3 and an age-group specific breathing shows that the varying breathing rates slightly affects the inhalation. The NO_x inhalation was affected more than the $PM_{2.5}$

inhalation. A time-of-day comparison between 10 A.M. and 3 P.M. was also done and found that the time-of-day has a slightly larger impact on the inhalation than the different breathing rates. The comparison of the $PM_{2.5}$ inhalation based on varying breathing rate does not account for the $PM_{2.5}$ correction factor, future work will look at implementing the correction factor along with the varying breathing rates.

3) The weighted results based on truck flow analysis shows that at 10 A.M. there is a greater reduction in $PM_{2.5}$ and NO_x inhalation, 54% and 43%, respectfully, when compared to the 3 P.M. scenario. This time-of-day effect can also be applied to reduce population inhalation as fleet operations. However, at 3 P.M. there is a greater reduction in CO_2 emissions which could be due to there being more HDDT traveling to the warehouse at 3 P.M. leading to larger weighted reduction, when compared to 10 A.M.. The weighted $PM_{2.5}$ inhalation results does not account for the $PM_{2.5}$ correction factor, future work will look at implementing the correction factor over the whole network.

These results suggest that effectiveness of the exposure-based routing depends on time of day and vary based on the population of residences and sensitivity receptors. Overall, the results demonstrate the potential for the exposure-based routing strategy to help mitigate the impacts of truck emission on a disadvantaged community.

Increased vehicle collisions along the LERs are also a concern and could be reduced with technology and education. Future work needs to be done to help mitigate the safety

concerns along the LERs. Some recommendations for the city and airport authority would include:

1) Meet with the freight transportation companies and discuss the frequent routes used.
2) Comprehensively inspects and improve the street sections for visibility (e.g., obstruction, signages, surface marking etc.) and mobility (e.g., potholes, pavement condition, traffic signal timing, etc.) issues to better accommodate future increase of heavy-duty vehicles.
3) Seek guidance and sponsorship through various funding resources [4,5,6]. Meet and inform the business and residents along the streets that will be impacted most. Provide education and support to improve their environmental health and safety.
4) Collect city-level data, for instance, total volume and heavy-duty vehicle volume by time of day at key locations and use them for future decision making.

5.6 Acknowledgment

The authors would like to acknowledge the California Strategic Growth Council for supporting this research as part of the Climate Smart Transportation and Communities Consortium effort. The authors would also like to thank Prof. JR DeShazo and Prof. Karthick Ramakrishnan and their teams for their valuable inputs. The contents of this paper reflect the views of the authors who are responsible for the facts and the accuracy of the data presented herein. The contents do not necessarily reflect the official views of or policy of the sponsor. This paper does not constitute a standard, specification, or regulation.

5.7 References

1. California Air Resources Board (2012). Diesel Particulate Matter Health Impacts. https://ww2.arb.ca.gov/resources/summary-diesel-particulate-matter-health-impacts#:~:text=As%20a%20significant%20fraction%20of,illnesses%2C%20and%20even%20premature%20death.
2. Wilson, S. J., Miller, M. R., & Newby, D. E. (2018). Effects of Diesel Exhaust on Cardiovascular Function and Oxidative Stress. *Antioxidants and Redox Signaling*, *28*(9), 819–836. https://doi.org/10.1089/ars.2017.7174
3. Poorfakhraei, A., Tayarani, M., & Rowangould, G. (2017). Evaluating health outcomes from vehicle emissions exposure in the long range regional transportation planning process. In *Journal of Transport and Health* (Vol. 6, pp. 501–515). https://doi.org/10.1016/j.jth.2017.05.177
4. California Environmental Protection Agency (2018). California Climate Investments to Benefit Disadvantaged Communities. https://calepa.ca.gov/envjustice/ghginvest/
5. California Legislative Information (2016). Assembly Bill No. 1550 Greenhouse gases: investment plan: disadvantaged communities. https://leginfo.legislature.ca.gov/faces/billNavClient.xhtml?bill_id=201520160AB1550
6. California Air Resources Board (2017c). Community Air Protection Program. https://ww2.arb.ca.gov/capp/about

7. Amazon Air Regional Air Hub (2019). Air Cargo Development at SBD International Airport. https://www.sbdairport.com/facilities-amenities/amazon-air-regional-air-hub/
8. San Bernardino Airport Communities (2020). https://sbairportcommunities.org/home
9. California Office of Environmental Health Hazard Assessment (2018). ArcGIS Online. SB 535 Disadvantaged Communities. https://oehha.maps.arcgis.com/apps/View/index.html?appid=c3e4e4e1d115468390cf61d9db83efc4
10. South Coast AQMD (2018). AB 617 - 2018-Designated Communities. http://www.aqmd.gov/nav/about/initiatives/environmental-justice/ab617-134/san-b
11. Boriboonsomsin, K. (2020). California Air Resources Board Project. Geofencing as a Strategy to Lower Emissions in Disadvantaged Communities. https://ww3.arb.ca.gov/research/single-project.php?row_id=68793
12. Luo, J., Barth, M.J. and Boriboonsomsin, K. (2018). Vehicle Routing to Mitigate Human Exposure to Traffic-Related Air Pollutants. In 2018 21st International Conference on Intelligent Transportation Systems (ITSC) (pp. 2765-2770). IEEE
13. California Air Resources Board (2017a). EMFAC2017 Web Database. https://arb.ca.gov/emfac/2017/
14. California Air Resources Board (2017b). MSEI - Modeling Tools - EMFAC Software and Technical Support Documentation. https://ww2.arb.ca.gov/our-

work/programs/mobile-source-emissions-inventory/road-documentation/msei-modeling-tools-emfac

15. Snyder, M. G. and Heist, D. K. (2013). User's Guide for R-LINE Model Version 1.2. https://www.cmascenter.org/r-line/documentation/1.2/RLINE_UserGuide_11-13-2013.pdf.
16. Community Modeling and Analysis System (2013). R-LINE Version 1.2. Available: https://www.cmascenter.org/r-line/
17. South Coast Air Quality Management District (2019). Meteorological Data for AERMOD. http://www.aqmd.gov/home/air-quality/meteorological-data/data-for-aermod.
18. U.S. Environmental Protection Agency (2011). Exposure Factors Handbook: 2011 Edition, September.
19. California Office of Environmental Health Hazard Assessment (2012). Technical Support Document for Exposure Assessment and Stochastic Analysis, August 2012. https://oehha.ca.gov/air/crnr/notice-adoption-technical-support-document-exposure-assessment-and-stochastic-analysis-aug
20. Gong Jr., H., W. S. Linn, S. L. Terrell, K. R. Anderson, K. W. Clark, C. Sioutas, W. E. Cascio, N. Alexis, and R. B. Devlin (2004). Exposures of elderly volunteers with and without chronic obstructive pulmonary disease (COPD) to concentrated ambient fine particulate pollution. Inhalation Toxicology, 16(11-12), 731-744.

21. Lim, Y. H., Kim, H., Kim, J. H., Bae, S., Park, H. Y., & Hong, Y. C. (2012). Air Pollution and Symptoms of Depression in Elderly Adults. *Environmental Health Perspectives*, *120*(7), 1023–1028. https://doi.org/10.1289/ehp.1104100
22. Grineski, S. E., Clark-Reyna, S. E., & Collins, T. W. (2016). School-based exposure to hazardous air pollutants and grade point average: A multi-level study. *Environmental Research*, *147*, 164–171. https://doi.org/10.1016/j.envres.2016.02.004
23. Salvi, S. (2007). Health effects of ambient air pollution in children. *Paediatric Respiratory Reviews*, *8*(4), 275–280. https://doi.org/10.1016/j.prrv.2007.08.008
24. Weichenthal, S., R. Kulka, P. Bélisle, L. Joseph, A. Dubeau, C. Martin, D. Wang, and R. Dales (2012). Personal exposure to specific volatile organic compounds and acute changes in lung function and heart rate variability among urban cyclists. Environmental Research, 118, 118-123.
25. U.S. Bureau of Labor Statistics (2017a). Monthly Labor Review. https://www.bls.gov/opub/mlr/2017/article/occupational-choices-of-the-elderly.htm
26. U.S. Bureau of Labor Statistics (2017b). Older Workers: Labor force trends and career options. https://www.bls.gov/careeroutlook/2017/article/older-workers.htm
27. Population Demographics for California 2020, 2019 (2020). https://suburbanstats.org/population/how-many-people-live-in-california
28. U.S. Bureau of Labor Statistics (2020). American Time Use Survey. https://www.bls.gov/tus/

29. Slate. The Day Care Dilemma (2013). https://slate.com/human-interest/2013/08/day-care-in-the-united-states-is-it-good-or-bad-for-kids.html
30. National Center for Education Statistics. Child Care (2019). https://nces.ed.gov/fastfacts/display.asp?id=4
31. May, A. A., Presto, A. A., Hennigan, C. J., Nguyen, N. T., Gordon, T. D., & Robinson, A. L. (2013a). Gas-particle partitioning of primary organic aerosol emissions: (1) Gasoline vehicle exhaust. Atmospheric Environment, 77, 128–139. https://doi.org/10.1016/j.atmosenv.2013.04.060
32. May, A. A., Presto, A. A., Hennigan, C. J., Nguyen, N. T., Gordon, T. D., & Robinson, A. L. (2013b). Gas-particle partitioning of primary organic aerosol emissions: (2) diesel vehicles. Environmental Science & Technology, 47(15), 8288–8296.
33. Robinson, A. L., Grieshop, A. P., Donahue, N. M., & Hunt, S. W. (2010). Updating the Conceptual Model for Fine Particle Mass Emissions from Combustion Systems. Journal of the Air & Waste Management Association, 60(10), 1204–1222. https://doi.org/10.3155/1047-3289.60.10.1204
34. Moretti A, Cocker D, Barth M (2021). Improved Prediction of Near-Road Vehicle Emissions for Gasoline and Diesel Vehicles Between Emission Simulators and Measured Data from PEMS and Laboratory Measurements. American Association for Aerosol Research - Abstract Submission. October 2021. http://aaarabstracts.com/2021/viewabstract.php?pid=222

35. University of California, Riverside. 200 Vehicle Study. https://www.cert.ucr.edu/200-vehicle-study
36. Robinson, A. L., Donahue, N. M., Shrivastava, M. K., Weitkamp, E. A., Sage, A. M., Grieshop, A. P., Lane, T. E., Pierce, J. R., & Pandis, S. N. (2007). Rethinking Organic Aerosols: Semivolatile Emissions and Photochemical Aging. Science, 315(March), 1259–1262. https://doi.org/10.1126/science.1133061
37. Google Maps (2021). https://maps.google.com
38. McCaffery C, Zhu H, Tang T, Li C, Karavalakis G, Cao S, Oshinuga A, Burnette A, Johnson KC, Durbin TD (2021). Real-world NO_x emissions from heavy-duty diesel, natural gas, and diesel hybrid electric vehicles of different vocations on California roadways. Sci Total Environ. 2021 Aug 25;784:147224. doi: 10.1016/j.scitotenv.2021.147224. Epub 2021 Apr 20. PMID: 33905931.
39. Kari, D., Wu, G. and Barth, M.J., (2014). Eco-friendly freight signal priority using connected vehicle technology: a multi-agent systems approach. In 2014 IEEE Intelligent Vehicles Symposium Proceedings (pp. 1187-1192). IEEE.
40. Guo, G. and Wang, Y., (2021). Eco-driving of freight vehicles with signal priority on congested arterial roads. IEEE Transactions on Vehicular Technology.
41. UC Berkeley (2020). Transportation Injury Mapping System. https://tims.berkeley.edu/.
42. California Department of Transportation (2020). Caltrans Performance Measurement System (PeMS). I-10W Truck Flow. http://pems.dot.ca.gov/?report_form=1&dow_0=on&dow_1=on&dow_2=on&do

w_3=on&dow_4=on&dow_5=on&dow_6=on&tod=all&tod_from=0&tod_to=0&holidays=on&agg=on&s_time_id=1590969600&e_time_id=1593561540&dnode=Freeway&fwy=10&dir=W

43. Hao, P., G. Wu, K. Boriboonsomsin, and M. J. Barth (2018). Eco-approach and departure (EAD) application for actuated signals in real-world traffic. IEEE Transactions on Intelligent Transportation Systems, Vol. 20, No. 1, 2018, pp. 30-40.

Chapter 6. Conclusions

One way that researchers can better predict near-road $PM_{2.5}$ and therefore human exposure is through the use of emission simulators; however, the predicted $PM_{2.5}$ from emission simulators is not in agreement with measured $PM_{2.5}$ from near-road studies. This dissertation bridged the gap between predicted and measured near-road $PM_{2.5}$ by creating a $PM_{2.5}$ correction factor that accounts for the gas-particle portioning that the organic $PM_{2.5}$ undergoes as it dilutes and cools in the ambient atmosphere.

Chapter 2 applied two statistical models to examine the relationship among the weather parameters, traffic data, and the near-freeway air pollutant concentration of $PM_{2.5}$ and NO_2 at two different near-road air monitoring stations in Southern California. Both statistical models showed that all weather parameters were significant variables, however the significance of traffic data depended on the air monitoring station location and pollutant of concern. Traffic data correlated better with near-freeway NO_2 concentrations than the $PM_{2.5}$ concentrations; this could be due to organic $PM_{2.5}$ undergoing gas-particle partitioning as it rapidly dilutes and cools in the ambient atmosphere. To better predict the near-road air pollutant concentrations the following recommendations are made: include heavy-duty diesel truck flow; measure ambient background $PM_{2.5}$; account for the gas-particle partitioning of the organic $PM_{2.5}$.

Chapter 3 developed a $PM_{2.5}$ correction factor based on the gas-particle partitioning of the organic aerosols emitted from on-road gasoline and diesel vehicles. Results indicate CF is sensitive to the sampling dilution & temperature (from the PEMS and dynamometers), ambient temperature and background $PM_{2.5}$, distance from the vehicle, and the vehicles

EC/TC ratio, and shows that there is a bias in predicted roadside $PM_{2.5}$ using the current transportation models.

Chapter 4 developed a look-up table and random forest models based off the correction factor developed in Chapter 3. In building the random forest generally the ambient temperature, vehicle's EC:OC and initial reactive organic gas (ROG_i) concentration were determined to be the most important variables for predicting the CF. The correction factor can be coupled with emission simulators or dispersion models to better predict near-road $PM_{2.5}$ and inhaled mass. The suggested future work for the $PM_{2.5}$ correction factor is to broaden the fuel types and types of vehicles, such as light duty diesel vehicles and natural gas vehicles to better predict a wide range of vehicle emitted $PM_{2.5}$. The correction factor should also be validated by direct measurement--the correction factor was built based on established science but field measurements and/or lab measurements would verify the results.

Chapter 5 evaluated the potential heavy-duty diesel truck trips from major freeway junctions to and from the airport and compared the travel time, distance, and inhalation values in a disadvantaged community as well as showed how the correction factor developed in Chapters 3 and 4 could be applied. Results suggest that effectiveness of the exposure-based routing depends on time of day and vary based on the population of residences and sensitive facilities. Implementing the correction factor, developed in Chapters 3 and 4, showed that when the gas-particle partitioning was considered that the emission simulator and dispersion model was underestimating the near-road $PM_{2.5}$ by 8% when 1m from the roadway and overestimating between 38% to 100% for 5m-600m from

the roadway. The $PM_{2.5}$ estimates suggest that rerouting trucks at least 100m away from the sensitive receptors and dense populations would reduce the $PM_{2.5}$ inhalation by an additional 75% or more. Overall, the results demonstrate the potential for the exposure-based routing strategy to help mitigate the impacts of truck emission on a disadvantaged community. The suggested future work is to investigate, with a portable emission measurement system, how the NO_x and/or $PM_{2.5}$ varies on atrial roads (with the slower speeds and higher stop-and-go scenarios) to see if the low exposure routes reduce the pollutant inhalation in real-world scenarios.

Appendix A introduces a new oxidation instrument that was built for the laboratory, the oxidation flow reactor (OFR). A preliminary experiment using α-pinene was conducted and showed that the OFR had comparable SOA produced, to that of Chhabra et al. 2010. Further work needs to be done to further optimize the OFR including flow simulation, examining wall loss, and varying the power supplied to the UV lamps and RH to understand how they affect the mixing ratios of O_3, OH and HO_2 generated inside the OFR.

The research presented in this dissertation is critical in understanding how vehicle emissions interact with the ambient air, immediately after being emitted, which can greatly improve our understanding of how vehicle emissions affect human health, air quality, and the environment. Currently, emission simulators are treating all $PM_{2.5}$ as non-volatile and are therefore not adjusting the $PM_{2.5}$ based on the gas-particle partitioning; this leads to emission simulators and dispersion models being unable to accurately predict the near-road $PM_{2.5}$. Implementing the correction factor with emission simulators and/or dispersion

models would allow for a more realistic $PM_{2.5}$ concentration thereby improving estimates of human exposure to $PM_{2.5}$.

Appendix A: Oxidation Flow Reactor

A.1 Abstract

This chapter introduces a new instrument, an oxidation flow reactor (OFR), built and initially characterized for the Atmospheric Process Lab to evaluate gas-phase chemical reactions leading to particulate formation. The OFR was built in 2018 and is a vertical cylindrical stainless steel continuous flow reactor, with a volume of ~14L and a nominal flow rate of 5LPM. A preliminary OFR experiment was ran with α-pinene to test the feasibility of the OFR. Comparing the HR-ToF-AMS m/z fragment table from the preliminary experiment to Chhabra et al. 2010 (Figure A.2) shows that the secondary organic aerosol (SOA) produced from the OFR is comparable to the SOA produced from Chhabra et al. 2010. The preliminary results indicate that the α-pinene is being oxidized by OH within the OFR. An initial OH calibration experiment was conducted by measuring the decay of benzene due to the reaction with OH; it was estimated that the OH exposure inside the OFR is about $1.33*10^{12}$ molecules s cm^{-3} ($7.8*10^{9}$ molecules cm^{-3}). This OH exposure level corresponds to about 10 days of atmospheric oxidation, assuming typical atmospheric OH levels of $1.5*10^{6}$ molecules cm^{-3}. Since the OFR was built my research went in another direction leading to me to be unable to optimize the OFR. However, the OFR has been a useful instrument within the laboratory for others to use, uses include being used as a radical source, additional aging, and to help understand additional influences on the particle composition.

A.2 Introduction

Organic aerosol (OA) accounts for ~20% to 90% of the aerosol mass in the lower troposphere [1]. Secondary OA (SOA) production is typically studied in environmental smog chambers. These smog chambers are large batch-style Teflon bags with volumes up to 90m^3 and residence times of several hours. Smog chambers are designed to simulate SOA formation and further oxidation within the atmosphere; however, they are not designed to track the fast changes of precursor gases due to their large volumes and therefore long response times [2]. An alternative approach is a direct, fast measurement of the aerosol formation potential using a small chamber, the oxidation flow reactor.

The concept of the Oxidation Flow Reactor (OFR) is that all precursor gases are rapidly oxidized with extreme amounts of oxidants resulting in aerosol formation [2]. Due to the highly oxidizing environment inside the OFR, it simulates atmospheric oxidation on a timescale ranging from a day to several days in a few minutes [2,3]; thus, allowing the OFR to produce atmospheric levels of oxidation that are not possible in the traditional environmental smog chambers [4].

A.3 Building the Oxidation Flow Reactor

The OFR was built in 2018 and is a vertical cylindrical stainless steel continuous flow reactor, with a volume of ~14L and a length of 46cm and a diameter of 20cm, a schematic diagram of the OFR is shown in Figure A.1. The flow rate through the chamber is 5LPM which gives a residence time of 170s; however, since the OFR does not exhibit a plug flow behavior; therefore, the outflow consists of a mix of residence times [2,5]

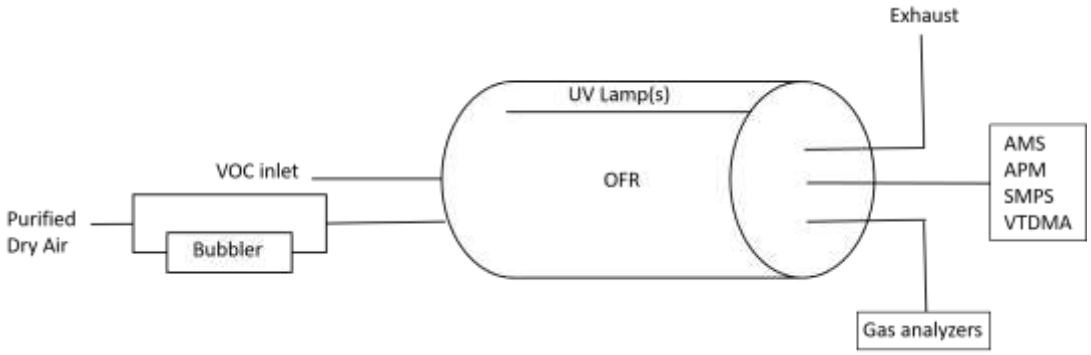

Figure A.1: Schematic diagram of the OFR chamber setup

There are 1-4 UV lamps inside of the OFR, the UV lamps are low pressure Hg lamps which produces mainly 185nm and 254nm light. OH radicals are generated inside the OFR due to the photolysis of water ($H_2O + hv(185\text{nm}) \rightarrow OH + H$) [6]. The water is introduced into the OFR by passing some of the purified dry air though a bubbler while the majority bypasses the bubbler to create the desired relative humidity. O_3 is also formed inside the OFR due to O_2 photolysis (Reaction A.1) with the amount of OH formed (n) depending on the amount of H_2O in the OFR [11].

Reaction A.1: OH and O_3 production inside the OFR [6]

$$O_2 \xrightarrow{hv\ (185\text{nm})} 2O(^3P) \xrightarrow{O_2} 2O_3 \xrightarrow{hv(254\text{nm})} 2O(^1D) \xrightarrow{H_2O} n\text{OH}$$

A.4 Results

A preliminary OFR experiment was ran with α-pinene to test the feasibility of the OFR. The preliminary experiment used: a Scanning Mobility Particle Sizer (SMPS) to measure the size distribution and number concentration [7], the Aerosol Particle Mass Monitor (APM, Kanomax) in series with an SMPS to measure particle effective density

[8], and the Aerodyne high-resolution time-of-flight Aerosol Mass Spectrometer (HR-ToF-AMS) to get the bulk chemical composition of organic particulates [9]. The goal of the preliminary experiment was to see if the α-pinene was reacting with the OH to produce SOA. The APM calculated a density of 1.4 g cm^{-3}, which is in agreement with the assumed SOA density. Comparing the HR-ToF-AMS m/z fragment table from the preliminary experiment to Chhabra et al. 2010 (Figure A.2) shows that the SOA produced from the OFR is comparable to the SOA produced from Chhabra et al. 2010 [10]. These results indicate that the α-pinene is being oxidized by OH inside the OFR.

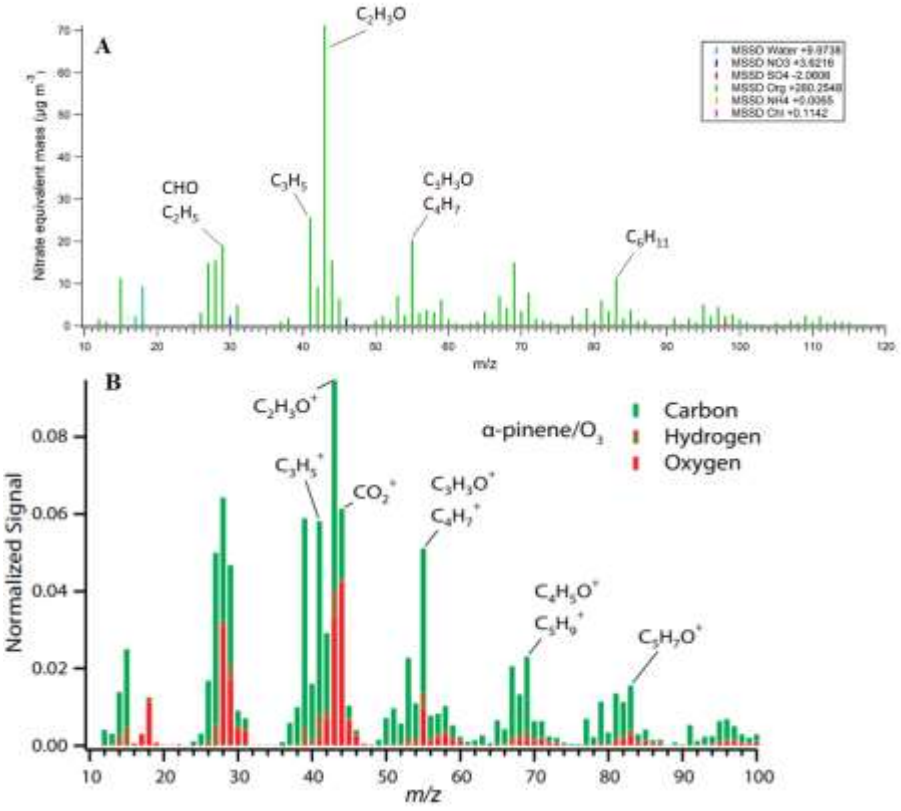

Figure A.2: M/Z fragment table for a-pinene. A) α-pinene/OH experiment from the OFR and B) α-pinene/O_3 experiment from Chhabra et al. 2010 [10]

The SOA likely comes from the reaction of OH with α-pinene, due to the reaction of α-pinene by O_3 being relatively slow compared to the reaction of α-pinene by OH. The rate constants of α-pinene with OH and O_3 are about $5.5*10^{-11}$ molecule^{-1} cm^3 s^{-1} and $8.2*10^{-17}$ molecule^{-1} cm^3 s^{-1} from 288K to 295K [2].

OH exposure in the OFR is defined as the OH concentration (molecules cm^{-3}) integrated over residence time of the OFR [12]. OH exposure determines how fast the precursor is oxidized within the OFR. An initial OH calibration experiment was conducted by measuring the decay of benzene due to the reaction with OH (rate constants ~ $1.22*10^{-12}$ cm^3 molecule^{-1} s^{-1} [11]. Using a gas chromatography (GC) it was estimated that the OH exposure inside the OFR is about $1.33*10^{12}$ molecules s cm^{-3} ($7.8*10^9$ molecules cm^{-3}). This OH exposure level corresponds to about 10 days of atmospheric oxidation, assuming typical atmospheric OH levels of $1.5*10^6$ molecules cm^{-3} [12].

A.5 Discussion & Conclusions

Since the OFR was built my research went in another direction leading to me to be unable to optimize the OFR. The OFR has been a tool within the laboratory that has been used as a radical source, used for additional aging, and to help understand additional influences on the particle composition.

Future steps to further optimize the OFR will include determining the flow inside the OFR, examine wall loss, and varying the power supplied to the UV lamps and RH to understand how they affect the mixing ratios of O_3, OH and HO_2 generated inside the OFR.

A.6 References

1 Kanakidou, M., Seinfeld, J. H., Pandis, S. N., Barnes, I., Dentener, F. J., Facchini, M. C., Van Dingenen, R., Ervens, B., Nenes, A., Nielsen, C. J., Swietlicki, E., Putaud, J. P., Balkanski, Y., Fuzzi, S., Horth, J., Moortgat, G. K., Winterhalter, R., Myhre, C. E. L., Tsigaridis, K., Vignati, E., Stephanou, E. G., Wilson, J. (2005). Organic aerosol and global climate modelling: a review. Atmospheric Chemistry and Physics, 5(4), 1053–1123.

2 Kang, E., Root, M. J., Toohey, D. W., & Brune, W. H. (2007). Introducing the concept of Potential Aerosol Mass (OFR). *Atmospheric Chemistry and Physics*, *7*(22), 5727–5744, http://doi.org/10.5194/acp-7-5727-2007.

3 PAM Wiki [online]. Available: https://sites.google.com/site/PAMwiki/ [Accessed: 05-June-2018].

4 Chen, S., Brune, W. H., Lambe, A. T., Davidovits, P., & Onasch, T. B. (2013). Modeling organic aerosol from the oxidation of a-pinene in a Potential Aerosol Mass (OFR) chamber. *Atmospheric Chemistry and Physics*, *13*(9), 5017–5031, https://doi.org/10.5194/acp-13-5017-2013.

5 Lambe, A. T., Ahern, A. T., Williams, L. R., Slowik, J. G., Wong, J. P. S., Abbatt, J. P. D., Brune, W. H., Ng, N. L., Wright, J. P., Croasdale, D. R., Worsnop, D. R., Davidovits, P., & Onasch, T. B. (2011). Characterization of aerosol photooxidation flow reactors: Heterogeneous oxidation, secondary organic aerosol formation and cloud condensation nuclei activity measurements. *Atmospheric Measurement Techniques*, *4*(3), 445–461. https://doi.org/10.5194/amt-4-445-2011.

6 Li, R., Palm, B. B., Ortega, A. M., Hlywiak, J., Hu, W., Peng, Z., Jimenez, J. L. (2015). Modeling the radical chemistry in an oxidation flow reactor: Radical formation and recycling, sensitivities, and the OH exposure estimation equation. *Journal of Physical Chemistry A*, *119*(19), 4418–4432, https://doi.org/10.1021/jp509534k.

7 Scanning Mobility Particle Sizer – TSI [online]. Available: http://www.tsi.com/Products/Particle-Sizers/Scanning-Mobility-Particle-Sizer-Spectrometers/Scanning-Mobility-Particle-Sizer-Spectrometer-3938.aspx [Accessed: 07-August-2018].

8 McMurry, P. H., Wang, X., Park, K., & Ehara, K. (2002). The relationship between mass and mobility for atmospheric particles: A new technique for measuring particle density. Aerosol Science and Technology, 36(2), 227–238. https://doi.org/10.1080/027868202753504083.

9 Jayne, J. T., Leard, D. C., Zhang, X., Davidovits, P., Smith, K. A., Kolb, C. E., & Worsnop, D. R. (2000). Development of an aerosol mass spectrometer for size and composition analysis of submicron particles. *Aerosol Science and Technology*, *33*(1–2), 49–70. https://doi.org/10.1080/027868200410840.

10 Chhabra, P. S., Flagan, R. C., & Seinfeld, J. H. (2010). Elemental analysis of chamber organic aerosol using an aerodyne high-resolution aerosol mass spectrometer. *Atmospheric Chemistry and Physics*, *10*(9), 4111–4131.

11 Seinfeld, J. H., Pandis, S. N. (2016). Atmospheric chemistry and physics: from air pollution to climate change. Wiley product, textbook.

12 Kang, E., Toohey, D. W., & Brune, W. H. (2011). Dependence of SOA oxidation on organic aerosol mass concentration and OH exposure: Experimental OFR chamber studies. Atmospheric Chemistry and Physics, 11(4), 1837–1852. https://doi.org/10.5194/acp-11-1837-2011.